

Determining the Molecular Underpinnings of Iron Homeostasis in Human Cells

By

April Lee

B.A. Biology
Cornell University, 2018

Submitted to the Biology Department in partial fulfillment
of the requirements for the degree of

DOCTOR OF PHILOSOPHY IN BIOLOGY

at the

MASSACHUSETTS INSTITUTE OF TECHNOLOGY

September 2025

©2025 April Lee. *All Rights Reserved.*

The author hereby grants to MIT a nonexclusive, worldwide, irrevocable, royalty-free license to exercise any and all rights under copyright, including to reproduce, preserve, distribute and publicly display copies of the thesis, or release the thesis under an open-access license.

Authored by
April Lee
Department of Biology
23 June 2025

Certified by
Joseph H. Davis
Associate Professor of Biology
Thesis Supervisor

Accepted by
Mary Gehring
Professor of Biology
Member, Whitehead Institute
Director, Biology Graduate Committee

Determining the Molecular Underpinnings of Iron Homeostasis in Human Cells

By

April Lee

Submitted to the Department of Biology
on 23 June 2025 in partial fulfillment of the requirements for the degree of
Doctor of Philosophy in Biology at the Massachusetts Institute of Technology

ABSTRACT

Precise regulation of nutrient availability is crucial for cellular function and survival. Iron, in particular, is tightly regulated as it serves as an essential cofactor for numerous enzymes but can catalyze the formation of toxic radicals at elevated levels. To maintain the necessary cytoplasmic iron concentration, cells store excess iron in large proteinaceous cages called ferritin and, when available iron levels fall, they degrade these cages, liberating the stored iron for use. This thesis focuses on the molecular mechanisms underlying cellular iron sensing, as well as the molecular interactions supporting regulated ferritin degradation and subsequent iron release. Specifically, this work interrogates the protein interactions involved in ferritinophagy, a form of selective autophagy that leads to the lysosomal degradation of ferritin. Extending prior work that identified key components supporting ferritinophagy, including the selective autophagy receptor protein NCOA4 and its cognate autophagosomal receptor GATE16, experiments described here uncover the molecular contacts between these proteins. I found that NCOA4 bears two short linear motifs that each bind to GATE16 with weak affinity. However, these binding motifs are highly avid and, in concert, support high-affinity binding of NCOA4 to oligomerized GATE16. I further describe that ferritin degradation in cultured human cells relies on the contacts I identified biochemically. Moreover, I found that iron decreases NCOA4's affinity for GATE16, providing a plausible mechanism for iron-dependent regulation of ferritinophagy. Taken together, this work suggests a general mechanism by which selective autophagy receptors can distinguish between inactive monomeric GATE16 and the active oligomerized forms that primarily drive autophagy. In related studies, I have biochemically probed the NCOA4•ferritin interface, with these experiments suggesting a novel function of NCOA4 in modulating ferritin cage structure – either through cage dismantling or through the formation of higher order structures. Taken together, these studies further define the molecular mechanisms by which NCOA4 aids cells in maintaining iron homeostasis, and they provide the requisite reagents for future work aimed at building a unified model for how mammalian cells regulate this vital but toxic metal.

Thesis Supervisor: Joseph H. Davis
Title: Associate Professor of Biology

ACKNOWLEDGMENTS

The work in this thesis would not have been possible without the guidance and support of many remarkable individuals. I would like to use this space to thank the following:

My advisor, Joey, for supporting my journey through graduate school. Your excellent input and advice helped direct this project to some truly interesting conclusions. You also assembled a lab environment that aided in the success of this.

My committee members, Cathy Drennan and Matt Vander Heiden, for your invaluable suggestions on my project through the years. Special thanks to my outside committee member, Mike Ragusa.

My fellow Davis lab members, especially those who have spent countless hours with me in North Lab and made my day to day life joyous. Andrew, thank you for your mentorship in the early years of my PhD.

My undergraduate lab advisor, Joshua Chappie, for being instrumental in leading me to pursue a PhD at MIT.

My dear MIT friends, Michael Das, Michael Stubna and Peter Wang, for all the hangouts, trips and debriefs. Das, you especially have been one of the most important parts of my life these past few years.

Finally, my parents, for their constant support and counsel throughout this process and for always pushing me to do my best in life.

Table of Contents

Chapter 1: Introduction	6
1.1 Homeostasis of nutrients is essential for cellular function	7
1.2 Maintenance of a stable cytosolic pool of iron	8
1.3 Interplay of the proteasome and lysosome in protein degradation	10
1.4 Selective autophagy as a specific form of lysosomal degradation	13
1.5 LC3 interacting motifs regulate selective autophagy	15
1.6 Ferritinophagy facilitates ferritin degradation	16
1.7 Research summary	19
1.8 Figures	22
1.9 References	25
Chapter 2: NCOA4 initiates ferritinophagy by binding GATE16 using two highly avid short linear interaction motifs	31
2.1 Abstract	32
2.2 Introduction	33
2.3 Results	36
2.4 Discussion	43
2.5 Materials and Methods	48
2.6 Figures	61
2.7 References	80
Chapter 3: A minimal fragment of the ferritinophagy receptor NCOA4 dismantles heavy ferritin cages	85
3.1. Abstract	86
3.2. Introduction	87
3.3. Results	90
3.4. Discussion	94
3.5. Materials and Methods	98
3.6. Figures	104
3.7. References	109
Chapter 4: Conclusions and future directions	112
4.1. NCOA4 initiates ferritinophagy by binding GATE16 using two highly avid short linear interaction motifs	113
4.2. Future directions in interrogating NCOA4•GATE16 interactions	114
4.3. Putative role of NCOA4 in dismantling ferritin cages	116
4.4. Future directions for NCOA4 ³⁸³⁻⁵²² dependent cage dismantling	117
4.5. Contribution to the role of NCOA4 in ferritinophagy regulation	118
4.6. Figures	120
4.7. References	122

List of Figures

Chapter 1: Introduction

- 1.1. Maintenance of the labile pool of iron in the cell.
- 1.2. Types of mammalian autophagy.
- 1.3. NCOA4 as the regulator of ferritinophagy.

Chapter 2: NCOA4 initiates ferritinophagy by binding GATE16 using two highly avid short linear interaction motifs

- 2.1. NCOA4³⁸³⁻⁵²² binds directly to (GST-GATE16)₂.
- 2.2. Oligomeric states of GATE16 and NCOA4³⁸³⁻⁵²² in solution.
- 2.3. NCOA4³⁸³⁻⁵²² and (GST-GATE16)₂ binding kinetics measured by BLI.
- 2.4. NCOA4³⁸³⁻⁵²² binding to (GST-GATE16)₂ via peptide array.
- 2.5. Sequence conservation of the two LIR-like motifs of NCOA4³⁸³⁻⁵²².
- 2.6. NCOA4³⁸³⁻⁵²² binds to (GST-GATE16)₂ through two LIR-like motifs
- 2.7. Impact of NCOA4³⁸³⁻⁵²² mutants on protein stability.
- 2.8. Contribution of LDS in NCOA4³⁸³⁻⁵²² binding to (GST-GATE16)₂.
- 2.9. Binding of NCOA4³⁸³⁻⁵²² to (GST-GATE16)₂ requires avidity.
- 2.10. Assessment of nonspecific binding of NCOA4³⁸³⁻⁵²² to GST in far-westerns.
- 2.11. Assessing nonspecific association of NCOA4³⁸³⁻⁵²² to (GST)₂ in BLI.
- 2.12. Load-dependent BLI response.
- 2.13. Cellular levels of NCOA4³⁸³⁻⁵²² and associated mutants.
- 2.14. NCOA4³⁸³⁻⁵²² supports ferritin degradation *in vivo* and requires both LIR-like motifs.
- 2.15. LC3B can form puncta independent of ATG7 in ferritinophagy inducing conditions.
- 2.16. NCOA4³⁸³⁻⁵²²•(GST-GATE16)₂ binding is iron dependent.
- 2.17. Assessing nonspecific association of MBP to (GST-GATE16)₂ in BLI.

Chapter 3: A minimal fragment of the ferritinophagy receptor NCOA4 dismantles heavy ferritin cages

- 3.1. MBP-NCOA4³⁸³⁻⁵²²-mNeon binds specifically to hfH.
- 3.2. NCOA4³⁸³⁻⁵²² dependent loss of heavy ferritin cages in analytical SEC.
- 3.3. NCOA4³⁸³⁻⁵²² dependent loss of heavy ferritin cages in cryo-EM.
- 3.4. NCOA4³⁸³⁻⁵²² dependent loss of heavy ferritin cages in mass photometry.
- 3.5. Cage dismantling activity of NCOA4³⁸³⁻⁵²² requires free C-terminus.

Chapter 4: Conclusions and future directions

- 4.1. Iron regulation of NCOA4•GATE16 dependent ferritinophagy.
- 4.2. Hypothesized NCOA4 dependent degradation of ferritin via the proteasome and lysosome.

Chapter 1

An introduction to cellular homeostasis and ferritinophagy

AUTHOR CONTRIBUTIONS

AL wrote following text with editorial support from JHD.

1.1 Homeostasis of nutrients is essential for cellular function.

Cells require nutrients such as sugars, lipids, amino acids and trace metals to survive. As such, mammalian cells have developed a wide array of mechanisms to sense and respond to changes in nutrient levels internally and in their environment. Indeed, an array of molecular sensors detect changes to nutrient levels and can trigger signaling cascades that result in either uptake, export, synthesis or degradation of the target nutrient (Sung *et al*, 2023). One well studied example of such a eukaryotic nutrient sensor and effector is the kinase mTOR (mechanistic target of rapamycin), which binds to an assortment of other protein factors to form biochemically defined complexes that can differentially sense and respond to a wide array of growth factors, nucleotides, and other chemicals correlated with cell state (Condon & Sabatini, 2019). For instance, kinase activity in mTOR complex 1 (mTORC1) is regulated by levels of amino acids in the lysosome, a degradative compartment of the cell. When amino acids are abundant, they bind to proteins in the lysosomal membrane, causing the recruitment and activation of mTORC1 kinase activity, which downregulates the degradative process of autophagy through phosphorylation of key autophagy initiation components (Efeyan *et al*, 2012). However, when amino acid levels are low, mTORC1 remains in an inactive form in the cytosol, instead promoting autophagy (Efeyan *et al.*, 2012). Autophagy can then degrade various proteins to liberate amino acids for use by the cell in the synthesis of new proteins (He, 2022). Thus, mTORC1 both senses and regulates the availability of amino acids.

Interestingly, mTOR also senses and regulates a variety of metal ions, which serve vitals roles in metabolism as enzymatic cofactors (Nelson, 1999). For example, mTORC1 can respond to altered levels of cellular calcium via interaction with the calcium binding

protein calmodulin (Amemiya *et al*, 2023). Moreover, chelation, and thus depletion, of iron was reported to inhibit mTORC1 signaling, indicating its ability to sense iron levels (Shang *et al*, 2020). Additionally, mTOR can regulate iron homeostasis by altering the stability of proteins involved in iron transport across the cell membrane (Bayeva *et al*, 2012). Dysregulation of mTORC1 signaling, and by extension nutrient level maintenance, has been linked to human diseases including cancer, metabolic disorders, autoimmune diseases and neurological disorders, thus highlighting the importance of cellular nutrient homeostasis (Dibble & Manning, 2013).

1.2 Maintenance of a stable cytosolic pool of iron.

The regulation of iron levels is crucial for cellular health. Iron is a required co-factor for many essential enzymes, especially those involved in energy metabolism and oxygen transport, in part due to its ability to convert from the reduced state (Fe^{2+}) to the oxidized state (Fe^{3+}), which aids in shuttling electrons and coordinating catalysis. As such, iron is an integral part of mitochondria function where it forms heme groups and iron sulfur clusters (Teh *et al*, 2024). However, when dysregulated or present at high levels, iron can catalyze the formation of reactive oxygen species (ROS) - highly reactive radicals generated through Fenton chemistry (Meyerstein, 2021). These reactive species can damage organelles and tissues, leading to a variety of oxidative stress responses and diseases (Wang & Pantopoulos, 2011). Specifically, dysregulations in free Fe^{2+} levels are linked to neurodegenerative disorders, including Alzheimer's (Ward *et al*, 2014) and Parkinson's (Sofic *et al*, 1988) diseases.

Given the dichotomy between the importance but potential damaging effects of iron, it is critical that cells tightly control the levels of free Fe^{2+} . To accomplish this, cells

maintain a labile pool of cytosolic Fe^{2+} , whose concentration is regulated at the levels of uptake, export, usage and storage (**Figure 1.1**). To support uptake, iron can be either imported by receptor mediated endocytosis of transferrin bound to Fe^{3+} before reduction to Fe^{2+} in endosomes or first converted to Fe^{2+} by cell surface ferrireductases and then shuttled into the cell through transmembrane transporters (Lane *et al*, 2015). Both mechanisms serve to increase the amount of usable iron in the labile pool. Conversely, the labile pool can be decreased by using iron metabolically in the mitochondria or exporting it from the cell via ferroportin (Lane *et al.*, 2015).

Additionally, iron may be stored as a ferrihydrite mineral core within in the proteinaceous cage called ferritin. Ferritin is a 24-mer comprised of heavy and light chain subunits that can sequester up to 4,500 Fe^{3+} in this ~5-8 nm amorphous mineral core (Arosio *et al*, 2017; Bossoni *et al*, 2023). The ferritin cage is highly symmetric and comprised of both three-fold hydrophilic and four-fold hydrophobic channels. The three-fold channels facilitate Fe^{2+} entry into the cage while the four-fold channels allow for proton transfer to balance overall charge as the oxidized mineral core is formed (Zhang *et al*, 2021). Due to the critical role of iron storage, the expression of ferritin is modulated by cellular iron concentrations. Specifically, levels of iron in the cell are able to translationally regulate the production of ferritin via the iron responsive element:iron responsive protein (IRE:IRP) system (Zhou & Tan, 2017). When iron levels are low, IRPs bind to ferritin mRNA IREs to prevent translation and production of ferritin protein, but in excess iron conditions, iron binds to IRPs, blocking their association with IREs and allowing for ferritin translation to proceed (Arosio *et al.*, 2017). Thus, in high iron conditions, more ferritin can be translated, facilitating increased iron storage and a

concomitant decrease in the cytosolic Fe^{2+} concentration. In addition to the translational regulation of ferritin to modulate iron levels, ferritin cages can also be degraded to release iron back into the labile pool to increase the available concentration of Fe^{2+} . In different studies ferritin degradation has been reported to occur via the lysosome (Zhang *et al*, 2010) via the proteasome (De Domenico *et al*, 2009), or through both pathways (Kwok & Richardson, 2004). Given the essential role of ferritin in modulating iron concentration, several diseases have been linked to ferritin misregulation. These diseases include hereditary ferritinopathy, which is caused by mutations in the ferritin light chain gene that causes formation of ferritin inclusion bodies and leads to excess iron deposition in the cytosol, resulting in production of oxidizing species that damage cellular proteins and lipids (Muhoberac & Vidal, 2019).

1.3 Interplay of the proteasome and lysosome in protein degradation.

In response to various signals, such as iron depletion, cells must adapt their proteome, upregulating or downregulating both the abundance and the activity of proteins like ferritin to suit the current environment. In some instances, this regulation can simply occur when cells tune the rates of degradation, synthesis (Munro *et al*, 2024) or sequestration (Buchler & Cross, 2009). Protein activity can be directly altered by post-translation modifications (PTMs) (Lee *et al*, 2023), which is commonly thought to offer a mechanism for the reversible regulation of protein activity by covalently adding functional groups like phosphate to amino acids to either activate or deactivate enzymatic activity (Seok, 2021). Alternatively, regions of the protein responsible for targeted degradation known as degrons may also be controlled by PTMs, whereby installation of a PTM either

increases or decreases protein stability (Lee *et al.*, 2023). In addition to altering protein levels, such degradation also liberates recycled amino acids that can then be used to synthesize new proteins with alternate functions that promote survival in the new environmental condition (Davies & Humphrey, 1978). Protein degradation in eukaryotic cells is driven primarily by either the ubiquitin-proteasome system (UPS) or lysosomal macroautophagy (Dikic, 2017).

The UPS aids cells in downregulating protein levels as well as clearing damaged or otherwise misfolded proteins. To do so, proteins are recognized by elements of the protein quality control pathway and, through the action of E1/E2/E3 ligases, are marked with ubiquitin tags (Li *et al.*, 2022). These tags are then commonly thought to target the substrate for proteasomal degradation (LaPlante & Zhang, 2021), though emerging evidence suggests that such tagging can also promote lysosomal degradation (Komander & Rape, 2012). The proteasome translocates substrates in an ATP-dependent manner into its inner chamber, where the unfolded polypeptide is proteolyzed and released (Bard *et al.*, 2018). The proteasome has been implicated in a wide array of cellular processes, including the cell cycle, signal transduction and stress response (Bard *et al.*, 2018).

While the proteasome is thought to primarily target small, short-lived proteins, macroautophagy, which directs proteins to the lysosome for degradation is generally thought to act on large, heterogenous complexes like protein aggregates and organelles (Dikic, 2017). Macroautophagy begins when environmental signals converge on the multi protein complex of ULK1 kinase (Yu *et al.*, 2018) and, as noted above, one of the most well studied stimuli for macroautophagy regulation is nutrient deprivation as sensed via mTOR pathway components. Specifically, in nutrient rich conditions mTORC1

phosphorylation inhibits the ULK1 complex, whereas in starvation conditions, these marks are stripped by cellular phosphatases and AMPK phosphorylation marks are installed that are thought to activate the ULK1 complex (Antonioli *et al.*, 2017). Once activated, ULK1 then triggers a downstream cascade to activate the PI3KC3 complex (Lin & Hurley, 2016), which in turn nucleates the formation of an autophagosome precursor membrane (Antonioli *et al.*, 2017). This precursor double membrane expands with the recruitment of lipids via ATG9 before encapsulating the desired target (Antonioli *et al.*, 2017). The fully formed autophagosome finally fuses with the lysosome, where hydrolytic enzymes degrade the target and release the contents for reuse by the cell (Dikic, 2017).

Although initially studied as two independent pathways, recent studies have indicated that there is crosstalk and potential compensation between the UPS and macroautophagy (Cui *et al.*, 2024). This means that there are various substrates, such as ferritin, which can be degraded by both the proteasome and lysosome (De Domenico *et al.*, 2009; Kwok & Richardson, 2004; Zhang *et al.*, 2010). This compensatory relationship was first noted upon discovery that proteasome inhibition or overload could induce macroautophagy (Dikic, 2017; Ge *et al.*, 2009). Reciprocally, studies have demonstrated that macroautophagy inhibition can increase proteasomal activity and upregulate the production of proteasomal subunits (Wang *et al.*, 2013). In some cancer cells, it has been observed that upon impairing macroautophagic pathways, cell lines that begin as highly macroautophagy-dependent can adapt to instead rely on the proteasome (Towers *et al.*, 2019). While some studies demonstrate the compensatory relationship of the lysosome and proteasome, other studies have found that impairment of one pathway may lead to dysfunction of the other. For instance, Korolchuk *et al.* observed that macroautophagy

inhibition causes impaired flux of substrates through the UPS (Korolchuk *et al*, 2009). This may be due to the fact that macroautophagy is efficacious at clearing large aggregates and more complex structures that the proteasome cannot effectively tackle. Moreover, inhibition of one degradative pathway may lead to accumulation of substrates that overwhelm the capacity of the other, causing cellular dysfunction. Given this complex dynamic, it is important that when studying the degradation of substrates, both pathways are considered.

1.4 Selective autophagy as a specific form of lysosomal degradation.

While autophagy converges on the lysosome to facilitate proteolytic degradation of substrates, there are multiple pathways in mammalian cells by which it can proceed, namely chaperone mediated autophagy (CMA), microautophagy and macroautophagy. CMA is highly specific as all substrates contain a pentapeptide targeting motif (KFERQ), which is recognized by chaperone proteins such as HSP8A for direct delivery to the lysosome (Fred Dice, 1990) (**Figure 1.2a**). At the lysosomal membrane, the target protein•HSP8A complex binds LAMP2A, a CMA substrate receptor, causing multimerization of LAMP2A and forming a translocation complex (Parzych & Klionsky, 2014). The substrate is then transferred into the lysosome where it is degraded. The CMA pathway is largely regulated by levels of active LAMP2A in the lysosomal membrane (Cuervo & Dice, 2000). Distinct from CMA, microautophagy involves the uptake of substrates into the lysosome by direct invagination of the lysosomal membrane (Parzych & Klionsky, 2014) (**Figure 1.2b**). Unlike both CMA and microautophagy which require direct interaction of the substrate/substrate receptor complex with the lysosome,

macroautophagy is unique in that the substrate is first sequestered in a double membraned structure of the autophagosome prior to lysosomal fusion (**Figure 1.2c**). Macroautophagy (autophagy, hereafter) can be categorized into two separate types: nonselective and selective. In nonselective macroautophagy portions of cytoplasm are engulfed by an autophagosome without being directly tethered to the core autophagic machinery, whereas selective macroautophagy (selective autophagy, hereafter) targets organelles or protein complexes by physically linking them to the autophagosome through specific binding interactions (Feng *et al*, 2014).

To achieve the required specificity of selective autophagy, cargos are often recognized by a class of proteins termed selective autophagy receptors (SARs). The unifying characteristic for SARs is that they simultaneously bind to both the target cargo and the autophagosomal machinery - specifically members of the LC3/GABARAPs family of ubiquitin-like modifier proteins (Lamark & Johansen, 2021) (**Figure 1.2d**). This definition of a SAR is largely based on the initial discovery that p62, one of the first SARs, recognizes polyubiquitinated protein aggregates, linking them to the autophagy machinery by binding to an LC3 family member (Bjørkøy *et al*, 2005; Lamark & Johansen, 2021). As autophagy must be tightly regulated to respond to environmental cues and cellular maintenance, SARs are also stringently modulated, often through a variety of PTMs. Ubiquitination of SARs can target them for degradation via the proteasome, thus depleting the amount present to conduct autophagy. Moreover, other PTMs like phosphorylation and acetylation can promote or inhibit the interaction of SARs and LC3s (Gubas & Dikic, 2022). Additionally, the activity of SARs can be regulated by their oligomeric state, with their higher order oligomeric forms often driving autophagy (Gubas

& Dikic, 2022). These SARs have been implicated in the degradation of many complexes and organelles including, but not limited to the ER, mitochondria, aggregates and ferritin (Lamark & Johansen, 2021).

1.5 LC3 interacting motifs regulate selective autophagy.

Selective autophagy receptors are thought to bind specifically to members of the Microtubule-associated proteins 1A/1B light chain 3B (LC3/GABARAP) family of integral autophagosomal proteins (Lee & Lee, 2016). This family consists of six homologs: LC3A, LC3B, LC3C, GABARAP, GEC1 and GATE16. Upon induction of autophagy, soluble LC3/GABARAPs are conjugated to a lipid through the action of the E1-like enzyme, ATG7, and a E2/E3-like system composed of ATG12/ATG5, such that they are covalently linked to phosphatidyl ethanolamine headgroups of phospholipids in the autophagosomal membrane (Kabeya *et al*, 2004; Kraft *et al*, 2014; Liu *et al*, 2024). SARs generally then bind to these membrane-associated LC3/GABARAPs via an LC3 interacting motif (LIR), which are short linear motifs typically following a consensus sequence of [W/F/Y]-X-X-[I/L/V], often accompanied by an N-terminal patch of acidic residues (Johansen & Lamark, 2020). Structural studies have demonstrated that LIR motifs bind in the LIR docking site (LDS) region of LC3/GABARAPs, which consists of two hydrophobic pockets that support docking of the aromatic and aliphatic residues of the LIR motif (Johansen & Lamark, 2020).

Interest in LIR motifs stems both from their role in autophagy, and the fact that they are part of a broader group known as short linear motifs (SLiMs). SLiMs range from three to ten amino acids and are typically found in intrinsically disordered regions of proteins

(Davey *et al*, 2023). They bind to targets generally with micromolar affinity and regulate a variety of cellular processes by altering protein localization, stability and binding site availability (Davey *et al.*, 2023). Interestingly, SLiMs contain very low information content such that they are highly prevalent through the proteome, which raises questions of how specificity is achieved. In one model, it has been speculated that their low information content sequence profiles allow for multiple SLiMs to exist in a single protein or protein complex (Maiti & De, 2022). Thus, if a binding partner exposed multiple SLiM binding pockets, it is possible that multivalent interactions could be used to achieve tight binding and thus a higher level of specificity. Stated directly, in this model isolated SLiMs with individual weak affinity would not support a sustained protein interaction as such a complex would stably form only when multiple (highly avid) SLiMs were bound to a partner protein or protein complex (Errington *et al*, 2019; Lluís Garcés *et al*, 2009). If true, it would follow that cells could thus regulate specific binding of SLiM-containing proteins by altering their oligomeric state or local concentration through changes in PTM status (Lee *et al.*, 2023), localization (Gotte & Menegazzi, 2023), membrane association (Sawa-Makarska *et al*, 2014), or by modulating the availability of scaffolding proteins (Hata & Iida, 2009). Below, I discuss the relationship between SLiMs and the regulation of ferritin levels through a process known as ferritinophagy, which relies on SLiM-based interactions.

1.6 Ferritinophagy facilitates ferritin degradation.

One mechanism by which ferritin is degraded in response to decreased iron levels is

ferritinophagy, a type of selective autophagy. In this process, ferritin is selectively recognized and targeted to the lysosome for degradation (**Figure 1.3a**). Proteases in the highly acidic lysosome open and degrade ferritin cages, allowing for reduction of iron by the lysosomal ferrireductase, STEAP3, and the subsequent transport of Fe^{2+} into the cytoplasm by ion channels TRPML1/2 and Nramp1 (LeVine, 2023; Zhang *et al.*, 2021).

Ferritinophagy is thought to rely on the protein Nuclear Receptor Coactivator 4 (NCOA4). NCOA4 was first identified as a selective autophagy receptor in an LC-MS/MS based proteomics approach targeting proteins that copurified with autophagosomes (Mancias *et al.*, 2014). Mancias *et al.* found that NCOA4 binds to the heavy chain of ferritin via residues I489 and W497 (Mancias *et al.*, 2015) while also colocalizing and interacting with LC3s (Mancias *et al.*, 2014), thus acting as a link between ferritin and the autophagosomal machinery. Furthermore, it was determined that although the full length NCOA4 structure is predicted to be highly disordered, the biochemically amenable fragment NCOA4³⁸³⁻⁵²² is sufficient for ferritin binding (Gryzik *et al.*, 2017; Hoelzgen *et al.*, 2024; Mancias *et al.*, 2015). Isothermal titration calorimetry experiments were consistent with eight NCOA4³⁸³⁻⁵²² molecules binding per highly symmetric ferritin cage (Srivastava *et al.*, 2020). Additionally, it was recently reported that NCOA4³⁸³⁻⁵²² is loaded with a [3Fe-4S] iron sulfur cluster coordinated by four cysteines (Zhao *et al.*, 2024). This cluster was identified in iron replete conditions (Zhao *et al.*, 2024). Notably, it was previously observed that the E3 ligase HERC2 ubiquitylates and promotes degradation of NCOA4 in an iron-dependent manner (**Figure 1.3b**), though the identity of this iron sulfur cluster was not known at the time (Mancias *et al.*, 2015). Conversely, iron-free NCOA4 has higher affinity for ferritin, which presumably fosters enhanced ferritin degradation in iron deplete

conditions (Zhao *et al.*, 2024). Given this complicated set of iron-dependent interactions, NCOA4 is thought to act as a linchpin in the regulation of ferritinophagy by sensing iron availability, presumably through this iron sulfur cluster.

Although ferritinophagy is widely accepted to be dependent on NCOA4, the molecular mechanisms of the pathway remain largely underexplored and it seems that multiple NCOA4 dependent pathways can occur in cells. Canonical autophagy relies on the assumption that the selective receptor, NCOA4, binds to both the intended degradation substrate, ferritin, and LC3s that have been lipidated by ATG7 and inserted into autophagosomal membranes (de la Ballina *et al.*, 2020) (**Figure 1.3a**). Several studies report that NCOA4 dependent ferritinophagy follows this model of canonical autophagy (Dowdle *et al.*, 2014; Mancias *et al.*, 2014). However, others have observed that ferritinophagy does not require ATG7 and by extension lipidated LC3s, but instead relies on TAX1BP1, a known cargo receptor (Goodwin *et al.*, 2017). This TAX1BP1 pathway represents a lysosomal, NCOA4-dependent pathway that functions as a form of non-canonical autophagy. Ohshima and colleagues have proposed that NCOA4 drives formation of ferritin•NCOA4 phase separated condensates, which can be degraded through both LC3-dependent autophagy and endosomal microautophagy and that both mechanisms are dependent on TAX1BP1 (Ohshima *et al.*, 2022). Further complicating matters, experiments to assess ferritinophagy often rely on the increased signal afforded either by the exogenous addition of iron to the cells in the form of ferric ammonium citrate (FAC), the chelation of iron with deferoxamine (DFO), or a combination of the two, with some studies indicating that details in the application of these additives (e.g. exposure times, concentrations, cell types, etc.) can alter the pathway by which ferritin is degraded.

For example, Kuno and colleagues reported that prolonged iron treatment causes the formation of NCOA4•ferritin condensates that are delivered to the lysosomes by a noncanonical ATG7-independent, TAX1BP1-dependent pathway, whereas in iron depleted conditions ferritin degradation proceeded through canonical autophagy via NCOA4 (Kuno *et al*, 2022). Given these various reports it is unclear how exactly ferritinophagy functions and the relation between the several possible pathways.

1.7 Research summary.

In this thesis, I use a biochemical reductionist approach to characterize the interactions of key proteins involved in the regulation of ferritinophagy. Specifically, I focus on the binding modes of NCOA4 to GATE16, a member of the LC3/GABARAP family, and to ferritin.

In chapter 2, the primary research of this thesis, I elucidate the molecular details of the NCOA4•GATE16 binding interface. Whereas NCOA4 was previously shown to colocalize and strongly interact with GATE16, the molecular mechanisms of this interaction remained unknown (Mancias *et al.*, 2014). Thus, I employed a biochemically amenable fragment of NCOA4, NCOA4³⁸³⁻⁵²², which was demonstrated to be sufficient for ferritin binding, to characterize the NCOA4•GATE16 interaction (Mancias *et al.*, 2015). Through this study, I first found that NCOA4³⁸³⁻⁵²² binds to GATE16 directly and does so through two LIR-like motifs, as confirmed through a series of mutational analyses. I observed that these LIR-like motifs present in NCOA4 each bind to the LDS of GATE16 with weak affinity, but are highly avid and together promote tight overall binding of NCOA4 to GATE16. When assessing stoichiometry of the complex, I found that one NCOA4

molecule exposes two LIR-like motifs that are each bound by a separate GATE16 which, in my system, was dimerized through a GST tag. In related work, I then probed the importance of these motifs *in vivo* in human cell lines expressing stably integrated NCOA4³⁸³⁻⁵²² or NCOA4³⁸³⁻⁵²² motif mutants. I found that in my tested conditions, NCOA4³⁸³⁻⁵²² is sufficient to promote ferritinophagy and requires both LIR-like motifs, as demonstrated by lysosomal colocalization and ferritin degradation changes. This work supports the notion that in some cellular contexts, my proposed avidity model of NCOA4•GATE16 binding is critical in supporting ferritinophagy. Importantly, by using cells lacking ATG7, I demonstrated that LC3s can form puncta and by extension, oligomerize, independent of their lipidation status, revealing a plausible mechanism for highly avid interactions to occur in both wild type and ATG7Δ genetic backgrounds. This model of NCOA4 requiring GATE16 to be oligomerized provides a potential mechanism by which selective autophagy receptors can distinguish between inactive, monomeric LC3s and oligomeric, active LC3s. Finally, I compared the affinity of iron-free NCOA4³⁸³⁻⁵²² to reconstituted, iron-bound NCOA4³⁸³⁻⁵²² to assess the effect of iron on the NCOA4•GATE16 interaction. I found that iron-bound NCOA4³⁸³⁻⁵²² has decreased affinity for GATE16, indicating that iron can regulate ferritinophagy at the level of NCOA4•GATE16 complex formation. Overall, my work in this chapter reveals key molecular mechanisms by which NCOA4 binds to GATE16 and it describes how this interaction may support the regulation of ferritinophagy both by oligomerization of LC3s and response to iron levels.

In chapter 3, I interrogate the molecular details of how NCOA4 interacts with ferritin. I determined that NCOA4³⁸³⁻⁵²² can bind directly to heavy ferritin and, consistent with my

observation, this interface has since been resolved in atomic detail through a cryo-EM structure of the co-complex (Hoelzgen *et al.*, 2024; Mancias *et al.*, 2015). However, initial experiments I have conducted suggest that NCOA4³⁸³⁻⁵²² may have an alternate function beyond just binding to ferritin. Using a combination of analytical size exclusion chromatography, electron microscopy and mass photometry, I have generated preliminary evidence showing that ferritin cages disappear, or fall apart, upon addition of NCOA4³⁸³⁻⁵²². Given these results, I propose two models to explain this observation: in one, NCOA4³⁸³⁻⁵²² facilitates the dismantling of ferritin cages upon binding; and in the second, NCOA4³⁸³⁻⁵²² facilitates the formation of higher order ferritin cage oligomers, which may form condensates. If model one is true, my cage dismantling model would provide a mechanism by which cells could directly release iron into the cytosol without the need to degrade ferritin cages via either the lysosome or proteasome.

1.8 FIGURES

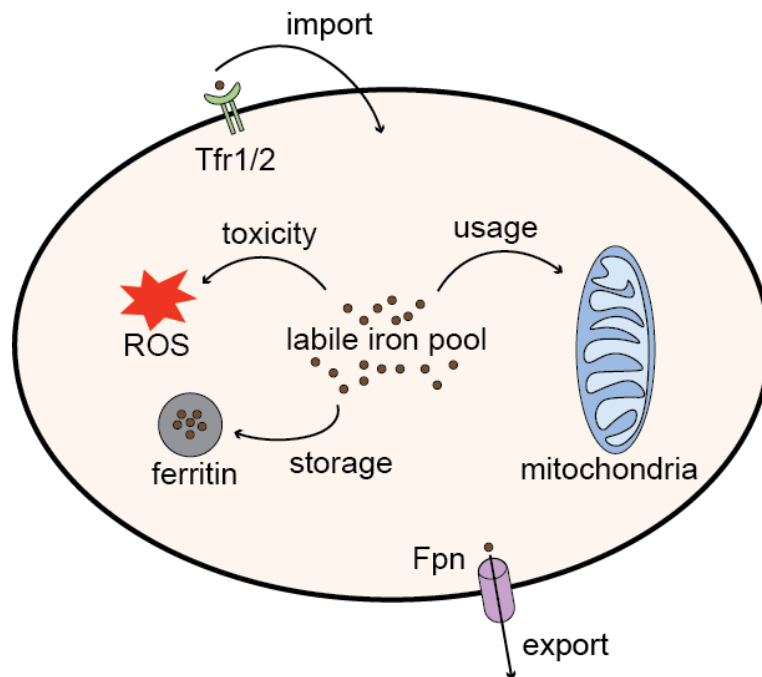


Figure 1.1: Maintenance of the labile pool of iron in the cell.

The cytosolic labile iron pool is regulated by import via transferrin receptors (Trf1/2) and export via ferroportin (Fpn) channels. Iron is a widely used enzymatic cofactor, particularly by the mitochondria. Finally, iron is stored in the protein cage, ferritin, which can be degraded in iron deplete conditions. Tight regulation of iron is crucial as, when present at high levels, it can catalyze the formation of damaging reactive oxygen species (ROS).

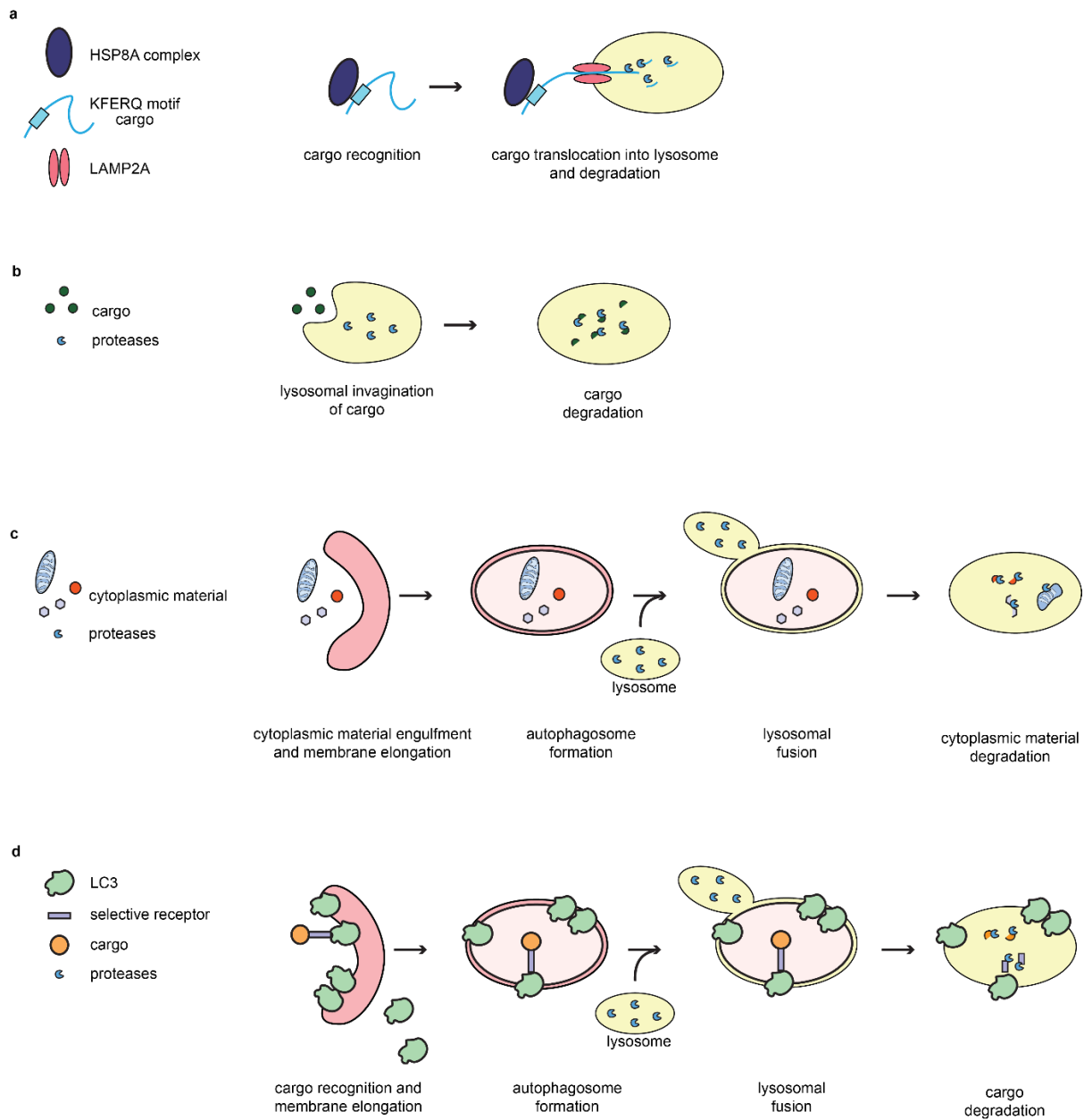


Figure 1.2: Types of mammalian autophagy.

(a) Chaperone mediated autophagy (CMA). Target cargo bears a KFERQ motif which is recognized by the HSP8A complex and directly translocated into the lysosome via a LAMP2 oligomer for proteolytic degradation.

(b) Microautophagy. Cargo material is directly invaginated into the lysosome.

(c) Bulk macroautophagy. Cytoplasmic material is engulfed in a double membrane autophagosome that forms de novo and later fuses with the lysosome.

(d) Selective macroautophagy. Cargo is recognized by a selective receptor, which links cargo to the nascent autophagosome via LC3/GABARAP family members for subsequent autophagosomal engulfment and lysosomal fusion.

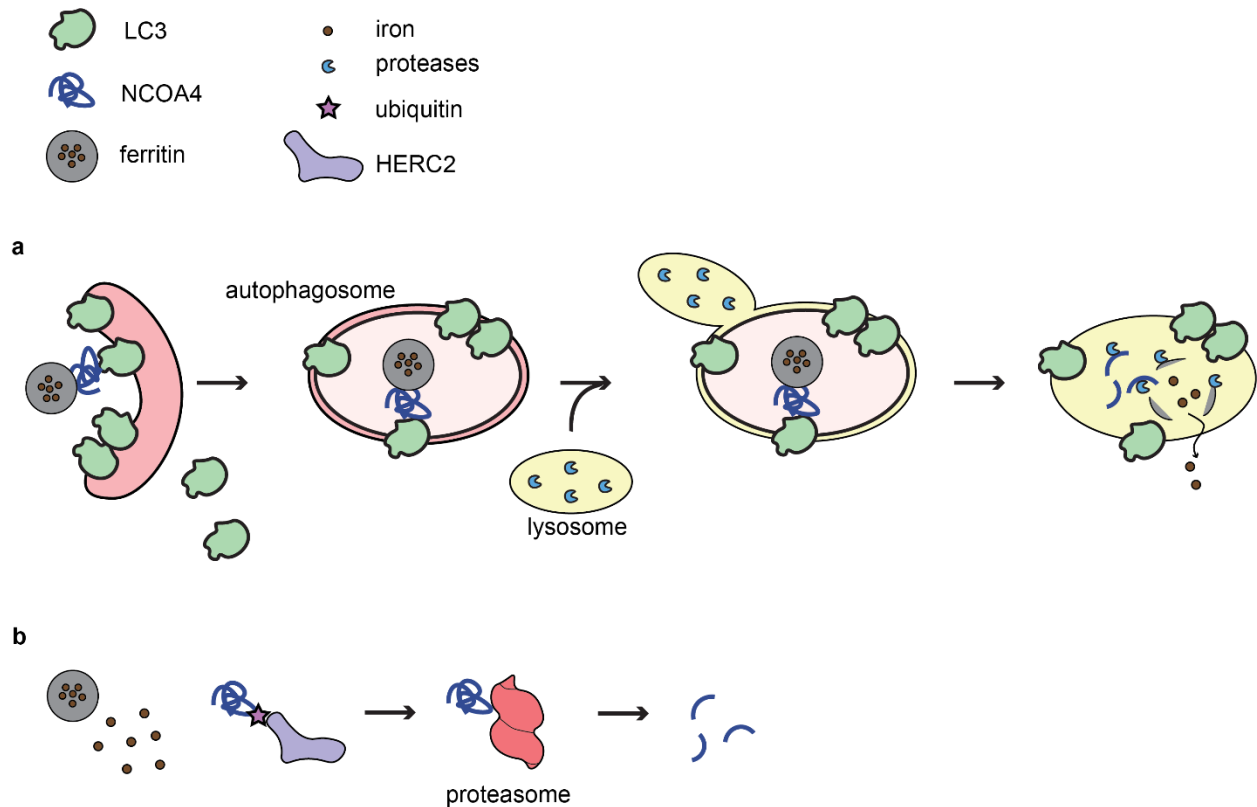


Figure 1.3: NCOA4 as the regulator of ferritinophagy.

(a) In iron limiting conditions, NCOA4 recognizes the substrate, iron-loaded ferritin cages, and simultaneously binds to LC3 in the nascent autophagosome. After substrate recognition, a double membraned autophagosome forms around the complex before fusing with the lysosome. In the lysosome, ferritin cages are degraded by lysosomal proteases and iron is released into the cytosol.

(b) In iron replete conditions, NCOA4 is ubiquitinated by the E3 ligase, HERC2, and brought to the proteasome where it is degraded. Thus, ferritin cages are not degraded by NCOA4 in these conditions.

1.9 REFERENCES

- Amemiya Y, Maki M, Shibata H, Takahara T (2023) New Insights into the Regulation of mTOR Signaling via Ca²⁺-Binding Proteins. *International Journal of Molecular Sciences* 24: 3923
- Antonoli M, Di Rienzo M, Piacentini M, Fimia GM (2017) Emerging Mechanisms in Initiating and Terminating Autophagy. *Trends Biochem Sci* 42: 28-41
- Arosio P, Elia L, Poli M (2017) Ferritin, cellular iron storage and regulation. *IUBMB Life* 69: 414-422
- Bard JAM, Goodall EA, Greene ER, Jonsson E, Dong KC, Martin A (2018) Structure and Function of the 26S Proteasome. *Annu Rev Biochem* 87: 697-724
- Bayeva M, Khechaduri A, Puig S, Chang HC, Patial S, Blackshear PJ, Ardehali H (2012) mTOR regulates cellular iron homeostasis through tristetraprolin. *Cell Metab* 16: 645-657
- Bjørkøy G, Lamark T, Brech A, Outzen H, Perander M, Overvatn A, Stenmark H, Johansen T (2005) p62/SQSTM1 forms protein aggregates degraded by autophagy and has a protective effect on huntingtin-induced cell death. *J Cell Biol* 171: 603-614
- Bossoni L, Labra-Muñoz JA, van der Zant HSJ, Čaluković V, Lefering A, Egli R, Huber M (2023) In-depth magnetometry and EPR analysis of the spin structure of human-liver ferritin: from DC to 9 GHz. *Phys Chem Chem Phys* 25: 27694-27717
- Buchler NE, Cross FR (2009) Protein sequestration generates a flexible ultrasensitive response in a genetic network. *Molecular Systems Biology* 5: 272
- Condon KJ, Sabatini DM (2019) Nutrient regulation of mTORC1 at a glance. *J Cell Sci* 132
- Cuervo AM, Dice JF (2000) Regulation of Lamp2a Levels in the Lysosomal Membrane. *Traffic* 1: 570-583
- Cui DS, Webster SM, Davis JH (2024) Integrated proteasomal and lysosomal activity shape mTOR-regulated proteome remodeling. *bioRxiv*. 2024.2007.2020.603815
- Davey NE, Simonetti L, Ivarsson Y (2023) The next wave of interactomics: Mapping the SLiM-based interactions of the intrinsically disordered proteome. *Current Opinion in Structural Biology* 80: 102593
- Davies DD, Humphrey TJ (1978) Amino Acid Recycling in Relation to Protein Turnover. *Plant Physiology* 61: 54-58

- De Domenico I, Ward DM, Kaplan J (2009) Specific iron chelators determine the route of ferritin degradation. *Blood* 114: 4546-4551
- de la Ballina LR, Munson MJ, Simonsen A (2020) Lipids and Lipid-Binding Proteins in Selective Autophagy. *J Mol Biol* 432: 135-159
- Dibble CC, Manning BD (2013) Signal integration by mTORC1 coordinates nutrient input with biosynthetic output. *Nature Cell Biology* 15: 555-564
- Dikic I (2017) Proteasomal and Autophagic Degradation Systems. *Annu Rev Biochem* 86: 193-224
- Dowdle WE, Nyfeler B, Nagel J, Elling RA, Liu S, Triantafellow E, Menon S, Wang Z, Honda A, Pardee G *et al* (2014) Selective VPS34 inhibitor blocks autophagy and uncovers a role for NCOA4 in ferritin degradation and iron homeostasis in vivo. *Nat Cell Biol* 16: 1069-1079
- Efeyan A, Zoncu R, Sabatini DM (2012) Amino acids and mTORC1: from lysosomes to disease. *Trends Mol Med* 18: 524-533
- Errington WJ, Bruncsics B, Sarkar CA (2019) Mechanisms of noncanonical binding dynamics in multivalent protein–protein interactions. *Proceedings of the National Academy of Sciences* 116: 25659-25667
- Feng Y, He D, Yao Z, Klionsky DJ (2014) The machinery of macroautophagy. *Cell Research* 24: 24-41
- Fred Dice J (1990) Peptide sequences that target cytosolic proteins for lysosomal proteolysis. *Trends in Biochemical Sciences* 15: 305-309
- Ge PF, Zhang JZ, Wang XF, Meng FK, Li WC, Luan YX, Ling F, Luo YN (2009) Inhibition of autophagy induced by proteasome inhibition increases cell death in human SHG-44 glioma cells. *Acta Pharmacol Sin* 30: 1046-1052
- Goodwin JM, Dowdle WE, DeJesus R, Wang Z, Bergman P, Kobylarz M, Lindeman A, Xavier RJ, McAllister G, Nyfeler B *et al* (2017) Autophagy-Independent Lysosomal Targeting Regulated by ULK1/2-FIP200 and ATG9. *Cell Rep* 20: 2341-2356
- Gotte G, Menegazzi M (2023) Protein Oligomerization. *Int J Mol Sci* 24
- Gryzik M, Srivastava A, Longhi G, Bertuzzi M, Gianoncelli A, Carmona F, Poli M, Arosio P (2017) Expression and characterization of the ferritin binding domain of Nuclear Receptor Coactivator-4 (NCOA4). *Biochim Biophys Acta Gen Subj* 1861: 2710-2716
- Gubas A, Dikic I (2022) A guide to the regulation of selective autophagy receptors. *The FEBS Journal* 289: 75-89

- Hata Y, Iida J (2009) Scaffold Protein. In: *Encyclopedia of Neuroscience*, Binder M.D., Hirokawa N., Windhorst U. (eds.) pp. 3613-3616. Springer Berlin Heidelberg: Berlin, Heidelberg
- He C (2022) Balancing nutrient and energy demand and supply via autophagy. *Current Biology* 32: R684-R696
- Hoelzgen F, Nguyen TTP, Klukin E, Boumaiza M, Srivastava AK, Kim EY, Zalk R, Shahar A, Cohen-Schwartz S, Meyron-Holtz EG *et al* (2024) Structural basis for the intracellular regulation of ferritin degradation. *Nat Commun* 15: 3802
- Johansen T, Lamark T (2020) Selective Autophagy: ATG8 Family Proteins, LIR Motifs and Cargo Receptors. *J Mol Biol* 432: 80-103
- Kabeya Y, Mizushima N, Yamamoto A, Oshitani-Okamoto S, Ohsumi Y, Yoshimori T (2004) LC3, GABARAP and GATE16 localize to autophagosomal membrane depending on form-II formation. *Journal of cell science* 117: 2805-2812
- Komander D, Rape M (2012) The ubiquitin code. *Annu Rev Biochem* 81: 203-229
- Korolchuk VI, Mansilla A, Menzies FM, Rubinsztein DC (2009) Autophagy inhibition compromises degradation of ubiquitin-proteasome pathway substrates. *Mol Cell* 33: 517-527
- Kraft LJ, Nguyen TA, Vogel SS, Kenworthy AK (2014) Size, stoichiometry, and organization of soluble LC3-associated complexes. *Biophysical Journal* 106: 734a-735a
- Kuno S, Fujita H, Tanaka YK, Ogra Y, Iwai K (2022) Iron-induced NCOA4 condensation regulates ferritin fate and iron homeostasis. *EMBO Rep* 23: e54278
- Kwok JC, Richardson DR (2004) Examination of the mechanism(s) involved in doxorubicin-mediated iron accumulation in ferritin: studies using metabolic inhibitors, protein synthesis inhibitors, and lysosomotropic agents. *Mol Pharmacol* 65: 181-195
- Lamark T, Johansen T (2021) Mechanisms of Selective Autophagy. *Annu Rev Cell Dev Biol* 37: 143-169
- Lane DJ, Merlot AM, Huang ML, Bae DH, Jansson PJ, Sahni S, Kalinowski DS, Richardson DR (2015) Cellular iron uptake, trafficking and metabolism: Key molecules and mechanisms and their roles in disease. *Biochim Biophys Acta* 1853: 1130-1144
- LaPlante G, Zhang W (2021) Targeting the Ubiquitin-Proteasome System for Cancer Therapeutics by Small-Molecule Inhibitors. *Cancers* 13: 3079
- Lee JM, Hammarén HM, Savitski MM, Baek SH (2023) Control of protein stability by post-translational modifications. *Nature Communications* 14: 201

Lee YK, Lee JA (2016) Role of the mammalian ATG8/LC3 family in autophagy: differential and compensatory roles in the spatiotemporal regulation of autophagy. *BMB Rep* 49: 424-430

LeVine SM (2023) Examining the Role of a Functional Deficiency of Iron in Lysosomal Storage Disorders with Translational Relevance to Alzheimer's Disease. *Cells* 12: 2641

Li Y, Li S, Wu H (2022) Ubiquitination-Proteasome System (UPS) and Autophagy Two Main Protein Degradation Machineries in Response to Cell Stress. *Cells* 11

Lin MG, Hurley JH (2016) Structure and function of the ULK1 complex in autophagy. *Curr Opin Cell Biol* 39: 61-68

Liu J, Xiao Y, Cao L, Lu S, Zhang S, Yang R, Wang Y, Zhang N, Yu Y, Wang X *et al* (2024) Insights on E1-like enzyme ATG7: functional regulation and relationships with aging-related diseases. *Communications Biology* 7: 382

Lluís Garcés J, Rey-Castro C, David C, Madurga S, Mas F, Pastor I, Puy J (2009) Model-Independent Link between the Macroscopic and Microscopic Descriptions of Multidentate Macromolecular Binding: Relationship between Stepwise, Intrinsic, and Microscopic Equilibrium Constants. *The Journal of Physical Chemistry B* 113: 15145-15155

Maiti S, De S (2022) Identification of potential short linear motifs (SLiMs) in intrinsically disordered sequences of proteins by fast time-scale backbone dynamics. *Journal of Magnetic Resonance Open* 10-11: 100029

Mancias JD, Pontano Vaites L, Nissim S, Biancur DE, Kim AJ, Wang X, Liu Y, Goessling W, Kimmelman AC, Harper JW (2015) Ferritinophagy via NCOA4 is required for erythropoiesis and is regulated by iron dependent HERC2-mediated proteolysis. *Elife* 4

Mancias JD, Wang X, Gygi SP, Harper JW, Kimmelman AC (2014) Quantitative proteomics identifies NCOA4 as the cargo receptor mediating ferritinophagy. *Nature* 509: 105-109

Meyerstein D (2021) Re-examining Fenton and Fenton-like reactions. *Nature Reviews Chemistry* 5: 595-597

Muhoberac BB, Vidal R (2019) Iron, Ferritin, Hereditary Ferritinopathy, and Neurodegeneration. *Front Neurosci* 13: 1195

Munro V, Kelly V, Messner CB, Kustatscher G (2024) Cellular control of protein levels: A systems biology perspective. *Proteomics* 24: e2200220

- Nelson N (1999) Metal ion transporters and homeostasis. *The EMBO Journal* 18: 4361-4371-4371
- Ohshima T, Yamamoto H, Sakamaki Y, Saito C, Mizushima N (2022) NCOA4 drives ferritin phase separation to facilitate macroferritinophagy and microferritinophagy. *J Cell Biol* 221
- Parzych KR, Klionsky DJ (2014) An overview of autophagy: morphology, mechanism, and regulation. *Antioxid Redox Signal* 20: 460-473
- Sawa-Makarska J, Abert C, Romanov J, Zens B, Ibiricu I, Martens S (2014) Cargo binding to Atg19 unmasks additional Atg8 binding sites to mediate membrane–cargo apposition during selective autophagy. *Nature Cell Biology* 16: 425-433
- Seok SH (2021) Structural Insights into Protein Regulation by Phosphorylation and Substrate Recognition of Protein Kinases/Phosphatases. *Life (Basel)* 11
- Shang C, Zhou H, Liu W, Shen T, Luo Y, Huang S (2020) Iron chelation inhibits mTORC1 signaling involving activation of AMPK and REDD1/Bnip3 pathways. *Oncogene* 39: 5201-5213
- Sofic E, Riederer P, Heinsen H, Beckmann H, Reynolds GP, Hebenstreit G, Youdim MB (1988) Increased iron (III) and total iron content in post mortem substantia nigra of parkinsonian brain. *J Neural Transm* 74: 199-205
- Srivastava AK, Flint N, Kreckel H, Gryzik M, Poli M, Arosio P, Bou-Abdallah F (2020) Thermodynamic and Kinetic Studies of the Interaction of Nuclear Receptor Coactivator-4 (NCOA4) with Human Ferritin. *Biochemistry* 59: 2707-2717
- Sung Y, Yu YC, Han JM (2023) Nutrient sensors and their crosstalk. *Experimental & Molecular Medicine* 55: 1076-1089
- Teh MR, Armitage AE, Drakesmith H (2024) Why cells need iron: a compendium of iron utilisation. *Trends Endocrinol Metab* 35: 1026-1049
- Towers CG, Fitzwalter BE, Regan D, Goodspeed A, Morgan MJ, Liu CW, Gustafson DL, Thorburn A (2019) Cancer Cells Upregulate NRF2 Signaling to Adapt to Autophagy Inhibition. *Dev Cell* 50: 690-703.e696
- Wang J, Pantopoulos K (2011) Regulation of cellular iron metabolism. *Biochem J* 434: 365-381
- Wang XJ, Yu J, Wong SH, Cheng AS, Chan FK, Ng SS, Cho CH, Sung JJ, Wu WK (2013) A novel crosstalk between two major protein degradation systems: regulation of proteasomal activity by autophagy. *Autophagy* 9: 1500-1508

Ward RJ, Zucca FA, Duyn JH, Crichton RR, Zecca L (2014) The role of iron in brain ageing and neurodegenerative disorders. *Lancet Neurol* 13: 1045-1060

Yu L, Chen Y, Tooze SA (2018) Autophagy pathway: Cellular and molecular mechanisms. *Autophagy* 14: 207-215

Zhang N, Yu X, Xie J, Xu H (2021) New Insights into the Role of Ferritin in Iron Homeostasis and Neurodegenerative Diseases. *Molecular Neurobiology* 58: 2812-2823

Zhang Y, Mikhael M, Xu D, Li Y, Soe-Lin S, Ning B, Li W, Nie G, Zhao Y, Ponka P (2010) Lysosomal proteolysis is the primary degradation pathway for cytosolic ferritin and cytosolic ferritin degradation is necessary for iron exit. *Antioxid Redox Signal* 13: 999-1009

Zhao H, Lu Y, Zhang J, Sun Z, Cheng C, Liu Y, Wu L, Zhang M, He W, Hao S, Li K (2024) NCOA4 requires a [3Fe-4S] to sense and maintain the iron homeostasis. *J Biol Chem* 300: 105612

Zhou ZD, Tan E-K (2017) Iron regulatory protein (IRP)-iron responsive element (IRE) signaling pathway in human neurodegenerative diseases. *Molecular Neurodegeneration* 12: 75

Chapter 2

NCOA4 initiates ferritinophagy by binding GATE16 using two highly avid short linear interaction motifs

The following chapter is adapted from a manuscript published on bioRxiv and currently under revision for journal publication.

AUTHOR CONTRIBUTIONS

AL and JHD conceived the work, designed and interpreted the experiments, and wrote the manuscript. AL performed all experiments.

2.1 ABSTRACT

Cells carefully regulate cytosolic iron, which is a vital enzymatic cofactor, yet is toxic in excess. In mammalian cells, surplus iron is sequestered in ferritin cages that, in iron limiting conditions, are degraded through the selective autophagy pathway ferritinophagy to liberate free iron. Prior work identified the ferritinophagy receptor protein NCOA4, which links ferritin and LC3/GABARAP-family member GATE16, effectively tethering ferritin to the autophagic machinery. Here, we elucidate the molecular mechanism underlying this interaction, discovering two short linear motifs in NCOA4 that each bind GATE16 with weak affinity. These binding motifs are highly avid and, in concert, support high-affinity NCOA4•GATE16 complex formation. We further find the minimal NCOA4³⁸³⁻⁵²² fragment bearing these motifs is sufficient for ferritinophagy and that both motifs are necessary for this activity. This work suggests a general mechanism wherein selective autophagy receptors can distinguish between the inactive pools of monomeric LC3/GABARAPs and the active oligomerized forms that drive autophagy. Finally, we find that iron decreases affinity of the NCOA4³⁸³⁻⁵²² fragment for GATE16, providing a plausible mechanism for iron-dependent regulation of ferritinophagy.

2.2 INTRODUCTION

All cells must tightly regulate nutrient levels, including metals such as iron that act as crucial cofactors for essential enzymes. Whereas ample labile iron is vital for cellular function, excess iron can be toxic due, in part, to its ability to form damaging reactive oxygen species (Wang & Pantopoulos, 2011). Indeed, iron dysregulation has been connected to a variety of neurological diseases including hereditary ferritinopathy, Alzheimer's (Ward *et al*, 2014) and Parkinson's (Sofic *et al*, 1988) diseases. Mammalian cells are thought to maintain an appropriate pool of cytosolic iron by balancing iron uptake and storage in ferritin cages with the release of ferritin-sequestered iron through degradation of these proteinaceous cages (Arosio *et al*, 2009).

One mechanism by which ferritin is degraded upon depletion of free iron pools is ferritinophagy, a type of selective autophagy (Mancias *et al*, 2015) wherein select cellular components are recognized by an autophagy receptor protein and encapsulated in a double-membraned vesicle that is targeted to the lysosome for proteolysis (Zaffagnini & Martens, 2016). Ferritinophagy is thought to rely on the protein Nuclear Receptor Coactivator 4 (NCOA4), which was first identified as a selective autophagy receptor in an LC-MS/MS based proteomics approach targeting proteins that copurified with autophagosomes (Mancias *et al*, 2014). The activity of NCOA4 is regulated via iron-dependent changes in affinity for ferritin (Zhao *et al*, 2024) as well as the E3 ligase HERC2, which can promote NCOA4 degradation via the proteasome (Mancias *et al*, 2015). An NCOA4 fragment composed of residues 383-522 (NCOA4³⁸³⁻⁵²², hereafter) was subsequently found to be sufficient to bind directly to ferritin (Hoelzgen *et al*, 2024; Mancias *et al*, 2015).

To link the intended substrate and the autophagic machinery, selective cargo receptors typically bind to one or more of the six members of the Microtubule-associated proteins 1A/1B light chain 3B (LC3/GABARAP) family of integral autophagosomal proteins (Lee & Lee, 2016). These homologs, which include LC3A, LC3B, LC3C, GABARAP, GEC1, and GATE16, exchange between a monomeric soluble form, and a lipid-conjugated form wherein they are covalently linked to phosphatidyl ethanolamine headgroups of phospholipids in the autophagosomal membrane (Kabeya *et al*, 2004; Kraft *et al*, 2014). Selective autophagy receptors are thought to tether bound substrates to the autophagosomal membrane by simultaneously binding to LC3/GABARAPs via a short linear motif known as an LC3 interacting region (LIR). These motifs are hydrophobic in nature and have a consensus sequence of [W/F/Y]-X-X-[I/L/V], often accompanied by an N-terminal patch of acidic residues (Johansen & Lamark, 2020). Structural studies have further shown that the LC3/GABARAPs contain a LIR docking site (LDS) consisting of two hydrophobic pockets that support docking of the aromatic and aliphatic residues of the LIR motif (Johansen & Lamark, 2020).

Autophagy receptors are typically thought to associate with LC3/GAPARAPs using a single LIR, with affinity often in the low micromolar range (Johansen & Lamark, 2020). However, the LIR motif is common in the proteome and multiple instances can be found in most autophagy receptors, raising the possibility of highly avid, multivalent interactions to arrays of oligomerized LC3/GABARAP-family proteins. In such a model, multiple binding motifs on the same receptor, each with weak intrinsic affinity, would act in concert to increase the effector receptor protein concentration and thus support high affinity binding to multimerized LC3/GABARAPs (Errington *et al*, 2019; Lluís Garcés *et al*, 2009)

such as those found on an autophagosomal membrane densely decorated by LC3/GABARAPs or tethered in proximity by other scaffold proteins or aggregates.

Here, to biochemically define the interactions supporting ferritinophagy, we extend the work of Mancias *et al.*, who previously identified the LC3/GABARAP family protein GATE16 as a strong NCOA4 interactor (Mancias *et al.*, 2014). Specifically, using a purified NCOA4³⁸³⁻⁵²² fragment, we identify and characterize two LIR-like motifs in NCOA4³⁸³⁻⁵²² that each weakly bind to GATE16. We further show that these LIR-like motifs are highly avid and that robust GATE16•NCOA4 complex formation requires oligomerized GATE16. Furthermore, we show that this minimal NCOA4³⁸³⁻⁵²² fragment is sufficient for lysosomal degradation of ferritin in cells and that such degradation requires the two identified motifs. Finally, we demonstrate that binding of iron to NCOA4³⁸³⁻⁵²² decreases its affinity for GATE16.

2.3 RESULTS

NCOA4 binds directly to GATE16.

Though it has been previously reported that NCOA4 interacts with GATE16, this interaction was exclusively demonstrated through co-immunoprecipitations from cell lysates and cellular co-localization studies with full length NCOA4 (Dowdle *et al.*, 2014; Mancias *et al.*, 2014). Such evidence does not preclude indirect GATE16•NCOA4 binding through a protein intermediate. Thus, we sought to determine whether NCOA4 and GATE16 can, in fact, bind directly. For these experiments we used the biochemically amenable fragment of NCOA4³⁸³⁻⁵²² (**Figure 2.1a-b**) that is sufficient to bind ferritin (Hoelzgen *et al.*, 2024), but lacks both the putative coiled-coil domain and domains that overlap with the β -isoform, which does not bind ferritin or support ferritinophagy (Mancias *et al.*, 2015). After purifying NCOA4³⁸³⁻⁵²² and GST-GATE16 that, in our assay, were monomeric and dimeric, respectively (**Figure 2.2**), we assessed binding via far-western blots and biolayer interferometry (BLI). We observed concentration-dependent association in both assays (**Figure 2.1c-d**) consistent with NCOA4³⁸³⁻⁵²² having directly bound to this dimeric (GST-GATE16)₂. Notably, careful inspection of the BLI traces revealed biphasic binding kinetics in the association and dissociation phases, consistent with the presence of at least two binding events (**Figure 2.3**).

NCOA4³⁸³⁻⁵²² binds to GATE16 via two LIR-like motifs.

NCOA4³⁸³⁻⁵²² contains several putative LIR-like sequence motifs. To determine if such motifs supported GATE16•NCOA4 binding, we constructed a tiled array of peptides, each 20 amino acids long, that spanned the NCOA4³⁸³⁻⁵²² sequence, and we probed this array for binding with (GST-GATE16)₂. The peptide array revealed two candidate linear

interacting regions within the NCOA4 fragment – specifically ⁴¹³FAECV⁴¹⁷ and ⁴⁸⁵SFQVI⁴⁸⁹ (**Figure 2.4**). Of note, whereas the ⁴⁸⁵SFQVI⁴⁸⁹ motif contained a canonical LIR sequence, the ⁴¹³FAECV⁴¹⁷ motif bore cysteine substituted for the L/I/V residue specified by the canonical four residue LIR motif. We found that these identified motifs were highly conserved amongst NCOA4 orthologs, with the limited observed sequence variation preserving the hydrophobic nature of the key residues, including this noted cysteine (**Figure 2.5**). To directly assess the impact of these motifs on NCOA4•GATE16 binding, we individually substituted alanine for the key aromatic residues (⁴¹³F:A; ⁴⁸⁶F:A) in the identified LIR motifs in NCOA4³⁸³⁻⁵²² and tested the impact of these mutations on (GST-GATE16)₂ binding using both far-western blots (**Figure 2.6a**) and BLI (**Figure 2.6b**). In each assay, mutations to these putative binding motifs decreased (GST-GATE16)₂ binding, consistent with the necessity of each motif. Notably, the effect was not due to simply unfolding NCOA4³⁸³⁻⁵²², as the mutations did not impact global protein stability as assayed by a SYPRO Orange-based protein thermal stability shift assay (**Figure 2.7**).

NCOA4•GATE16 binding relies on avidity *in vitro*.

Having identified two motifs in NCOA4³⁸³⁻⁵²² that were each necessary for GATE16 association, we next sought to determine where on GATE16 those peptides bound. Since LIR motifs typically bind to LC3/GABARAP family proteins in regions known as LIR-docking sites (LDS) (Johansen & Lamark, 2020), we hypothesized the LDS was a likely binding location. To assess this, we first mutated known key LDS residues Y49 and L50 of (GST-GATE16)₂ (LDS*, hereafter) to alanines and tested binding to NCOA4³⁸³⁻⁵²² via BLI. Interestingly, these mutations improved binding of GATE16 to NCOA4³⁸³⁻⁵²² (**Figure**

2.8a) (Wirth *et al*, 2019). To better understand whether NCOA4³⁸³⁻⁵²² interacts with the LDS, we probed the ability of a peptide derived from ATG4B that is known to bind to the LDS to disrupt the binding of NCOA4³⁸³⁻⁵²² to (GST-GATE16)₂ in BLI (Skytte Rasmussen *et al*, 2017). The ATG4B peptide did in fact inhibit NCOA4•GATE16 binding in a concentration dependent manner, further indicating that NCOA4³⁸³⁻⁵²² is interacting with the LDS of GATE16 (**Figure 2.8b**). Additionally, we performed competitive fluorescence anisotropy assays in which an unlabeled peptide containing either of the identified NCOA4³⁸³⁻⁵²² motifs was added to a solution bearing monomeric GATE16 and a fluorescently labeled ATG4B peptide. Though the NCOA4³⁸³⁻⁵²²-derived peptides displaced the ATG4B peptide in a sequence-dependent manner, consistent with competitive binding to the LDS, they did so with weak apparent affinity (**Figure 2.9a-b**).

The observed discrepancy in NCOA4 affinity for monomeric GATE16 and dimeric (GST-GATE16)₂ led us to hypothesize that the two LIR motifs synergistically facilitated NCOA4•GATE16 binding. In our model, we reasoned that binding of one LIR-like motif to a dimerized copy of GATE16 could increase the effective concentration of the second LIR-like motif, thereby facilitating its binding to the GST-dimerized GATE16 copy. To more directly test this model, we assayed the binding of NCOA4³⁸³⁻⁵²² to GATE16 as a function of GATE16's oligomeric state using either monomeric His₆-GATE16 or dimeric (GST-GATE16)₂ (**Figure 2.2**). Our BLI-based binding assay showed improved binding with (GST-GATE16)₂ relative to monomeric His₆-GATE16 (**Figure 2.9c**). Of note, GST alone was unable to bind NCOA4³⁸³⁻⁵²² in any of our BLI, far-western, or peptide array assays (**Figures 2.4, 2.10, 2.11**).

To further assess the impact of multiple NCOA4³⁸³⁻⁵²² motifs on GATE16 binding, we generated single and double mutants of the identified motifs. Mutation of either motif alone significantly decreased binding to (GST-GATE16)₂ as assayed by BLI, though neither was sufficient to completely abrogate binding (**Figure 2.9d**). Notably, replacing the FAEC of the FAECV motif with a tetra-alanine linker further abrogated binding relative to the ⁴¹³F:A mutant, likely due to contribution of the cysteine residue to binding (**Figure 2.9d**). In the double mutant (⁴¹³F:A, ⁴⁸⁶F:A), we observed even weaker binding, consistent with each motif contributing to the overall NCOA4³⁸³⁻⁵²²•GATE16 interaction (**Figure 2.9e**).

We next assessed the oligomeric state of NCOA4³⁸³⁻⁵²² in the context of our observed NCOA4³⁸³⁻⁵²²•GATE16 binding to obtain a more complete binding model. In contrast to previous studies reporting NCOA4³⁸³⁻⁵²² can dimerize despite lacking the N-terminal coiled-coil oligomerization domain contained in the full-length protein (Gryzik *et al*, 2017), we found that NCOA4³⁸³⁻⁵²² was monomeric at our working concentrations, as assessed by SEC-MALS (**Figure 2.2**). However, since the BLI binding assays require that NCOA4³⁸³⁻⁵²² be immobilized on an assay probe tip, it was still formally possible that NCOA4³⁸³⁻⁵²² was positioned in such a way that it was acting as an artificial dimer. To assess whether NCOA4³⁸³⁻⁵²² was acting as a monomer or a dimer in this assay, we performed two complementary tests via BLI, probing for NCOA4³⁸³⁻⁵²² binding to (GST-GATE16)₂ either in “*cis*” to monomeric NCOA4³⁸³⁻⁵²², or in “*trans*” to an apparently dimeric form (**Figure 2.9f-g**). In the first assay, the two individual motif mutants (⁴¹³F:A and ⁴⁸⁶F:A) were mixed in a 1:1 ratio, loaded on the probe and their binding to (GST-GATE16)₂ was measured. If NCOA4³⁸³⁻⁵²² were acting as a dimer in this assay, we expected binding

similar to NCOA4³⁸³⁻⁵²² lacking motif mutations, as each singly mutated NCOA4³⁸³⁻⁵²² would still have one motif available to bind to one subunit of the GST-GATE16 dimer. Instead, we observed strongly reduced binding (**Figure 2.9h-i**). In a complementary assay, we mixed NCOA4³⁸³⁻⁵²² and the double mutant (⁴¹³F:A, ⁴⁸⁶F:A) in a 1:1 ratio, loaded the probe at 2-fold higher density and measured binding to (GST-GATE16)₂. Of note, loading the probe with twice the amount of NCOA4³⁸³⁻⁵²² produced a proportional increase in observed binding response (**Figure 2.12**). As such, if NCOA4³⁸³⁻⁵²² were acting as a monomer in this assay, then we would expect this protein mixture loaded to at the 2-fold higher density to produce similar binding to that observed with mutation-free type protein loaded at the standard density. We observe binding at a level predicted by the monomeric model (**Figure 2.9f**) and thus conclude that a monomeric NCOA4³⁸³⁻⁵²² uses two binding motifs to associate with dimeric GST-GATE16 (**Figure 2.9h-i**).

NCOA4³⁸³⁻⁵²² requires two LIR-like motifs to direct lysosomal degradation of ferritin *in vivo*.

Having established the importance of these two LIR-like motifs *in vitro*, we next assessed the role of these motifs *in vivo*. To do so, we stably integrated NCOA4³⁸³⁻⁵²² or variants mutated in the LIR-like motifs into NCOA4 knockout HeLa cells (NCOA4Δ, hereafter) (Gryzik *et al*, 2021). We measured similar levels of NCOA4 in each transfected cell line (**Figure 2.13**). With these cell lines, we first determined whether the NCOA4³⁸³⁻⁵²² fragment could facilitate the degradation of ferritin by comparing the extent of ferritin degradation in WT, NCOA4Δ and NCOA4³⁸³⁻⁵²² cells upon iron chelation with deferoxamine (DFO). Using quantitative western blots (see Methods), we observed that

ferritin was not degraded in NCOA4 Δ cells, whereas ferritin degradation was robust in wild-type cells and those bearing the NCOA4³⁸³⁻⁵²² (**Figure 2.14a,c**). Notably, the WT cells exhibited greater chelation-induced degradation than those expressing the NCOA4³⁸³⁻⁵²² fragment, suggesting additional contributions to ferritinophagy outside of this biochemically amenable NCOA4 fragment.

Given that NCOA4³⁸³⁻⁵²² facilitated ferritin degradation, we next assessed the impact of mutations to the two LIR-like motifs. Consistent with our *in vitro* binding data, mutation of either motif was sufficient to prevent NCOA4³⁸³⁻⁵²²-dependent ferritin degradation (**Figure 2.14b,d**), supporting the hypothesis that both motifs are required for stable NCOA4³⁸³⁻⁵²² binding to LC3/GABARAP-family proteins and by extension for ferritin degradation in cells.

Finally, to assess whether the observed ferritin degradation occurred in the lysosome, we performed colocalization studies via immunofluorescence to measure the impact of these identified LIR motifs on NCOA4:lysosome colocalization. Specifically, we stained for GFP-NCOA4³⁸³⁻⁵²² and lysosomes (LAMP1) in our NCOA4³⁸³⁻⁵²² and NCOA4³⁸³⁻⁵²² mutant cell lines in the presence of DFO. Strikingly, we saw significant colocalization of NCOA4³⁸³⁻⁵²² with lysosomes, consistent with NCOA4-mediated ferritin degradation through the autophagy-lysosomal pathway (**Figure 2.14e**). Furthermore, we found that mutation of either NCOA4³⁸³⁻⁵²² LIR-like motif resulted in significantly decreased NCOA4:lysosome colocalization (**Figure 2.14f,g**).

The dependence of NCOA4:lysosome colocalization on both NCOA4³⁸³⁻⁵²² LIR-like motifs further indicates that NCOA4³⁸³⁻⁵²² relies on avidity, and by extension binding to oligomerized GATE16, *in vivo*. However, some previous studies have shown that

ferritinophagy can still occur in cells that lack the LC3 lipidation machinery (ATG7) and thus do not have densely LC3 populated membranes to facilitate multimerization (Goodwin *et al*, 2017; Kuno *et al*, 2022). Hence, we sought to test whether LC3s can oligomerize independent of ATG7. To do so, we probed the ability of both WT and ATG7 knockout (ATG7 Δ , hereafter) HeLa cells to form LC3B puncta. Both cell lines formed puncta in DFO and FAC+DFO conditions, albeit ATG7 Δ to a much lesser degree, suggesting that LC3s can oligomerize independent of ATG7 specific lipidation under ferritinophagy inducing conditions (**Figure 2.15**).

Iron regulates the binding of NCOA4³⁸³⁻⁵²² to GATE16.

Given that the NCOA4•GATE16 interaction is crucial in the progression of ferritinophagy, an iron sensing pathway, we next asked whether iron could regulate this interaction. It was recently reported that NCOA4³⁸³⁻⁵²² can bind an iron-sulfur cluster coordinated by four cysteines (Zhao *et al.*, 2024). Importantly, one of these four cysteines, residue 416, is present in the ⁴¹³FAECV⁴¹⁷ LIR-like motif we have described. Thus, we hypothesized that were NCOA4³⁸³⁻⁵²² iron-loaded, the FAECV motif would be occluded, which would prevent robust GATE16 binding. To test this, we chelated iron from purified NCOA4³⁸³⁻⁵²², or reconstituted the protein with iron anaerobically (see Methods). We used a ferene assay (Fish, 1988; Levitz *et al*, 2022; McCarthy & Booker, 2018) to measure the equivalents of iron bound in each sample (**Figure 2.16a**). For each of these samples we then measured binding to (GST-GATE16)₂, observing a marked decrease in (GST-GATE16)₂ binding in the iron-bound NCOA4³⁸³⁻⁵²² sample (**Figure 2.16b**), consistent with a role for iron in negatively regulating NCOA4•GATE16 binding.

2.4 DISCUSSION

Taken together, our biochemical study has revealed that NCOA4³⁸³⁻⁵²², a biochemically amenable fragment of the selective autophagy receptor for ferritin, can bind directly to GATE16 through two LIR-like motifs: ⁴¹³EAECV⁴¹⁷ and ⁴⁸⁵SEQVI⁴⁸⁹. We found that in isolation each motif binds GATE16 weakly and that NCOA4 relies on avidity between these motifs to achieve tight binding. Moreover, we observed that to robustly form this complex, GATE16 must be oligomeric, though NCOA4 need not be. Our work further showed that the fragment NCOA4³⁸³⁻⁵²² is sufficient for ferritinophagy and that each LIR-like motif is indispensable for this activity *in vivo*. Finally, we found that binding of iron to NCOA4³⁸³⁻⁵²² reduces its affinity for GATE16, providing a mechanistic link between cellular iron levels and targeted ferritinophagy.

An expanded LIR motif.

Work over the prior 15 years has resulted in an ever-expanding collection of canonical and non-canonical peptide sequences that support binding to LC3/GABARAP-family proteins (Chatzichristofi *et al*, 2023; Johansen & Lamark, 2020). One of the peptides we identified (⁴⁸⁵SEQVI⁴⁸⁹) follows the canonical LIR pattern (*i.e.*, [W/F/Y]-x-x-[I/L/V]), whereas the other (⁴¹³EAECV⁴¹⁷) is, to our knowledge, the first instance of a cysteine acting as a core hydrophobic residue in a mammalian LIR. By some measures reduced cysteine is hydrophobic and often found in the hydrophobic core of proteins (Nagano *et al*, 1999), making it a reasonable candidate to occupy one of the hydrophobic pockets on GATE16. Combining this and other observed non-canonical residues at this position (Farnung *et al*, 2023) with structures demonstrating flexibility in the number of residues separating the two core LIR residues (Keown *et al*, 2018; Knaevelsrud *et al*,

2013), leads to a conclusion that the canonical LIR motif is overly stringent, and that the proteome displays an even larger array of potential LC3/GABARAP-family interacting peptides than currently appreciated. Such an expanded understanding of this interface further highlights the challenges in achieving specificity, emphasizing the importance of our described avidity model.

Highly avid binding can support LC3/GABARAP-family protein interactions.

In cells, LC3/GABARAP-family proteins are relatively abundant (Beck *et al*, 2011; Huang *et al*, 2023) and the canonical LIR motif of [W/F/Y]-X-X-[I/L/V] is of low information content and thus common in the human proteome. How then do cells achieve the high binding selectivity one would expect given the degradative capacity of the autophagy-lysosomal pathway? Whereas additional selectivity determinants outside of the core LIR, including a previously described acidic patch N-terminal of the core LIR (Birgisdottir *et al*, 2013; Johansen & Lamark, 2020), likely play a role, our work additionally suggests that avidly linking multiple LIR-like motifs in a single complex can contribute to specificity and affinity. Under this model, selective receptors, or complexes thereof, would need to expose multiple LIRs to support tight binding to LC3s, with such a multivalency requirement adding an additional layer of binding selectivity. Notably, in this model, cells could regulate whether such LIRs were displayed in a condition-specific manner, providing a direct means to modulate selective autophagy.

In support of this avidity model, we have identified two LIR-like motifs in NCOA4³⁸³⁻⁵²² that cooperatively facilitate binding to GATE16. In this model, binding of one motif to a single subunit of (GST-GATE16)₂ increases the local concentration of the dimer-linked

GATE16 protomer, which facilitates the second binding event. As we have shown that each motif is indispensable for ferritinophagy *in vivo*, we hypothesize that LC3/GABARAP-family proteins must also act as oligomers to support NCOA4 binding in cells. While our work has focused on GATE16 binding specifically, NCOA4 is thought to interact with multiple members of the LC3/GABARAP family (Mancias *et al.*, 2014), which would allow for avid interactions across the LC3/GABARAP-family members. The fact that the LC3/GABARAPs are conjugated to the autophagosomal membrane, which can proximally situate them at high concentration on a 2D surface, offers one potential mechanism by which they could mimic an oligomeric state. However, some reports find that NCOA4 mediated ferritinophagy does not require ATG7 lipidated LC3s under certain conditions (Goodwin *et al.*, 2017; Kuno *et al.*, 2022). In our work we have shown that LC3s are still able to form puncta and by extension oligomerize independent of ATG7 mediated lipidation. In agreement with this observation, Runwal *et al.* discovered LC3 puncta in ATG(7/10) knockdown cells and puncta of non-conjugatable mutants of LC3B, GABARAP and Gec-1 in ATG16 knockout cells (Runwal *et al.*, 2019). Taken together, this suggests that LC3/GABARAPs can oligomerize in alternate modes that could still support avid interactions for ferritinophagy. In addition to there being multiple pathways by which LC3s may operate in ferritinophagy, prior reports have also cited a dependence on TAX1BP1 for particular conditions, further expanding the potential alternate pathways for ferritinophagy (Goodwin *et al.*, 2017; Ohshima *et al.*, 2022).

It has become increasingly clear that avidity plays a large role in the progression of autophagy (Zaffagnini & Martens, 2016). In addition to the NCOA4•GATE16 model proposed here, a similar mechanism has been suggested in yeast where avidity is used

to support the selective receptor Atg19 binding to Atg8, the yeast homolog of the LC3/GABARAPs (Sawa-Makarska *et al*, 2014), and in mammalian cells where the selective autophagy receptors p62 and OPTN were each shown to self-oligomerize to facilitate the degradation of their respective cargo (Wurzer *et al*, 2015; Ying *et al*, 2010). Moreover, at the most extreme end of low affinity, high avidity interactions, phase separation has been proposed to have a role in autophagic initiation and maturation (Fujioka *et al*, 2020; Zhang *et al*, 2018). Our work highlighting the role of avidity in facilitating NCOA4 binding to oligomerized LC3/GABARAPs complements these prior observations.

Iron regulation of ferritinophagy.

As the process of ferritinophagy releases iron predominantly in response to iron depletion, there are several proposed mechanisms linking ferritinophagy to levels of labile iron. In one model, in iron replete conditions, the E3 ubiquitin ligase HERC2 binds to NCOA4 and promotes its degradation via the proteasome (Mancias *et al.*, 2015; Zhao *et al.*, 2024), thereby negatively regulating ferritinophagy. Additionally, Zhao *et al.* recently showed that NCOA4 binds an iron-sulfur cluster, which is coordinated using cysteine residues 404, 410, 416 and 422, and that ablation of the iron-sulfur cluster increases NCOA4's affinity for ferritin (Zhao *et al.*, 2024). Interestingly, cysteine 416 is contained in our described GATE16-binding ⁴¹³FAECV⁴¹⁷ motif, raising the possibility of iron-sulfur dependent regulation of this binding activity. Here we showed that in an iron-bound state, NCOA4³⁸³⁻⁵²²'s affinity for GATE16 is greatly reduced. Hence the presence of iron dually inhibits GATE16 and ferritin binding, and thus ferritinophagy. We postulate that when

levels of labile iron fall, this iron-sulfur cluster could be removed from NCOA4, liberating the ⁴¹³FAECV⁴¹⁷ motif to bind GATE16 and facilitate ferritinophagy, effectively adding an additional layer of iron regulation to the ferritinophagy pathway.

2.5 MATERIALS AND METHODS

Protein expression and purification.

GST-tagged GATE16 was expressed from plasmid pGex-4T-2_GATE-16 (Addgene 73518; pl_JD338) in *E. coli* BL21 Tuner DE3 (st_JD494). His₆-tagged GATE16 was generated via Q5 site-directed mutagenesis PCR (New England Biolabs), replacing the GST tag with the sequence MHHHHHHGS, and this construct (pl_JD339) was expressed in *E. coli* strain st_JD494. The LDS* mutant of GST-GATE16 was generated by mutating Y49 and L50 to alanines. A g-block gene fragment (IDT) containing the sequence for NCOA4³⁸³⁻⁵²² was cloned into plasmid pDW363 (Addgene 8842) via HiFi assembly (New England Biolabs) such that it had an N-terminal Avitag followed by a His₆ tag and a C-terminal MBP (pl_JD337). This vector co-expresses the biotin ligase BirA, enabling NCOA4³⁸³⁻⁵²² biotinylation of its Avitag during expression. Mutants of NCOA4³⁸³⁻⁵²² (⁴¹³F:A, ⁴⁸⁶F:A, ⁴¹³F:A/⁴⁸⁶F:A, ⁴¹³FAEC:AAAA/⁴⁸⁶F:A, ⁴¹³FAEC:AAAA; corresponding to plasmids pl_JD344 – pl_JD348, respectively) were generated using Q5 site-directed mutagenesis PCR. All NCOA4³⁸³⁻⁵²² constructs were expressed in *E. coli* strain st_JD494.

For each protein purified, expression cultures (2L) were grown in 2xYT media at 37°C with aeration, and induced with 1mM isopropyl β-d-1-thiogalactopyranoside at an optical density of ~0.6. Media for expression of NCOA4³⁸³⁻⁵²² constructs was supplemented with 0.05mM biotin. Expression proceeded for three hours at 37°C for GATE16 constructs, or at 30°C for NCOA4³⁸³⁻⁵²² constructs before cells were harvested via centrifugation.

Cell pellets bearing GST-GATE16 were resuspended in 50mL buffer PBS (140mM NaCl, 2.7mM KCl, 10mM Na₂HPO₄, 1.8mM KH₂PO₄, pH 7.3), dounced until homogenous and sonicated using a Qsonica Sonicator (5sec on, 10sec off for 5min, amplitude 35%). The lysate was centrifuged at 251,000g for one hour in a Ti60 rotor, after which the soluble fraction was loaded on a 20mL glutathione-sepharose affinity column (GSTPrep FF 16/10, Cytiva), washed with three column volumes of resuspension buffer, and eluted with 5 column volumes of buffer EB (50mM Tris-HCl, 150 mM NaCl, 10mM reduced glutathione, pH 8.0). To generate monomeric GATE16 (mGATE16) for use in fluorescence anisotropy assays, the GST tag was then removed by addition of 20μL thrombin (Millipore 69671-3), and the sample was cleaved at 4°C overnight. The eluate or cleaved fractions for (GST-GATE16)₂ or mGATE16 respectively, were pooled, concentrated to 2mL and purified over a S75 16/600 size exclusion column in buffer SB (20mM Tris, 150mM NaCl, pH 7.5). Fractions bearing (GST-GATE16)₂ (~0.4CVs) or mGATE16 (~0.7CVs) were identified by SDS-PAGE, pooled, and concentrated via centrifugation in a 30kDa (GST-GATE16) or 3kDa (mGATE16) concentrator (UFC903024 and UFC900324, Millipore Sigma) to a stock concentration of ~500μM. GST was expressed and purified as described for (GST-GATE16)₂, using expression plasmid pl_JD340.

Cell pellets bearing His₆-GATE16 were resuspended in 50mL of buffer NLB (10mM K₂HPO₄, 300mM NaCl, 20mM KCl, 10mM imidazole, 5mM 2-mercaptoethanol, pH 8.0), lysed and clarified as above and then loaded onto a 5mL Ni-NTA column (Bio-Rad), washed with two column volumes of buffer NLB, and eluted over 20 column volumes in a linear gradient of buffer NLB with imidazole increasing from 10mM to 1M. Pooled fractions

totaling 18mL were then concentrated to 2mL using 3kDa centricon (Millipore Sigma UFC900324) and purified over a S75 16/600 size exclusion column in buffer SB. Fractions bearing His₆-GATE16 (~0.7CVs) were identified and concentrated as above.

Cell pellets bearing NCOA4³⁸³⁻⁵²² were resuspended in 50mL of buffer NLB, lysed, clarified, and purified on a Ni-NTA column as above. Eluate (~20mL) was then diluted 5-fold in buffer SB, loaded onto a 5mL MBPTrap HP column (Cytvia), washed with 5 column volumes of buffer SB, and eluted with 8 column volumes of buffer SB supplemented with 10mM maltose. Eluate was pooled, concentrated to 2mL and then purified over a S75 16/600 size exclusion column in buffer SB. Fractions (~0.4CVs) were identified and concentrated with a 30kDa centricon (Millipore Sigma UFC903024) to ~50μM.

Far-Western blots.

(GST-GATE16)₂ at the noted concentrations was spotted (2μL) on a nitrocellulose membrane (Amersham Protran) and allowed to dry at room temperature for 12 minutes. The membrane was then blocked in buffer TBST (20mM Tris, 150mM NaCl, 0.1% Tween-20, pH 7.5) supplemented with 3% bovine serum albumin for 15 minutes at room temperature before being incubated with a 0.1μM solution of the appropriate biotinylated NCOA4³⁸³⁻⁵²² protein construct. After washing three times for three minutes with TBST, the membrane was incubated with HRP conjugated streptavidin (Thermo 21130) diluted 1:100,000 and subsequently washed three times in TSBT as above, before applying high sensitivity enhanced chemiluminescent substrate (Thermo 34094). All membranes being compared were imaged concurrently over a two-minute exposure on an Azure Biosystems imager.

Biolayer interferometry (BLI).

All BLI experiments were conducted on an Octet Red96 instrument (Forte Bio) using streptavidin biosensors (Sartorius 18-5019). Streptavidin biosensors were preincubated with BLI buffer (20mM Tris, 150mM NaCl, 0.05% Tween-20, 1% BSA, 1mM DTT, pH 7.5) for ten minutes. Biotinylated NCOA4³⁸³⁻⁵²² constructs were diluted to 50nM in BLI buffer and loaded on the streptavidin biosensors to a response level of 0.6nm. The loaded biosensors were immersed in serial dilutions of the appropriate GATE16 construct at the noted concentrations at an orbital shake speed of 1,000rpm at 30°C for a 250 second association step, with a dissociation step in BLI buffer for 500 seconds between each concentration. For each experiment, background binding of GATE16 to the biosensor was measured using a biosensor lacking NCOA4, and the same process repeated for each concentration. This background binding was subtracted from the resulting assay curves. To generate height response curves as a function of concentration, the response values of the last 50 seconds of each previous dissociation step were averaged and subtracted from the response average of the last 50 seconds of the relevant association step for each concentration.

BLI to assess nonspecific binding of MBP to (GST-GATE16)₂ was conducted with biotinylated Avitag-MBP (from Avidity BIS-300 - BIS-300 positive and negative control protein kit), following the above protocol.

Disruption of NCOA4³⁸³⁻⁵²² binding to (GST-GATE16)₂ by ATG4B was assessed by measuring BLI response using an orbital shake speed of 1,000rpm at 30°C for a 100 second association step, with a dissociation step in BLI buffer for 150 seconds. ATG4B

peptide (EDEDFEILSL) was preincubated with 5 μ M (GST-GATE16)₂ before measuring response at noted concentrations.

BLI for chelated and iron bound NCOA4³⁸³⁻⁵²² were initiated using protein prepared in a 4°C anaerobic glove box (MBraun, under 100% nitrogen gas) before immediately transferring to the Octet Red96 for assessment. The biotinylated NCOA4³⁸³⁻⁵²² constructs were diluted to 250nM in degassed, anaerobic BLI buffer supplemented with 5mM DTT and loaded to a response level of 0.35nm on the streptavidin biosensors. The loaded biosensors were immersed in 10 μ M (GST-GATE16)₂ at an orbital shake speed of 1,000rpm at 10°C for a 100 second association step, followed by a dissociation step in anaerobic BLI buffer for 150 seconds. Each measurement was performed in triplicate.

Spotted peptide array binding assay.

A peptide array spanning the NCOA4³⁸³⁻⁵²² construct consisted of 20mers offset by three amino acids that were synthesized on a cellulose membrane via SPOT synthesis by the MIT Biopolymers Laboratory. Peptides containing known GATE16 binding peptides (Olsvik *et al*, 2015; Pankiv *et al*, 2007; Skytte Rasmussen *et al.*, 2017) derived from p62/SQSTM1 (³³²SGGDDDWTHLSS³⁴³), ATG4B (³⁸⁴EDEDFEILSL³⁹³) and FYCO1 (¹²⁷⁶DDAVFDIITDEELCQIQE¹²⁹³) were included as positive controls and a poly His peptide (HHHHHHGSSHHHHHHGSSHH) was added as a negative control. The membrane was briefly soaked in methanol and then washed with TBST before blocking in buffer TBSTB (TBST with 3% BSA) for 30 minutes at room temperature. The membrane was then incubated with 4 μ g/mL (GST-GATE16)₂ or GST as a negative control in TBSTB for 30 minutes and subjected to three washes in TBST, each lasting three minutes. Next, bound protein was transferred to a new nitrocellulose membrane at 30V for one hour via

wet transfer, and this membrane was blocked in TBSTB for 30 minutes, incubated with HRP conjugated anti-GST antibody (Cytiva RPN1236) at a 1:5,000 dilution, washed with TBST three times for three minutes, exposed to high sensitivity enhanced chemiluminescent substrate (Thermo 34094) and imaged via chemiluminescence (Azure Biosystems Imager).

Fluorescence anisotropy.

Fluorescently labeled (AF Dye-488-TFP ester) and unlabeled peptides were synthesized and HPLC purified by the MIT Biopolymers Laboratory. The peptide sequences used were as follows:

Label	Sequence
ATG4B	*EDED <u>FEILSL</u>
ATG9	*RDTQKLFTSSNAIHHDKDK
SFQVI	*TKAPKAMTPSRIAD <u>SFQVI</u>
SAQVI	*TKAPKAMTPSRIAD <u>SAQVI</u>
FAECV	*NEPCT <u>SFAECV</u> CDENCEKEA
AAECV	*NEPCT <u>SAAECV</u> CDENCEKEA
* marks location of AF Dye 488	

For competitive fluorescence anisotropy assays, 1.5 μ M mGATE16 was mixed with 10nM labeled ATG4B peptide in a buffer FA (20mM Tris, 150mM NaCl, pH 7.5) at room temperature. Increasing concentrations of the relevant unlabeled peptide were added to individual aliquots of mGATE16 complexed to the labeled ATG4B peptide and incubated

for 20 minutes at room temperature. The emission for each 120 μ L sample at 520nm (excitation at 485nm) for both horizontally (I_{VH}) and vertically (I_{VV}) polarized signal, along with a G_{factor} , was measured on a Photon Technology International (PTI) fluorimeter in a quartz cuvette. From these measurements, an anisotropy value r was calculated by the PTI software as $(I_{VV} * G_{factor} - I_{VH}) / (I_{VV} + 2 * G_{factor} * I_{VH})$. ATG9 peptide was used as a negative control as this should not bind to the LDS of GATE16 (Nishimura & Tooze, 2020).

For fluorescence anisotropy assays to measure affinity, 10nM labeled ATG4B peptide was added to individual aliquots of increasing concentrations of His₆-GATE16 in buffer FA. After the peptide was incubated with His₆-GATE16 for 20 minutes at room temperature, the horizontally and vertically polarized fluorescence emission at 520nm, along with a G_{Factor} , was measured as stated above. These same measurements were also taken for all His₆-GATE16 concentrations as background without labeled peptide. Parallel and perpendicular emission signal intensities for His₆-GATE16 alone were subtracted from that of His₆-GATE16 with labeled peptide for each concentration before calculating an anisotropy value r . A curve of anisotropy as a function of His₆-GATE16 concentration was fit in Graphpad Prism to a binding isotherm to obtain a K_D .

Protein thermal stability shift assay.

NCOA4³⁸³⁻⁵²² constructs were diluted to 10 μ M in buffer FA and mixed 1:1000 (v/v) SYPRO Orange (Sigma-Aldrich S5692). Each construct was assayed in triplicate in a 384-well plate using an Applied Biosystems QuantStudio 5 Real-Time PCR System. A negative control consisting of SYPRO Orange in buffer was included in all assays. Melt curves for each sample were generated by tracking the fluorescence emission signal at 570nm (excitation at 470nm) as the samples were heated from 25°C to 95°C in 1°C

increments. Melting temperatures were calculated as the temperature corresponding to the maximum of the first derivative of the fluorescence signal.

Size exclusion chromatography coupled to multi-angle light scattering (SEC-MALS).

All SEC-MALS experiments were conducted using a Dawn 8 MALS with an in-line Optilab differential refractive index detector (Wyatt). For both NCOA4³⁸³⁻⁵²² and (GST-GATE16)₂, 100µL of 1mg/mL protein was injected onto an equilibrated WTC-030 HPLC SEC column in buffer FA at a flow rate of 0.5mL/min. The instrument was calibrated with a 2mg/mL BSA standard before each run. Data was analyzed with Astra software (Wyatt) to report apparent molecular weight.

Western blot assays of ferritinophagy *in vivo*.

Stably integrated NCOA4³⁸³⁻⁵²² cell lines were generated via retroviral transfection of the relevant NCOA4³⁸³⁻⁵²² construct in a CMV-enhancer bearing pMRX plasmid (Addgene 84573) into NCOA4Δ HeLa cells (a gift from Prof. M. Poli, University of Brescia, Italy) (Gryzik *et al.*, 2021). In this pMRX plasmid, EGFP was fused to the N-terminus of NCOA4³⁸³⁻⁵²² and its mutants with a 13 residue GS linker. HeLa cells were transfected and selected as described previously (Sena-Esteves & Gao, 2018).

WT HeLa (cl_JD066), NCOA4Δ (cl_JD065), NCOA4³⁸³⁻⁵²² (cl_JD074), ⁴¹³F:A (cl_JD075), and ⁴⁸⁶F:A (cl_JD076) cell lines were seeded in a 12-well cell culture plate in DMEM (Genesee Scientific) and incubated at 37°C, 5% CO₂. After 24 hours all media was aspirated and replaced with either DMEM or DMEM supplemented with 40µM ferric ammonium citrate (FAC). After an additional 24 hours all media was aspirated and

replaced with either DMEM or DMEM supplemented with 50 μ M deferoxamine (DFO). Following an additional 24-hour incubation, cells were trypsinized (200 μ L, 5min, 37°C), pelleted via centrifugation at 100g for one minute, resuspended in Dulbecco's PBS (Sigma Aldrich D8537), pelleted as above before undergoing flash freezing in liquid nitrogen and storage at -80°C.

Frozen cell pellets were resuspended in 100 μ L 4X Laemmli buffer with Halt protease and phosphatase inhibitor (Thermo Scientific 78440) and lysed with a 29-gauge syringe. Samples were mixed with 285mM dithiothreitol, boiled, and run on an SDS-PAGE gel before being transferred to a PVDF membrane (Invitrogen) using an iBlot2 transfer device (Invitrogen; 7min; 20V). Membranes were blocked overnight in TBSTB, incubated with rabbit anti-FTH1 antibody diluted 1:1,000 (Cell Signaling 3998S) or HRP conjugated anti-tubulin antibody diluted 1:20,000 (GeneTex GTX628802-01) as above. Anti-rabbit HRP conjugated secondary antibody (ABclonal AS014) was applied at a 1:1,000 dilution and washed, exposed to enhanced chemiluminescent substrate, and imaged as above. Ferritin levels were then measured by densitometry in FIJI (Schindelin *et al*, 2012) and normalized to tubulin intensity measured as above.

Fluorescence assays.

For colocalization assays, NCOA4³⁸³⁻⁵²² cell lines were seeded on glass coverslips in a 12-well cell culture plate in DMEM as above. After 24 hours, media was aspirated and replaced with DMEM supplemented with 50 μ M DFO, and cells were incubated an additional 24 hours. Cells were then fixed with 4% paraformaldehyde in PBS (150mM NaCl, 2.7mM KCl, 10mM Na₂HPO₄, 1.8mM KH₂PO₄, pH 8.0) for 15 minutes at room temperature, quenched with 100mM glycine in PBS for 10 minutes, and washed three

times with PBS. Cells were next permeabilized with 0.5% Triton X-100 in PBS for 10 minutes, washed once with PBS and blocked for 30 minutes in 2% BSA in PBS. Slides were next incubated in anti-GFP mouse antibody (Santa Cruz sc-9996) diluted 1:200, anti-LAMP1 rabbit antibody (Cell Signaling 9091T) diluted 1:200, and Hoechst stain (Invitrogen H3570) diluted 1:1,000, in 2% BSA in PBS for one hour. Following three 5-minute soaks in PBS, slides were incubated in Alexa Fluor 488 anti-mouse antibody (Thermo Fisher A-11001) diluted 1:200, and Alexa Fluor 568 anti-rabbit antibody (Thermo Fisher A-11036) diluted 1:200, for one hour. Slides were then soaked three times for 5 minutes in PBS, dried and mounted on slides with ProLong Gold mounting medium, set overnight, and sealed. Slides were imaged on a Dragonfly 505 spinning-disk confocal microscope with an iXon Ultra 888 EMCCD camera with the following settings: 60x objective pixel size (206 μ m*206 μ m), 40 μ m pin hole size, 0.5 μ m interval z stack slices, 405nm laser with 445/46 bandpass emission filter, 488nm laser with 521/38 bandpass filter and 561nm laser with 594/43 bandpass filter. A minimum of 100 cells were imaged per condition.

All image analysis was conducted in FIJI (Schindelin *et al*, 2012). To measure the area of overlap per cell, the best focused image from the z-stack was first manually chosen based on the nuclei in the 405nm channel. The in-focus image was then split into its respective green (NCOA4³⁸³⁻⁵²²) and pink (lysosome) channels before merging to a single RGB image. Images were viewed at fixed brightness and saturation when selecting regions of overlap (white). The overlapping regions were then measured and the area per nuclei recorded. The JACoP plugin for FIJI (Bolte & Cordelières, 2006) was used to estimate the fraction of lysosomes that colocalized with NCOA4³⁸³⁻⁵²². In brief, each z

stack was split into the respective channels, background subtracted with a rolling ball radius of 50 pixels and set to standard brightness values. For all images, threshold values were manually chosen for the pink and green channels, and the Manders' value, which calculates the fraction of pink signal that overlaps green signal, was recorded.

For LC3B puncta formation, WT HeLa or ATG7 Δ HeLa cells (gift from Dr. Terje Johansen, (Mejlvang *et al*, 2018)) were seeded on glass coverslips in a 12-well cell culture plate in DMEM. After 24 hours, media was aspirated and replaced with DMEM supplemented with 40 μ M FAC or regular DMEM, and cells were incubated an additional 24 hours. Media was then aspirated and replaced with DMEM supplemented with 50 μ M DFO with or without 400nM BafA or regular DMEM, and cells were incubated an additional 24 hours. Cells were then fixed and stained according to the above protocol using anti-LC3B primary antibody (Abcam EPR18709) and Alexa Fluor 568 anti-rabbit secondary antibody (Thermo Fisher A-11036). Slides were imaged on a Nikon Eclipse Ti2 inverted microscope at 60x objective pixel size using the RFP setting (50ms exposure, widefield fluorescence, 584nm emission).

NCOA4³⁸³⁻⁵²² iron chelation and reconstitution.

To obtain reconstituted NCOA4³⁸³⁻⁵²² sample, purified NCOA4³⁸³⁻⁵²² was diluted two-fold in buffer IC (20mM Tris, 150mM NaCl, 5mM DTT, pH 7.5, degassed and stored anaerobically) incubated with a 10-fold molar excess of ammonium iron (II) sulfate hexahydrate and sodium sulfide nonahydrate overnight at 20°C in an anaerobic glove box. Excess iron and sulfur were pelleted via centrifugation at 17,200g for 2mins and filtered using a centrifuge tube 0.22 μ m filter (Corning 8160) before loading onto an S200 10/300 increase size exclusion column run in buffer IC under anaerobic conditions.

Fractions eluting at ~0.57 column volumes were collected and concentrated with a 30kDa centricon for use in BLI.

To obtain chelated sample, purified NCOA4³⁸³⁻⁵²² was incubated with EDTA and potassium ferricyanide in molar ratios of 1:50 and 1:20 respectively for 30min at room temperature. This material was run over an S200 10/300 increase in buffer IC. Fractions eluting at ~0.57 column volumes were collected and concentrated for subsequent use in BLI.

Chelated and reconstituted NCOA4³⁸³⁻⁵²² were both tested in a ferene assay (Fish, 1988; Levitz *et al.*, 2022; McCarthy & Booker, 2018) to measure iron concentration. In brief, chelated and reconstituted NCOA4³⁸³⁻⁵²² samples were diluted to 2.5 μ M in buffer IC and iron (III) nitrate nonahydrate (Thermo 047282.AP) standards spanning 0 to 100 μ M were made in volumes of 100 μ L. Samples and standards were mixed with 100 μ L of Reagent A (156mM SDS, 113mM saturated sodium acetate) and 100 μ L of Reagent B (274mM ascorbic acid, 8mM sodium meta-bisulfite, 536mM saturated sodium acetate) and then incubated at 30°C for 15 minutes. 5 μ L of Reagent C (36mM ferene) was added before centrifuging samples at 21,130g for 5min. The absorbance at 592nm for 250 μ L of supernatant from each condition was then measured in a 96-well clear plate using a Molecular Devices plate reader. Three replicates of each protein sample were compared to a standard curve calculated from the standards to obtain an iron concentration.

ACKNOWLEDGMENTS

We thank Dante Avalos, Cathy Drennan, Michael Das, Allen Sanderlin and Gregory Dodge for helpful discussion, and the MIT Biophysical Instrumentation Facility and MIT Biopolymers Laboratory for supporting access to key instrumentation. This work was supported by NIH grants 5T32-GM007287, and NSF-CAREER grant 2046778, and the Whitehead Family.

AUTHOR CONTRIBUTIONS

AL and JHD conceived the work, designed and interpreted the experiments and wrote the manuscript. AL performed all experiments. The authors declare that they have no conflict of interest.

2.6 FIGURES

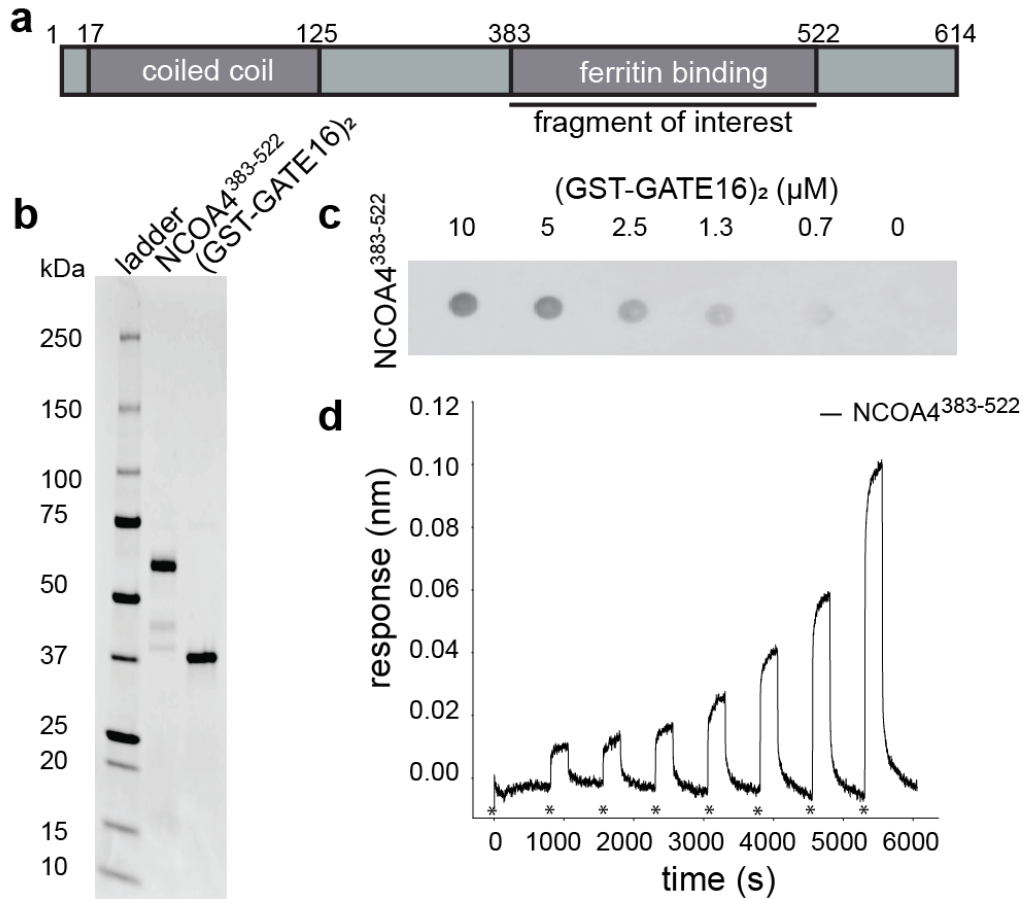


Figure 2.1: NCOA4³⁸³⁻⁵²² binds directly to (GST-GATE16)₂.

(a) Schematic of NCOA4 domain architecture. The fragment of interest (NCOA4³⁸³⁻⁵²²) used here is noted.

(b) SDS-PAGE gel of purified biotinylated AviTag-His₆-NCOA4³⁸³⁻⁵²²-MBP (NCOA4³⁸³⁻⁵²²) and (GST-GATE16)₂.

(c) Far-western of NCOA4³⁸³⁻⁵²² binding to decreasing concentrations of (GST-GATE16)₂ which was spotted on the membrane at indicated concentration. Signal was detected by HRP-conjugated streptavidin directed to soluble, Avi-tagged NCOA4³⁸³⁻⁵²², which was incubated on membrane at a concentration of 0.1 μM.

(d) Biolayer interferometry (BLI) trace of NCOA4³⁸³⁻⁵²² binding to (GST-GATE16)₂ where NCOA4³⁸³⁻⁵²² was immobilized to the probe and was incubated with increasing concentrations (0nM, 78nM, 156nM, 313nM, 625nM, 1.25 μM, 2.5 μM, 5 μM) of (GST-GATE16)₂. Initialization of each incubation noted by asterisks. Trace depicted is background corrected for binding of (GST-GATE16)₂ alone to the probe at each concentration.

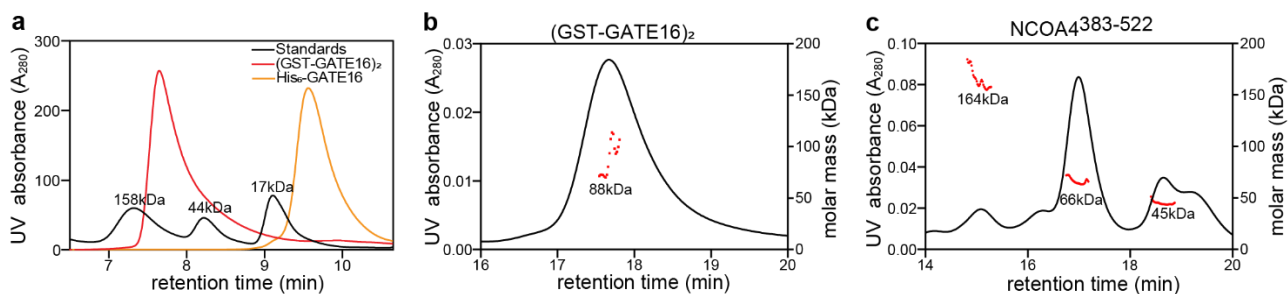


Figure 2.2: Oligomeric states of GATE16 and NCOA4³⁸³⁻⁵²² in solution.

(a) HPLC trace of (GST-GATE16)₂ and His₆-GATE16. Gel filtration standards annotated with molecular weight. Note a monomer of His₆-GATE16 is 15kDa in mass.

(b) SEC-MALS analysis of (GST-GATE16)₂. Black curve traces UV absorbance at 280nm. Red dots represent determined molar mass across the given peak. Measured mass of peak is 88±14kDa. Note a dimer of GST-GATE16 is 80kDa in mass.

(c) SEC-MALS analysis of NCOA4³⁸³⁻⁵²². Black curve and red dots as in (b). Measured masses from peaks left to right are 164±7.3kDa, 66.2±2.0kDa, 44.8±2.0kDa. Note a monomer of the biotinylated AviTag-His₆-NCOA4³⁸³⁻⁵²²-MBP construct used in all *in vitro* assays is 61kDa and isolated MBP is 40kDa in mass.

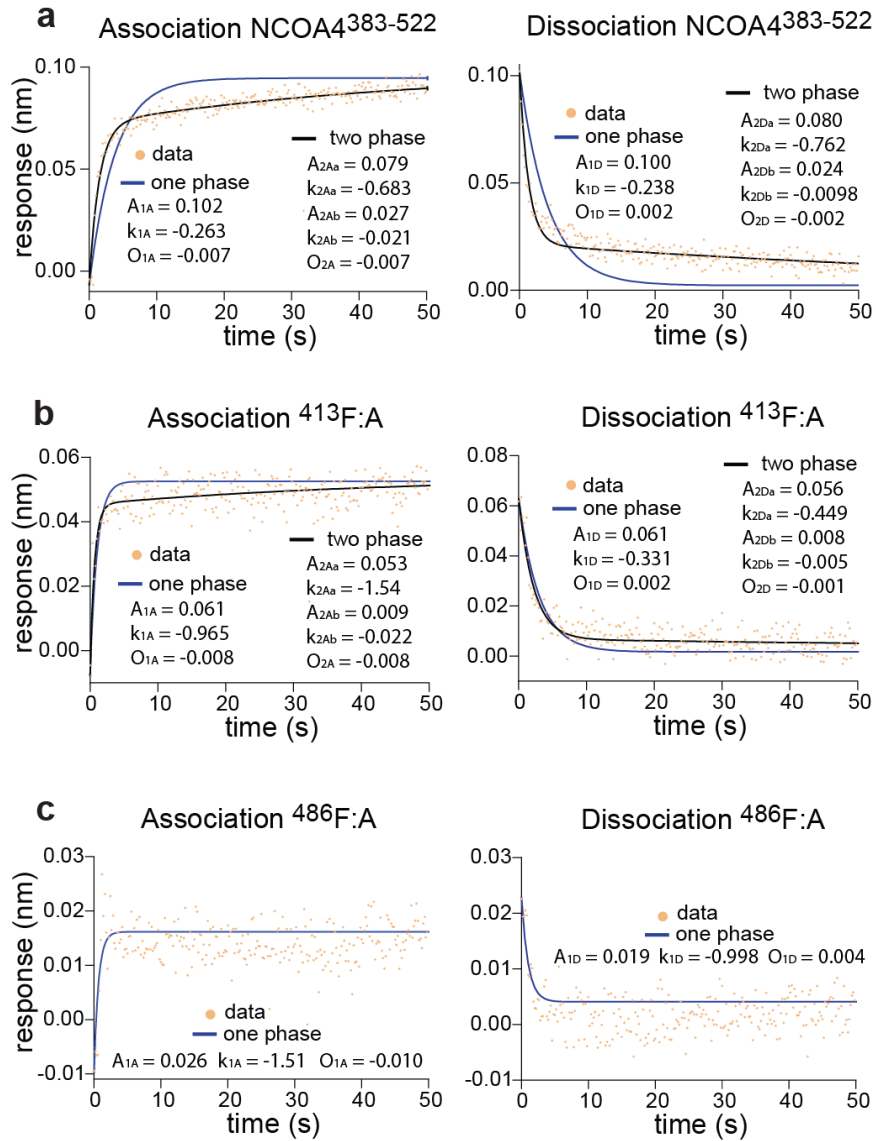


Figure 2.3: NCOA4³⁸³⁻⁵²² and (GST-GATE16)₂ binding kinetics measured by BLI.

(a) BLI association and dissociation curves of NCOA4³⁸³⁻⁵²² binding to 5μM (GST-GATE16)₂. BLI response data fit in Prism to one- and two-phase models as follows:

$$A_{1A}(1-e^{k_{1A}t})+O_{1A} \quad | \quad \text{one-phase association}$$

$$A_{1D}e^{k_{1D}t}+O_{1D} \quad | \quad \text{one-phase dissociation}$$

$$A_{2Aa}(1-e^{k_{2Aa}t})+A_{2Ab}(1-e^{k_{2Ab}t})+O_{2A} \quad | \quad \text{two-phase association}$$

$$A_{2Da}e^{k_{2Da}t}+A_{2Db}e^{k_{2Db}t}+O_{2D} \quad | \quad \text{two-phase dissociation}$$

(b) BLI response curves of ⁴¹³F:A binding fit as in (a).

(c) BLI response curves of ⁴⁸⁶F:A binding fit as in (a)

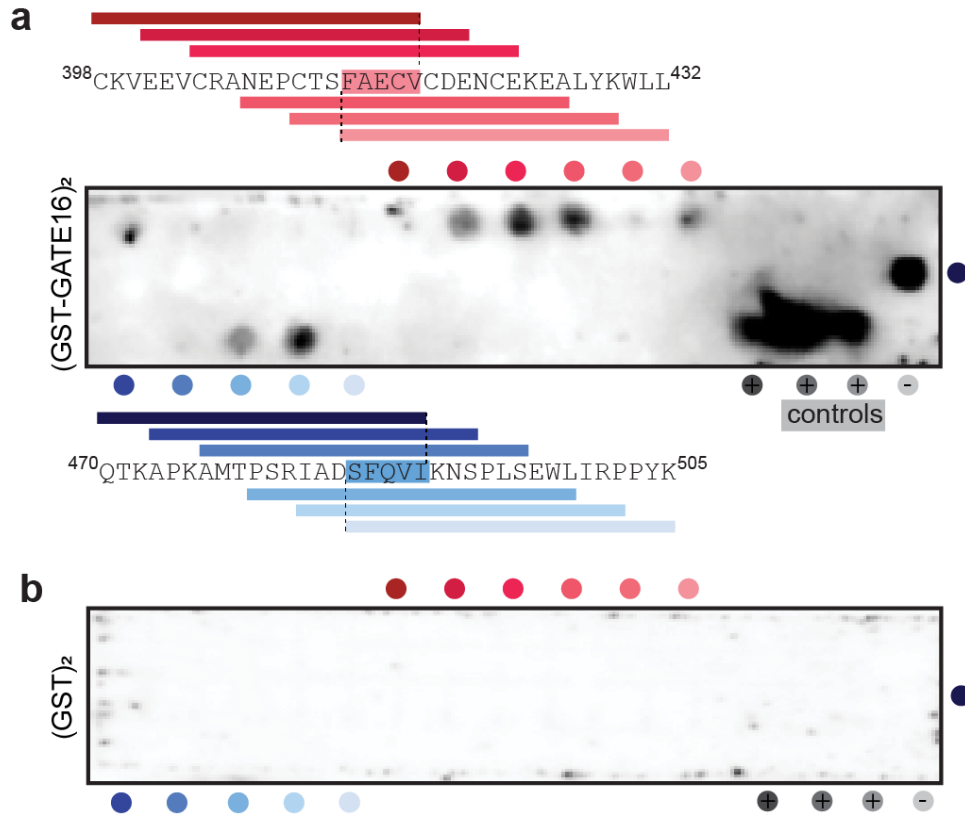


Figure 2.4: NCOA4³⁸³⁻⁵²² binding to (GST-GATE16)₂ via peptide array.

(a) Binding of (GST-GATE16)₂ to a peptide spot array composed of 20mers tiled across the NCOA4³⁸³⁻⁵²² sequence. (GST-GATE16)₂ binding detected using an HRP-conjugated anti-GST antibody. Sites of (GST-GATE16)₂ binding are indicated by colored dots adjacent to peptide array, with corresponding peptide sequence spans depicted. Positive control peptides arrayed left-to-right are noted with grey circles, and were derived from p62/SQSTM1 (SGGDDDWTHLSS), ATG4B (EDEDFEILSL), and FYCO1 (DDAVFDIITDEELCQIQE), with known LIR motif underlined. Negative control peptide noted by light grey circle corresponded to a poly-His peptide (HHHHHHGSSHHHHHHGSSH).

(b) Far-western as in (a), with GST replacing (GST-GATE16)₂.

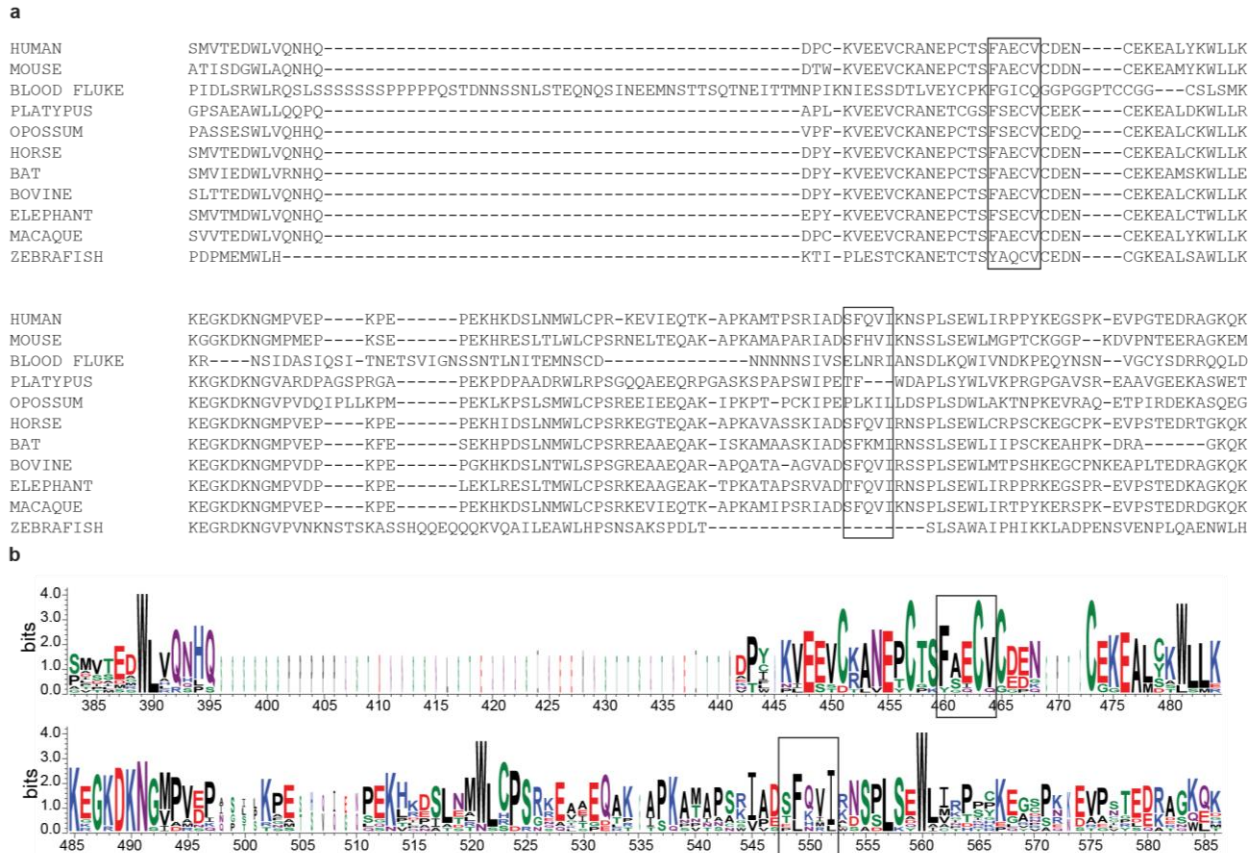


Figure 2.5: Sequence conservation of the two LIR-like motifs of NCOA4³⁸³⁻⁵²².

(a) Sequence alignment of human NCOA4³⁸³⁻⁵²² and orthologs. Identified LIR-like motifs are indicated with boxes.

(b) Sequence logo of the alignment in (a) generated by WebLogo 3.7.4 (Crooks et al., 2004). Motifs are indicated with boxes. Height at each position indicates overall sequence conservation at that position and height of individual letters at each position indicates relative frequency of the residue for that position. The width of each position is proportional to the number of aligned sequences at that position.

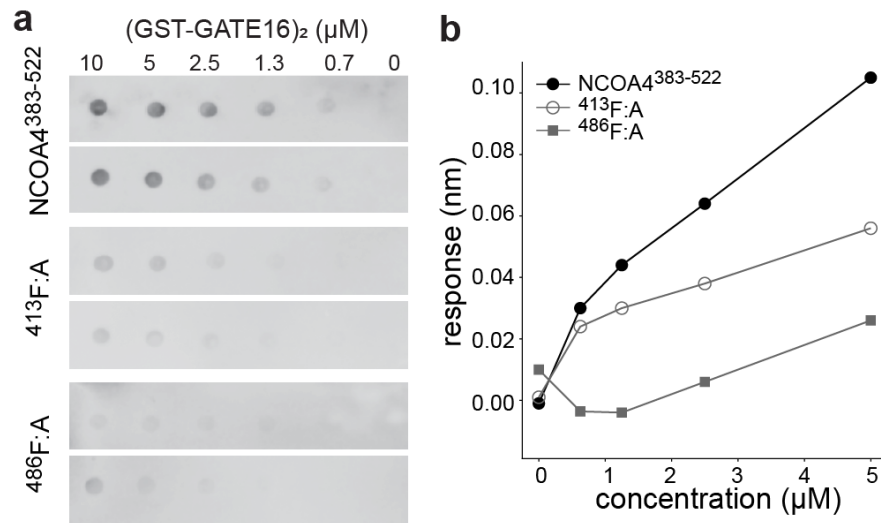


Figure 2.6: NCOA4³⁸³⁻⁵²² binds to (GST-GATE16)₂ through two LIR-like motifs

(a) Far-western of NCOA4³⁸³⁻⁵²² and NCOA4³⁸³⁻⁵²² motif mutants binding to (GST-GATE16)₂, which was spotted on membrane at indicated concentrations. Binding was detected using HRP-conjugated streptavidin directed to soluble, Avi-tagged NCOA4³⁸³⁻⁵²², which was incubated on membrane at a concentration of 0.1 μM. NCOA4³⁸³⁻⁵²² and motif mutants assayed in duplicate.

(b) BLI response curve of NCOA4³⁸³⁻⁵²² and motif mutants binding to (GST-GATE16)₂, where the NCOA4³⁸³⁻⁵²² construct was immobilized to the probe and tested against increasing concentrations (0nM, 625nM, 1.25 μM, 2.5 μM, 5 μM) of (GST-GATE16)₂. FAECV motif mutant noted as ⁴¹³F:A and SFQVI mutant labeled as ⁴⁸⁶F:A.

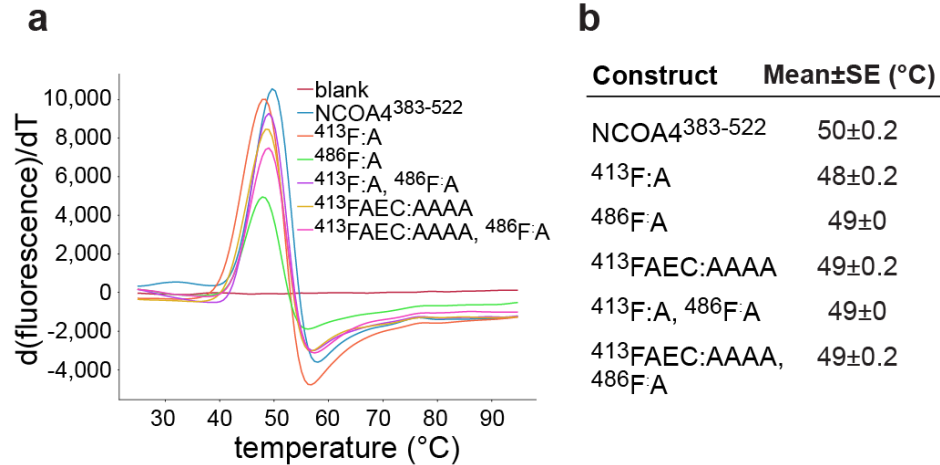


Figure 2.7: Impact of NCOA4³⁸³⁻⁵²² mutants on protein stability.

(a) Protein thermal shift assay melting curves plotting the first derivative of SYPRO Orange fluorescence emission as a function of temperature for NCOA4³⁸³⁻⁵²² and NCOA4³⁸³⁻⁵²² mutants (see Methods).

(b) Table of melting temperature for NCOA4³⁸³⁻⁵²² and NCOA4³⁸³⁻⁵²² mutants measured in (a). Mean and standard error of three replicates for each construct denoted.

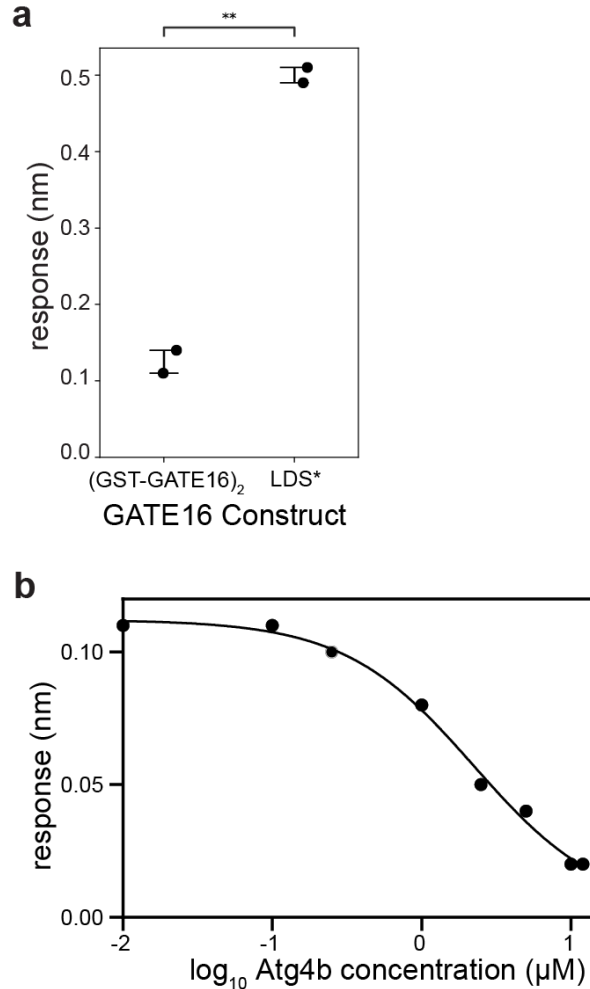


Figure 2.8: Contribution of LDS in NCOA4³⁸³⁻⁵²² binding to (GST-GATE16)₂.

(a) Quantification of NCOA4³⁸³⁻⁵²² binding to 5μM (GST-GATE16)₂ or ΔLDS (GST-GATE16)₂ as indicated. Each assayed in duplicate. Statistical significance calculated via independent t-test (ns:p<1, *:p<0.05, **p<0.01, ***p<0.001, ****p<0.0001).

(b) BLI response curve of NCOA4³⁸³⁻⁵²² binding to (GST-GATE16)₂ where NCOA4³⁸³⁻⁵²² construct is immobilized to the probe and tested against 5μM (GST-GATE16)₂ in the presence of increasing concentrations of ATG4B peptide (EDEDFEILSL) (10nM, 100nM, 250nM, 1μM, 2.5μM, 5μM, 10μM).

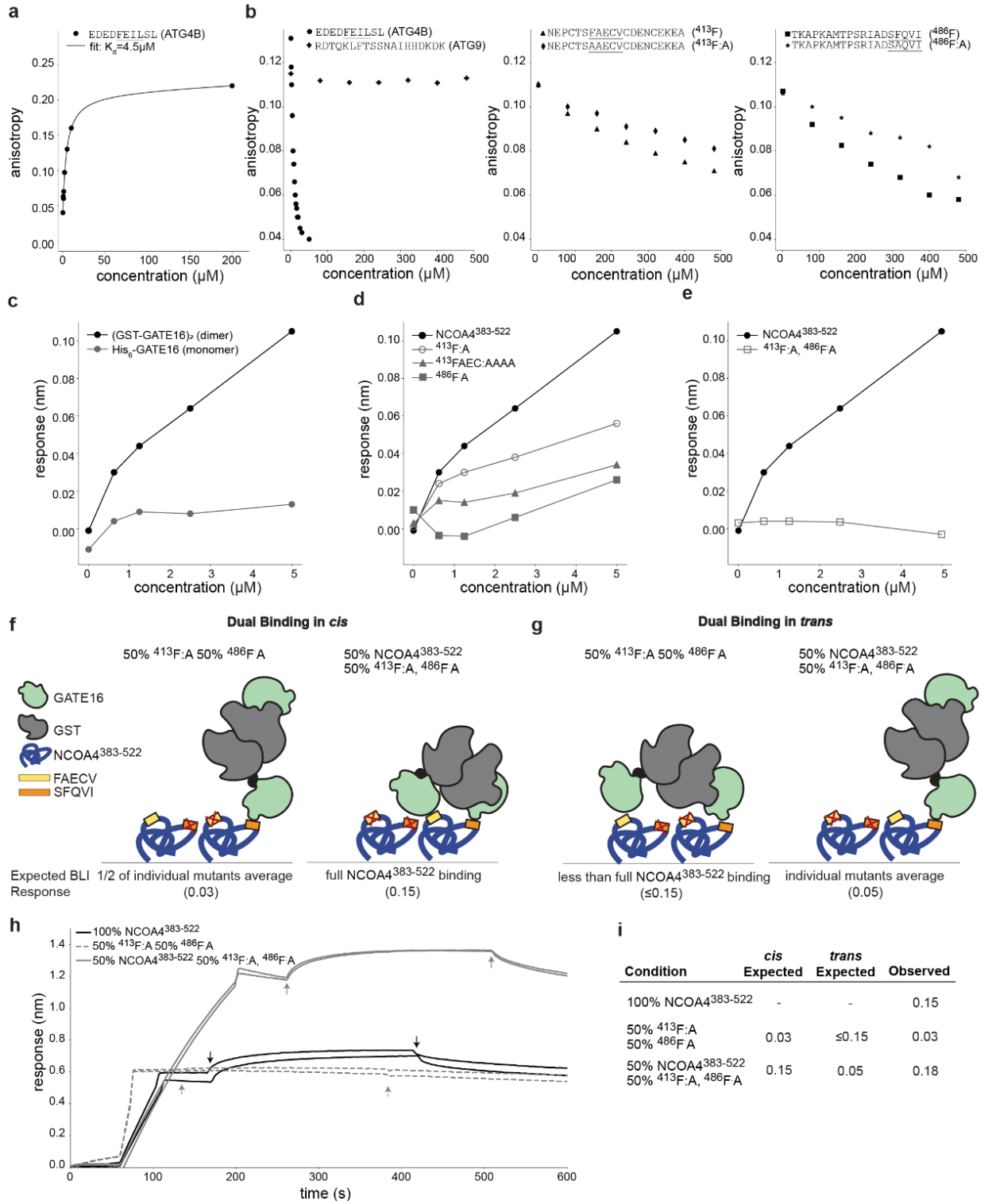


Figure 2.9: Binding of NCOA4³⁸³⁻⁵²² to (GST-GATE16)₂ requires avidity.

- (a)** Fluorescence anisotropy of dye-labeled peptide containing the ATG4B LIR binding to His₆-GATE16. Data fit to standard binding isotherm with apparent K_D noted.
- (b)** Competition fluorescence anisotropy assay of dye-labeled ATG4B LIR peptide competing for binding to monomeric GATE16 against increasing concentrations of unlabeled peptides derived from ATG4B, ATG9, NCOA4³⁸³⁻⁵²² or NCOA4³⁸³⁻⁵²² motif mutants, as noted.
- (c)** BLI response curve of NCOA4³⁸³⁻⁵²² binding to His₆-GATE16 or (GST-GATE16)₂ where NCOA4³⁸³⁻⁵²² construct is immobilized to the probe and tested against increasing concentrations (0nM, 625nM, 1.25μM, 2.5μM, 5μM) of either GATE16 construct.
- (d,e)** BLI assay of (GST-GATE16)₂ binding to noted NCOA4³⁸³⁻⁵²² constructs, probed at (GST-GATE16)₂ concentrations as described in (c).
- (f,g)** Schematic of hypothesized binding modes for (GST-GATE16)₂ binding in “*cis*” (f) or in “*trans*” (g) to NCOA4³⁸³⁻⁵²². BLI response expected for each model at the noted ratios of each protein construct detailed below schematic.
- (h)** BLI traces of assays performed as depicted in (f,g). Two replicates of each assay shown. Each assay used 5μM (GST-GATE16)₂.
- (i)** Expected responses for *cis* and *trans* models and quantification of response for BLI traces in (g).

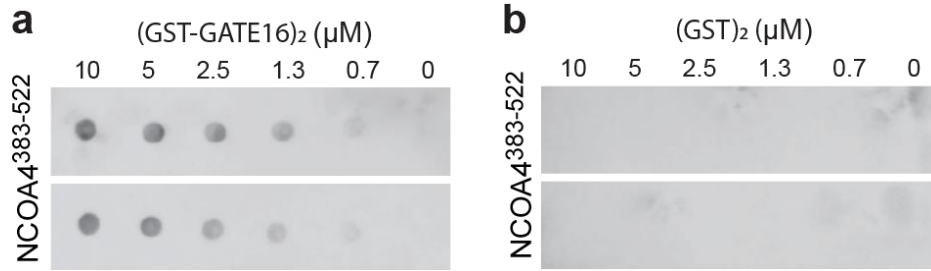


Figure 2.10: Assessment of nonspecific binding of NCOA4³⁸³⁻⁵²² to GST in far-westerns.

(a) Far-western of NCOA4³⁸³⁻⁵²² binding to (GST-GATE16)₂, which was spotted on membrane at indicated concentration. NCOA4³⁸³⁻⁵²² incubated on membrane at 0.1 μM. Signal detected by HRP conjugated streptavidin. Two replicates shown.

(b) Far-western as in (a), with GST replacing (GST-GATE16)₂.

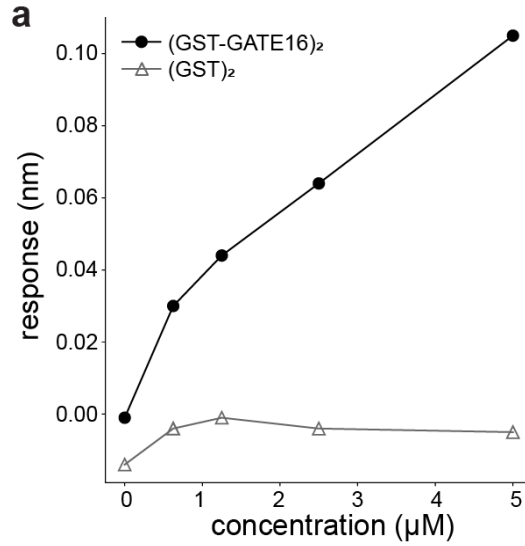


Figure 2.11: Assessing nonspecific association of NCOA4³⁸³⁻⁵²² to (GST)₂ in BLI.

(a) BLI response measurement of NCOA4³⁸³⁻⁵²² binding to (GST-GATE16)₂ and isolated (GST)₂ alone where NCOA4³⁸³⁻⁵²² construct was immobilized to the probe and tested against increasing concentrations (0nM, 625nM, 1.25μM, 2.5μM, 5μM) of either GST construct. Response height measured at each concentration.

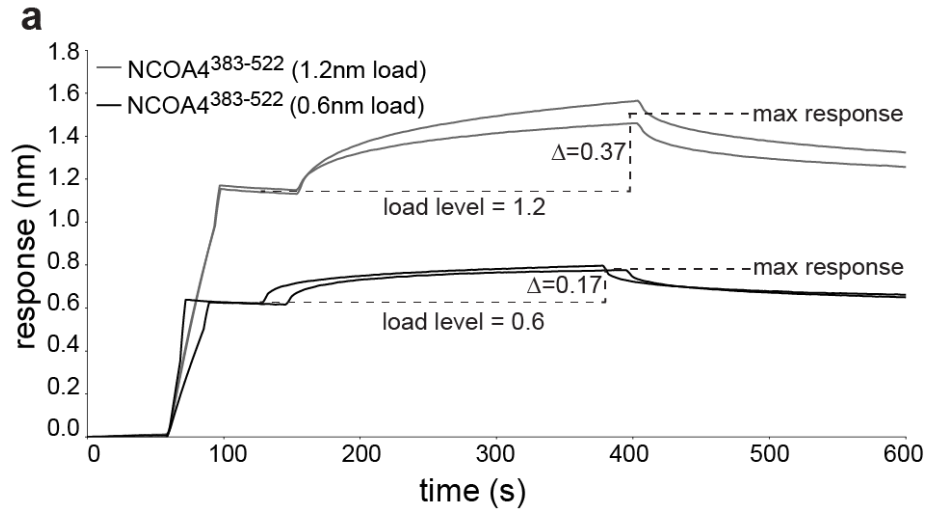
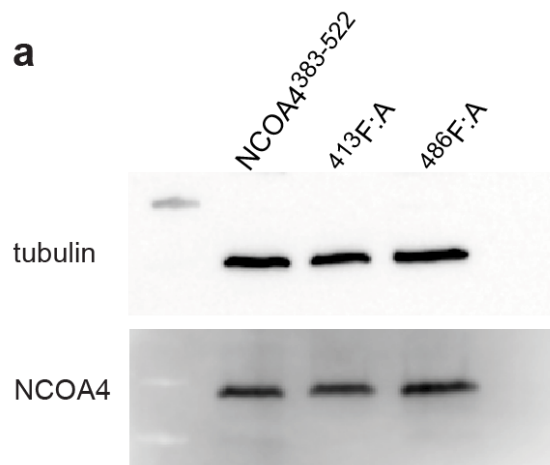


Figure 2.12: Load-dependent BLI response.

(a) BLI association and dissociation curves of NCOA4³⁸³⁻⁵²² binding to 5 μ M (GST-GATE16)₂ where NCOA4³⁸³⁻⁵²² construct is immobilized to the probe. Replicates at NCOA4³⁸³⁻⁵²² loading levels of 0.6 nm and 1.2 nm shown. Average BLI response across replicates denoted as difference (Δ) of max response and load level.



b

Cell Line	Relative NCOA4 Abundance
NCOA4 ³⁸³⁻⁵²²	1
413F:A	1.2
486F:A	1.2

Figure 2.13: Cellular levels of NCOA4³⁸³⁻⁵²² and associated mutants.

(a) Western blot assessing levels of NCOA4³⁸³⁻⁵²², 413F:A, and 486F:A expressed under steady-state conditions in HeLa cell lines. NCOA4 levels probed using an anti-GFP antibody against the GFP-fused NCOA4. Tubulin levels also probed by Western to assess relative sample loading.

(b) Table reporting NCOA4 abundance of each mutant relative to NCOA4³⁸³⁻⁵²² as measured in (a). In each instance, levels were normalized using the tubulin loading control.

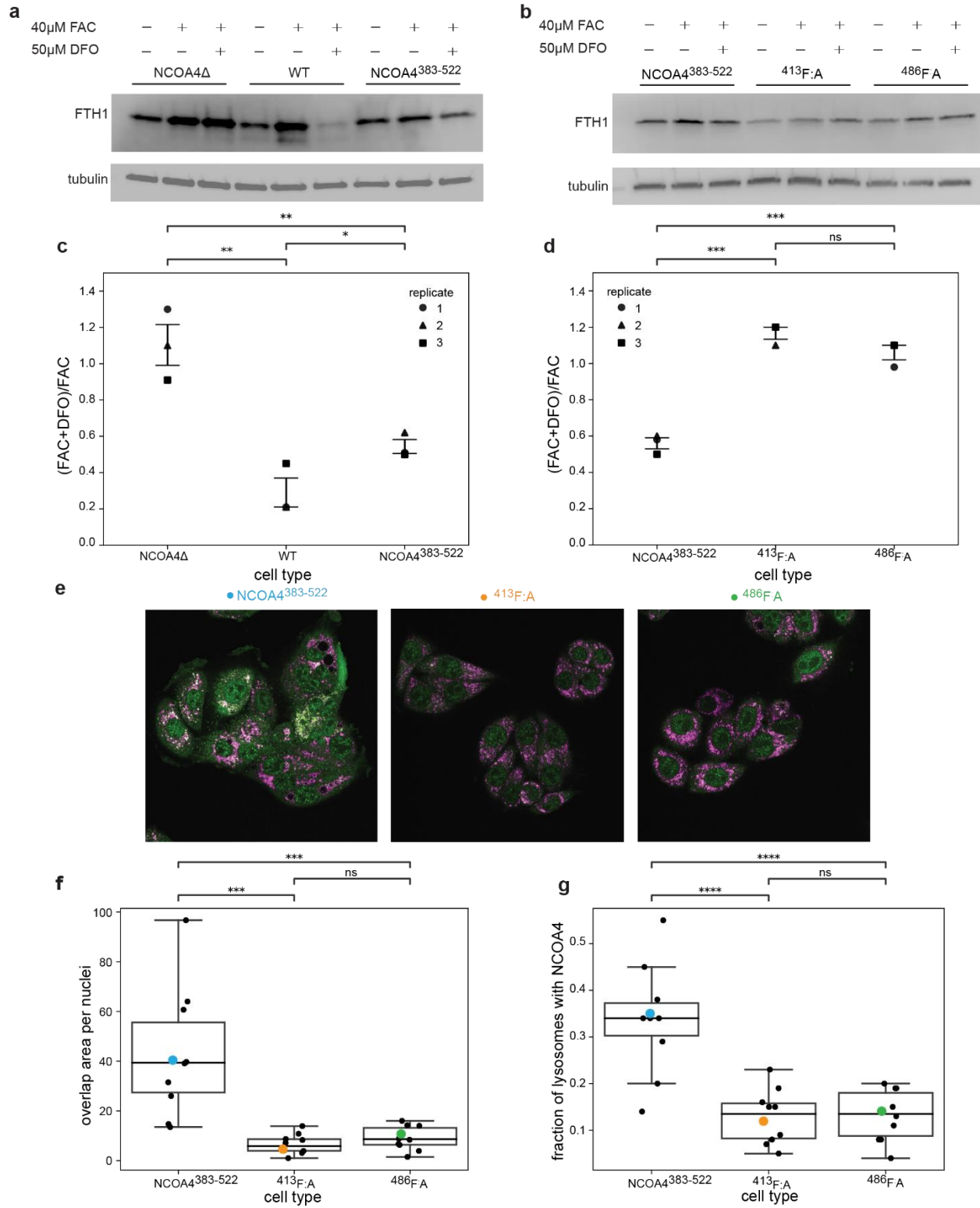


Figure 2.14: NCOA4³⁸³⁻⁵²² supports ferritin degradation *in vivo* and requires both LIR-like motifs.

(a) Western blots against ferritin heavy chain (FTH1) and tubulin in NCOA4Δ, WT and NCOA4³⁸³⁻⁵²² cell lines. Cells either untreated, treated for 24 hours with ferric ammonium citrate (FAC), or treated with FAC before undergoing a 24-hour treatment with deferoxamine (DFO).

(b) Western blots as described in (a) in either NCOA4³⁸³⁻⁵²², ⁴¹³F:A, or ⁴⁸⁶F:A cell lines.

(c,d) Quantification of triplicate ferritin degradation assays described in (a-b). Bars denote standard error of the mean. Fraction ferritin degraded calculated in FIJI (Schindelin et al., 2012) using condition-dependent band intensities as follows:

$$\frac{((\text{FAC}+\text{DFO})_{\text{FTH1}})/(\text{FAC}+\text{DFO})_{\text{tubulin}}}{(\text{FAC}_{\text{FTH1}}/\text{FAC}_{\text{tubulin}})}$$

Statistical significance calculated via independent t-test (ns:p<1, *:p<0.05, **:p<0.01, ***p<0.001, ****p<0.0001).

(e) Representative images probing for colocalization of GFP- NCOA4³⁸³⁻⁵²² and lysosomes in NCOA4³⁸³⁻⁵²², ⁴¹³F:A, or ⁴⁸⁶F:A cell lines treated with 50μM DFO. Anti-GFP signal shown in green and anti-LAMP1 signal shown in pink. Overlapping areas are white.

(f) Boxplot of colocalization assay described in (e), with colocalization quantified as a function of area of overlap per nuclei. Black dots represent individual images, with colored dots corresponding to images in (e). Significance calculated via independent t-test (ns:p<1, *:p<0.05, **p<0.01, ***p<0.001, ****p<0.0001).

(g) Boxplot of colocalization assay described in (e), with colocalization quantified as a function of fraction of lysosomes containing NCOA4³⁸³⁻⁵²². Values calculated as Manders' coefficients in FIJI. Black dots represent individual images, with colored dots corresponding to images in (e). Significance calculated via independent t-test (ns:p<1, *:p<0.05, **p<0.01, ***p<0.001, ****p<0.0001).

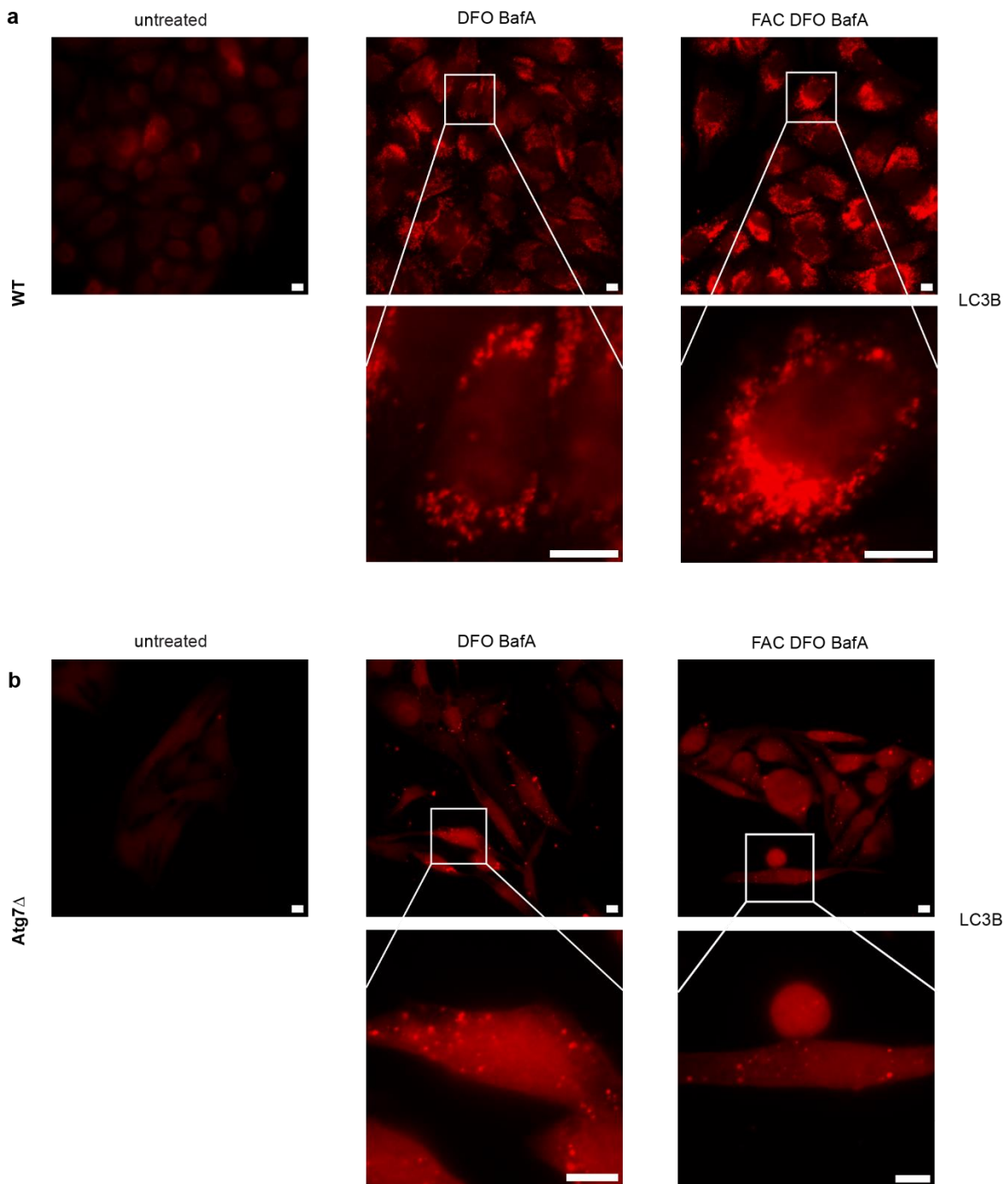


Figure 2.15: LC3B can form puncta independent of ATG7 in ferritinophagy inducing conditions.

(a) Representative images for WT HeLa cells untreated, treated with 40 μ M FAC, 50 μ M DFO, or 400nM BafA as indicated (see Methods). Anti-LC3B signal shown in red. 10 μ m scale bar in white in full image and enlarged inset.

(b) Images as described in (a) for *ATG7* Δ HeLa cells.

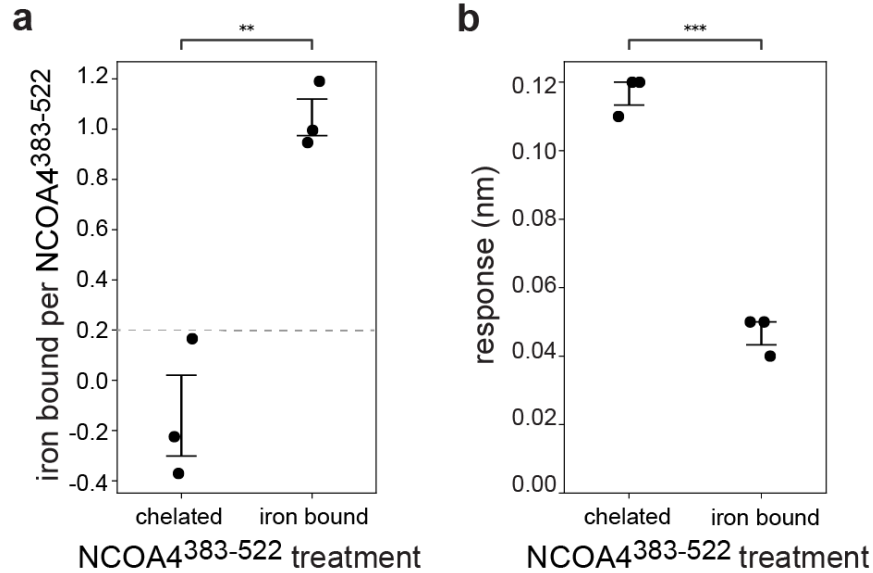


Figure 2.16: NCOA4³⁸³⁻⁵²²•(GST-GATE16)₂ binding is iron dependent.

(a) Quantification of iron bound per monomer of NCOA4³⁸³⁻⁵²² for chelated and reconstituted (iron bound) NCOA4³⁸³⁻⁵²² as measured in a ferene assay (Fish, 1988; Levitz et al., 2022; McCarthy & Booker, 2018). Each sample assayed in triplicate, and lower limit of detection noted with dashed line. Statistical significance calculated via independent t-test (ns:p<1, *:p<0.05, **p<0.01, ***p<0.001, ****p<0.0001).

(b) Quantification of chelated and iron bound NCOA4³⁸³⁻⁵²² binding to 10μM (GST-GATE16)₂ represented as response change in BLI. Each sample assayed in triplicate. Statistical significance calculated via independent t-test as in (a).

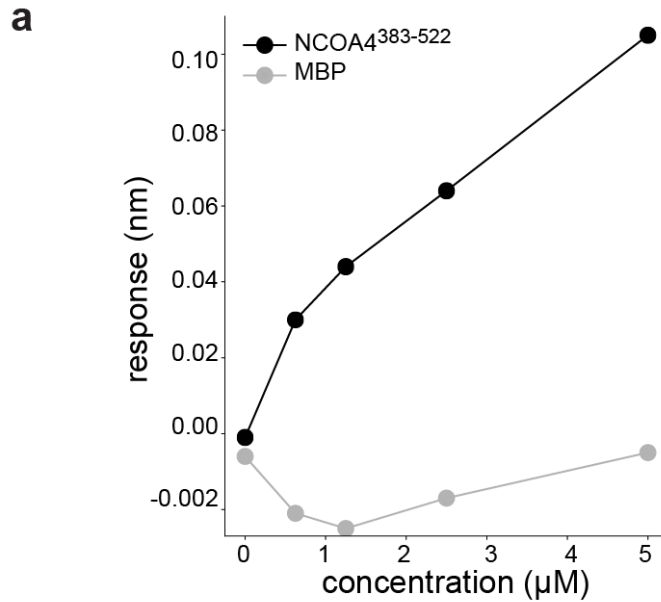


Figure 2.17: Assessing nonspecific association of MBP to (GST-GATE16)₂ in BLI.

(a) BLI response measurement of NCOA4³⁸³⁻⁵²² or MBP binding to (GST-GATE16)₂ where NCOA4³⁸³⁻⁵²² or MBP was immobilized to the probe and tested against increasing concentrations (0nM, 625nM, 1.25μM, 2.5μM, 5μM) of (GST-GATE16)₂. Response height measured at each concentration.

2.7 REFERENCES

- Arosio P, Ingrassia R, Cavadini P (2009) Ferritins: a family of molecules for iron storage, antioxidation and more. *Biochim Biophys Acta* 1790: 589-599
- Beck M, Schmidt A, Malmstroem J, Claassen M, Ori A, Szymborska A, Herzog F, Rinner O, Ellenberg J, Aebersold R (2011) The quantitative proteome of a human cell line. *Mol Syst Biol* 7: 549
- Birgisdottir AB, Lamark T, Johansen T (2013) The LIR motif - crucial for selective autophagy. *J Cell Sci* 126: 3237-3247
- Bolte S, Cordelières FP (2006) A guided tour into subcellular colocalization analysis in light microscopy. *J Microsc* 224: 213-232
- Chatzichristofi A, Sagris V, Pallaris A, Eftychiou M, Kalvari I, Price N, Theodosiou T, Iliopoulos I, Nezis IP, Promponas VJ (2023) LIRcentral: a manually curated online database of experimentally validated functional LIR motifs. *Autophagy* 19: 3189-3200
- Dowdle WE, Nyfeler B, Nagel J, Elling RA, Liu S, Triantafellow E, Menon S, Wang Z, Honda A, Pardee G *et al* (2014) Selective VPS34 inhibitor blocks autophagy and uncovers a role for NCOA4 in ferritin degradation and iron homeostasis in vivo. *Nat Cell Biol* 16: 1069-1079
- Errington WJ, Bruncsics B, Sarkar CA (2019) Mechanisms of noncanonical binding dynamics in multivalent protein–protein interactions. *Proceedings of the National Academy of Sciences* 116: 25659 - 25667
- Farnung J, Muhar M, Liang JR, Tolmachova KA, Benoit RM, Corn JE, Bode JW (2023) Semisynthetic LC3 Probes for Autophagy Pathways Reveal a Noncanonical LC3 Interacting Region Motif Crucial for the Enzymatic Activity of Human ATG3. *ACS Cent Sci* 9: 1025-1034
- Fish WW (1988) Rapid colorimetric micromethod for the quantitation of complexed iron in biological samples. *Methods Enzymol* 158: 357-364
- Fujioka Y, Alam JM, Noshiro D, Mouri K, Ando T, Okada Y, May AI, Knorr RL, Suzuki K, Ohsumi Y, Noda NN (2020) Phase separation organizes the site of autophagosome formation. *Nature* 578: 301-305
- Goodwin JM, Dowdle WE, DeJesus R, Wang Z, Bergman P, Kobylarz M, Lindeman A, Xavier RJ, McAllister G, Nyfeler B *et al* (2017) Autophagy-Independent Lysosomal Targeting Regulated by ULK1/2-FIP200 and ATG9. *Cell Rep* 20: 2341-2356

- Gryzik M, Asperti M, Denardo A, Arosio P, Poli M (2021) NCOA4-mediated ferritinophagy promotes ferroptosis induced by erastin, but not by RSL3 in HeLa cells. *Biochim Biophys Acta Mol Cell Res* 1868: 118913
- Gryzik M, Srivastava A, Longhi G, Bertuzzi M, Gianoncelli A, Carmona F, Poli M, Arosio P (2017) Expression and characterization of the ferritin binding domain of Nuclear Receptor Coactivator-4 (NCOA4). *Biochim Biophys Acta Gen Subj* 1861: 2710-2716
- Hoelzgen F, Nguyen TTP, Klukin E, Boumaiza M, Srivastava AK, Kim EY, Zalk R, Shahar A, Cohen-Schwartz S, Meyron-Holtz EG *et al* (2024) Structural basis for the intracellular regulation of ferritin degradation. *Nat Commun* 15: 3802
- Huang Q, Szklarczyk D, Wang M, Simonovic M, von Mering C (2023) PaxDb 5.0: Curated Protein Quantification Data Suggests Adaptive Proteome Changes in Yeasts. *Mol Cell Proteomics* 22: 100640
- Johansen T, Lamark T (2020) Selective Autophagy: ATG8 Family Proteins, LIR Motifs and Cargo Receptors. *J Mol Biol* 432: 80-103
- Kabaya Y, Mizushima N, Yamamoto A, Oshitani-Okamoto S, Ohsumi Y, Yoshimori T (2004) LC3, GABARAP and GATE16 localize to autophagosomal membrane depending on form-II formation. *J Cell Sci* 117: 2805-2812
- Keown JR, Black MM, Ferron A, Yap M, Barnett MJ, Pearce FG, Stoye JP, Goldstone DC (2018) A helical LC3-interacting region mediates the interaction between the retroviral restriction factor Trim5alpha and mammalian autophagy-related ATG8 proteins. *J Biol Chem* 293: 18378-18386
- Knaevelsrud H, Soreng K, Raiborg C, Haberg K, Rasmuson F, Brech A, Liestol K, Rusten TE, Stenmark H, Neufeld TP *et al* (2013) Membrane remodeling by the PX-BAR protein SNX18 promotes autophagosome formation. *J Cell Biol* 202: 331-349
- Kraft LJ, Nguyen TA, Vogel SS, Kenworthy AK (2014) Size, stoichiometry, and organization of soluble LC3-associated complexes. *Autophagy* 10: 861-877
- Kuno S, Fujita H, Tanaka YK, Ogra Y, Iwai K (2022) Iron-induced NCOA4 condensation regulates ferritin fate and iron homeostasis. *EMBO Rep* 23: e54278
- Lee YK, Lee JA (2016) Role of the mammalian ATG8/LC3 family in autophagy: differential and compensatory roles in the spatiotemporal regulation of autophagy. *BMB Rep* 49: 424-430
- Levitz TS, Brignole EJ, Fong I, Darrow MC, Drennan CL (2022) Effects of chameleon dispense-to-plunge speed on particle concentration, complex formation, and final resolution: A case study using the *Neisseria gonorrhoeae* ribonucleotide reductase inactive complex. *J Struct Biol* 214: 107825

Lluís Garcés J, Rey-Castro C, David C, Madurga S, Mas F, Pastor I, Puy J (2009) Model-Independent Link between the Macroscopic and Microscopic Descriptions of Multidentate Macromolecular Binding: Relationship between Stepwise, Intrinsic, and Microscopic Equilibrium Constants. *The Journal of Physical Chemistry B* 113: 15145-15155

Mancias JD, Pontano Vaites L, Nissim S, Biancur DE, Kim AJ, Wang X, Liu Y, Goessling W, Kimmelman AC, Harper JW (2015) Ferritinophagy via NCOA4 is required for erythropoiesis and is regulated by iron dependent HERC2-mediated proteolysis. *Elife* 4

Mancias JD, Wang X, Gygi SP, Harper JW, Kimmelman AC (2014) Quantitative proteomics identifies NCOA4 as the cargo receptor mediating ferritinophagy. *Nature* 509: 105-109

McCarthy EL, Booker SJ (2018) Biochemical Approaches for Understanding Iron-Sulfur Cluster Regeneration in Escherichia coli Lipoyl Synthase During Catalysis. *Methods Enzymol* 606: 217-239

Mejlvang J, Olsvik H, Svenning S, Bruun J-A, Abudu YP, Larsen KB, Brech A, Hansen TE, Brenne H, Hansen T *et al* (2018) Starvation induces rapid degradation of selective autophagy receptors by endosomal microautophagy. *Journal of Cell Biology* 217: 3640-3655

Nagano N, Ota M, Nishikawa K (1999) Strong hydrophobic nature of cysteine residues in proteins. *FEBS Lett* 458: 69-71

Nishimura T, Tooze SA (2020) Emerging roles of ATG proteins and membrane lipids in autophagosome formation. *Cell Discovery* 6: 32

Ohshima T, Yamamoto H, Sakamaki Y, Saito C, Mizushima N (2022) NCOA4 drives ferritin phase separation to facilitate macroferritinophagy and microferritinophagy. *J Cell Biol* 221

Olsvik HL, Lamark T, Takagi K, Larsen KB, Evjen G, Øvervatn A, Mizushima T, Johansen T (2015) FYCO1 Contains a C-terminally Extended, LC3A/B-preferring LC3-interacting Region (LIR) Motif Required for Efficient Maturation of Autophagosomes during Basal Autophagy. *J Biol Chem* 290: 29361-29374

Pankiv S, Clausen TH, Lamark T, Brech A, Bruun JA, Outzen H, Øvervatn A, Bjørkøy G, Johansen T (2007) p62/SQSTM1 binds directly to Atg8/LC3 to facilitate degradation of ubiquitinated protein aggregates by autophagy. *J Biol Chem* 282: 24131-24145

- Runwal G, Stamatakou E, Siddiqi FH, Puri C, Zhu Y, Rubinsztein DC (2019) LC3-positive structures are prominent in autophagy-deficient cells. *Scientific Reports* 9: 10147
- Sawa-Makarska J, Abert C, Romanov J, Zens B, Ibiricu I, Martens S (2014) Cargo binding to Atg19 unmasks additional Atg8 binding sites to mediate membrane-cargo apposition during selective autophagy. *Nat Cell Biol* 16: 425-433
- Schindelin J, Arganda-Carreras I, Frise E, Kaynig V, Longair M, Pietzsch T, Preibisch S, Rueden C, Saalfeld S, Schmid B *et al* (2012) Fiji: an open-source platform for biological-image analysis. *Nat Methods* 9: 676-682
- Sena-Esteves M, Gao G (2018) Production of High-Titer Retrovirus and Lentivirus Vectors. *Cold Spring Harb Protoc* 2018
- Skytte Rasmussen M, Mouilleron S, Kumar Shrestha B, Wirth M, Lee R, Bowitz Larsen K, Abudu Princely Y, O'Reilly N, Sjøttem E, Tooze SA *et al* (2017) ATG4B contains a C-terminal LIR motif important for binding and efficient cleavage of mammalian orthologs of yeast Atg8. *Autophagy* 13: 834-853
- Sofic E, Riederer P, Heinsen H, Beckmann H, Reynolds GP, Hebenstreit G, Youdim MB (1988) Increased iron (III) and total iron content in post mortem substantia nigra of parkinsonian brain. *J Neural Transm* 74: 199-205
- Wang J, Pantopoulos K (2011) Regulation of cellular iron metabolism. *Biochem J* 434: 365-381
- Ward RJ, Zucca FA, Duyn JH, Crichton RR, Zecca L (2014) The role of iron in brain ageing and neurodegenerative disorders. *Lancet Neurol* 13: 1045-1060
- Wirth M, Zhang W, Razi M, Nyoni L, Joshi D, O'Reilly N, Johansen T, Tooze SA, Mouilleron S (2019) Molecular determinants regulating selective binding of autophagy adapters and receptors to ATG8 proteins. *Nature Communications* 10: 2055
- Wurzer B, Zaffagnini G, Fracchiolla D, Turco E, Abert C, Romanov J, Martens S (2015) Oligomerization of p62 allows for selection of ubiquitinated cargo and isolation membrane during selective autophagy. *Elife* 4: e08941
- Ying H, Shen X, Park B, Yue BY (2010) Posttranslational modifications, localization, and protein interactions of optineurin, the product of a glaucoma gene. *PLoS One* 5: e9168
- Zaffagnini G, Martens S (2016) Mechanisms of Selective Autophagy. *J Mol Biol* 428: 1714-1724

Zhang G, Wang Z, Du Z, Zhang H (2018) mTOR Regulates Phase Separation of PGL Granules to Modulate Their Autophagic Degradation. *Cell* 174: 1492-1506 e1422

Zhao H, Lu Y, Zhang J, Sun Z, Cheng C, Liu Y, Wu L, Zhang M, He W, Hao S, Li K (2024) NCOA4 requires a [3Fe-4S] to sense and maintain the iron homeostasis. *J Biol Chem* 300: 105612

Chapter 3

A minimal fragment of the ferritinophagy receptor NCOA4 dismantles heavy ferritin cages

AUTHOR CONTRIBUTIONS

AL and JHD conceived the work, designed and interpreted the experiments. AL performed all experiments. AL wrote following text with editorial support from JHD. Upon completion of a set of additional experiments, we expect portions of this work will be submitted for publication, with AL and JHD as authors.

3.1 ABSTRACT

Regulation of iron levels in mammalian cells is critical for proper cellular function and survival. As such, cells tightly control the concentration of free, usable reduced iron (Fe^{2+}) by storing excess iron in an oxidized form (Fe^{3+}) in a large, proteinaceous cage called ferritin. In iron-limiting conditions, these cages can be degraded, thereby releasing iron into the cytosol, in an autophagic process that requires the selective autophagy receptor Nuclear Receptor Coactivator 4 (NCOA4). This receptor protein directly binds to ferritin and to core autophagy components. Here, we use a biochemically amenable fragment of NCOA4 (NCOA4³⁸³⁻⁵²²) to further interrogate the molecular details of the NCOA4•ferritin interaction via biochemical and biophysical techniques. *In vitro*, we observe an NCOA4³⁸³⁻⁵²²-dependent loss of heavy ferritin cages, in the absence of proteases, and propose a model in which NCOA4³⁸³⁻⁵²² directly dismantles ferritin cages, with this activity exhibiting a strong dependence on C-terminus of NCOA4³⁸³⁻⁵²². Our proposed cage dismantling model presents a potentially novel function for NCOA4, and would provide a mechanism by which cells could release iron directly into the cytosol.

3.2 INTRODUCTION

The regulation of iron availability and redox state is a vital process for mammalian cells. Iron is a critical cofactor for many enzymes, especially those involved in energy metabolism, but, when present in excess, can catalyze the formation of reactive oxygen species (ROS) via Fenton chemistry (Wang & Pantopoulos, 2011). These reactive oxygen species can lead to organelle and protein damage, ultimately resulting in cellular dysfunction. Given the critical yet potentially toxic nature of iron, cells have evolved a variety of mechanisms based on regulated uptake, export, and usage to tightly control the pool of free reduced iron (Fe^{2+}). Indeed, iron uptake is controlled by receptor mediated endocytosis of transferrin or it can be brought into the cell through transmembrane transporters (Lane *et al*, 2015). Conversely, iron can be incorporated into metabolic enzymes, often found in the mitochondria, or it can be exported via ferroportin (Lane *et al.*, 2015). Additionally, iron may be stored in the proteinaceous cage called ferritin.

Ferritin is a 24-mer protein comprised of heavy and light chains that can sequester up to 4,500 iron atoms as an oxidized mineral core (Arosio *et al*, 2017). The ferritin cage is highly symmetric and comprised of both three-fold hydrophilic and four-fold hydrophobic channels. The three-fold channels facilitate the entry of free reduced iron into the cage whereas the four-fold channels allow for proton transfer to balance overall charge as iron is oxidized, forming the ferrihydrite core (Zhang *et al*, 2021). This process of oxidation and sequestration minimizes excess ROS-forming reduced Fe^{2+} in the cytosol.

For cells to use iron stored in ferritin, it is commonly assumed that these highly stable ferritin cages must be degraded (Wang *et al*, 2017), with such degradation reported to occur via both the lysosome and the proteasome (De Domenico *et al*, 2009; Kwok &

Richardson, 2004; Zhang *et al*, 2010). As discussed in Chapters 1 and 2, the predominantly accepted mechanism by which ferritin is lysosomally degraded is called ferritinophagy, a type of selective autophagy. In this pathway, ferritin is recognized by the selective autophagy receptor Nuclear Receptor Coactivator 4 (NCOA4), which links the complex to an autophagosomal double membrane for subsequent engulfment, lysosomal fusion and degradation by hydrolases (Dikic, 2017; Mancias *et al*, 2014). Once ferritin is degraded in the lysosome, iron is released into the cytosolic pool.

Previous studies have shown that a minimal, biochemically amenable fragment of NCOA4, consisting of residues 383-522 (NCOA4³⁸³⁻⁵²², hereafter), is sufficient for binding to ferritin heavy chain (Hoelzgen *et al*, 2024; Mancias *et al*, 2015), with residues I489 and W497 of NCOA4 specifically required for ferritin binding (Mancias *et al.*, 2015). Isothermal titration calorimetry measurements are consistent with up to eight NCOA4³⁸³⁻⁵²² molecules binding per highly symmetric ferritin cage (Srivastava *et al*, 2020). However, NCOA4³⁸³⁻⁵²² is predicted to be largely disordered and, consistent with this prediction, a recent cryo-EM structure of NCOA4³⁸³⁻⁵²²•ferritin could only resolve the 16 amino acids of NCOA4³⁸³⁻⁵²² found at the NCOA4•ferritin binding interface (Hoelzgen *et al.*, 2024). Interestingly, NCOA4³⁸³⁻⁵²² has been reported to bind iron directly, which was shown to decrease NCOA4's affinity for ferritin (Zhao *et al*, 2024); the molecular mechanism by which such changes in ferritin affinity occur is unknown.

Here, we further investigate the NCOA4³⁸³⁻⁵²²•ferritin interaction, collecting data consistent with a novel cage dismantling activity in the NCOA4³⁸³⁻⁵²² fragment. Using a combination of analytical size exclusion chromatography (SEC), cryo-EM imaging and mass photometry we find that the addition of NCOA4³⁸³⁻⁵²² to heavy ferritin cages leads

to an apparent loss of ferritin cages, which by mass photometry appear to be dismantled into partial cages. With these preliminary data, we propose that NCOA4³⁸³⁻⁵²² can disassemble heavy ferritin cages, thereby proposing a new mechanism by which iron can be released directly into the cytosol.

3.3 RESULTS

NCOA4³⁸³⁻⁵²² binds specifically to ferritin heavy chain.

Despite high sequence and structural similarity between human ferritin's constituent light (hfL) and heavy (hfH) chains, NCOA4³⁸³⁻⁵²² was previously reported to bind specifically to hfH in both cell lysate co-immunoprecipitations (Dowdle *et al.*, 2014) and isothermal titration calorimetry experiments (Srivastava *et al.*, 2020). As ferritin cages can be composed exclusively of hfH, hfL, or a mixture of hfH and hfL, we hypothesized that when assessing binding of NCOA4 to ferritin cages, we could use hfL cages as an effective negative control. Thus, we sought to determine if, consistent with previous reports, our biochemically amenable NCOA4³⁸³⁻⁵²² (**Figure 3.1a**; MBP-NCOA4³⁸³⁻⁵²²-mNeon) construct also bound specifically to hfH, and we did so using a far-western assay to probe for NCOA4³⁸³⁻⁵²² binding to ferritin cages composed either hfH or hfL (**Figure 3.1b-c**). We found that NCOA4³⁸³⁻⁵²² bound to hfH in a concentration dependent manner, with no detectable binding to hfL, indicating that this fragment does in fact bind to hfH specifically and that the presence of additional tags did not impact this binding specificity.

Addition of NCOA4³⁸³⁻⁵²² causes a loss of hfH cages.

Having established that NCOA4³⁸³⁻⁵²² can bind specifically to hfH, we next sought to visualize the NCOA4³⁸³⁻⁵²²•hfH interaction interface by obtaining a co-structure of NCOA4³⁸³⁻⁵²² complexed to hfH cages. To do so, we first incubated pre-formed hfH₂₄ cages with an excess of His₆-NCOA4³⁸³⁻⁵²² and performed analytical size exclusion chromatography (SEC) on this solution, expecting to see the appearance of a larger molecular weight peak corresponding to the His₆-NCOA4³⁸³⁻⁵²²•hfH₂₄ cages. Surprisingly,

we instead observed a decrease in the intensity of the hfH₂₄ cage peak without any corresponding appearance of a larger His₆-NCOA4³⁸³⁻⁵²²•hfH₂₄ complex peak (**Figure 3.2a**). This pattern was also observed when His₆-NCOA4³⁸³⁻⁵²² was incubated with iron-loaded hfH₂₄ (Fe-hfH₂₄, hereafter) (**Figure 3.2b**). We next assessed whether this observed reduction in ferritin cage abundance was specific to the NCOA4³⁸³⁻⁵²²•hfH₂₄ interaction by conducting analytical SEC on His₆-NCOA4³⁸³⁻⁵²² incubated with hfL₂₄ cages. Interestingly, we did not observe a significant change in the peak intensity for the hfL₂₄ cages, suggesting that the loss of ferritin cages was dependent on the His₆-NCOA4³⁸³⁻⁵²²•hfH₂₄ interaction (**Figure 3.2c**). Ferritin cages composed of both heavy and light chains (hfHL) showed a subtle shift in chromatographic retention time, but also an overall loss of material (**Figure 3.2d**). Notably, the observed loss material in this assay was specific to the cage peak, as free ferritin subunits, which eluted at ~.85CV, were largely unaffected (**Figure 3.2e**).

To further interrogate the observed His₆-NCOA4³⁸³⁻⁵²²-dependent cage loss, and to visualize any changes to the hfH₂₄ cages, we attempted to probe the NCOA4³⁸³⁻⁵²²•hfH interaction using cryo-EM. Micrographs of hfH₂₄ or Fe-hfH₂₄ alone showed intact ferritin cages, with iron visible in the Fe-hfH₂₄ cages (**Figures 3.3a-b**). Strikingly, addition of NCOA4³⁸³⁻⁵²² caused a drastic decrease in the total number of cages present (**Figure 3.3c-d**). While this result is consistent with our analytical SEC observations and could be interpreted as an His₆-NCOA4³⁸³⁻⁵²²-dependent dismantling of ferritin cages, it is also possible that the NCOA4³⁸³⁻⁵²²•hfH material formed aggregates that were undetectable in cryo-EM micrographs due to denaturation at the air water interface or adhesion to the

grid's carbon supports; and that such higher order complexes adhered to an element of our chromatography apparatus, and were thus never observed.

NCOA4³⁸³⁻⁵²² disassembles hfH cages.

As described in these SEC-based and cryo-EM based assays, we observed a loss of ferritin cages, but did not detect the appearance of a smaller sized species – a clear prediction of any model involving cage dismantling. Given that such species could be outside the detection limits of these assays in size, contrast, homogeneity, or abundance, we tested the ability of mass photometry, which allows for sensitive detection of heterogeneous molecular weights in a solution, to detect such hypothesized species. Of note, these mass photometry assays were performed at concentrations ~1,000-fold more dilute than the analytical SEC and cryo-EM assays we performed. Consistent with our cryo-EM and SEC-based assays, incubation of His₆-NCOA4³⁸³⁻⁵²² with ferritin cages reduced the abundance of species with the approximate molecular mass of ferritin cages in hfH (510 kDa), Fe-hfH and hfHL (480 kDa) conditions, but not of cages composed of hfL (450 kDa) exclusively (**Figure 3.4a-d**). Critically, we newly observed the appearance of a lower molecular weight peak (~150 kDa) that was approximately the size of a ferritin chain octamer in the hfH, Fe hfH and hfHL conditions (**Figure 3.4a-b,d**). This result was consistent with a model in which His₆-NCOA4³⁸³⁻⁵²² acts to dismantle ferritin cages into constituent subunits, and does so in an hfH-dependent manner.

Cage dismantling ability of NCOA4³⁸³⁻⁵²² requires a free C-terminus.

Having observed that His₆-NCOA4³⁸³⁻⁵²² caused the disassembly of hfH₂₄ cages, we next wished to assess which region of NCOA4³⁸³⁻⁵²² was responsible for this activity. Of note, outside of its N-terminal coiled-coil domain, which is known to facilitate self-oligomerization (Mancias *et al.*, 2015), full length NCOA4 is predicted to be highly disordered (**Figure 3.5a**). To assess which region of NCOA4³⁸³⁻⁵²² contributed to the observed hfH₂₄ cage disassembly activity, we employed several NCOA4³⁸³⁻⁵²² constructs with a variety of bulky tags attached. Specifically, we compared the cage dismantling activity of a tagless NCOA4³⁸³⁻⁵²² (cNCOA4³⁸³⁻⁵²², hereafter) and His₆-NCOA4³⁸³⁻⁵²², a variant with sfGFP fused to the C-terminus (NCOA4³⁸³⁻⁵²²-sfGFP, hereafter) and dual termini tagged MBP-NCOA4³⁸³⁻⁵²²-mNeon (**Figure 3.5a**). To observe the effect of these tags on cage dismantling, we incubated hfH₂₄ with each of these NCOA4³⁸³⁻⁵²² constructs and analyzed the solution with SEC. We found that cNCOA4³⁸³⁻⁵²² and His₆-NCOA4³⁸³⁻⁵²² caused a loss of hfH₂₄ cage material, but introduction of a bulky tag at the C-terminus prevented this activity (**Figure 3.5b**). Accordingly, incubation with NCOA4³⁸³⁻⁵²²-sfGFP produced a higher molecular weight peak than hfH₂₄ alone, as did MBP-NCOA4³⁸³⁻⁵²²-mNeon, suggesting these C-terminally tagged NCOA4³⁸³⁻⁵²² constructs formed complexes with hfH₂₄ (**Figure 3.5b**). Thus, we reasoned that the cage dismantling activity is localized to the C-terminus of NCOA4³⁸³⁻⁵²², which raises the question of whether the endogenous C-terminus of NCOA4 (residues 523-614) support or suppress this activity.

3.4 DISCUSSION

Taken together, our biochemical studies of NCOA4³⁸³⁻⁵²² and ferritin suggest a novel function for selective autophagy receptor NCOA4³⁸³⁻⁵²². Here, consistent with prior work (Dowdle *et al.*, 2014; Srivastava *et al.*, 2020), we found that NCOA4³⁸³⁻⁵²² binds specifically to ferritin cages composed exclusively of hfH₂₄ and of mixtures of light and heavy chains, but not to cages bearing only light chains. Moreover, we observed a striking phenomenon wherein hfH₂₄ cages disappeared upon addition of NCOA4³⁸³⁻⁵²², as assayed by analytical size exclusion chromatography, cryo-EM and mass photometry assays. Notably, in our mass photometry-based assays, we observed the appearance of lower molecular weight species, consistent with the products of our proposed cage dismantling activity. Our analysis of a series of fusion constructs indicated that this observed dismantling activity was dependent on a free C-terminus of NCOA4³⁸³⁻⁵²². Overall, we these experiments led us to propose a preliminary model in which NCOA4³⁸³⁻⁵²² directly dismantles hfH₂₄ cages, and does so only when the C-terminus is not sterically occluded from interacting with ferritin cages by a globular protein domain, such as those found in our fusion constructs.

Interplay of NCOA4³⁸³⁻⁵²²-dependent cage dismantling and ferritinophagy.

As NCOA4 is typically accepted as the selective autophagy receptor for ferritinophagy, recognizing and targeting ferritin cages for lysosomal degradation, our proposed model of cage dismantling is seemingly contradictory to this canonical pathway (Mancias *et al.*, 2014). However, as we found that the disassembly of ferritin cages was inhibited by the fusion of a globular protein to the C-terminus of NCOA4³⁸³⁻⁵²², it is possible

that whether NCOA4 directs ferritinophagy or cage dismantles is dictated by the conformation of NCOA4. In conditions where the C-terminus is in a particular conformation, NCOA4 could facilitate canonical ferritinophagy through the lysosome, but when the C-terminus is in another conformation, NCOA4 could instead directly dismantle cages in the cytosol. If this hypothesis is true, one might speculate that post-translational modifications to NCOA4, or the binding of accessory proteins could regulate the availability of the C-terminus. For example, as I showed in Chapter 2 (Lee & Davis, 2024), the autophagosomal machinery proteins, LC3s, bind directly to NCOA4 to drive ferritinophagy. In doing so, they could induce an NCOA4 conformation that occludes the C-terminus and blocks this observed cage dismantling activity. Thus, the model we present here could act as another complementary pathway to the canonical ferritinophagy, further diversifying the variety of pathways have already been proposed (Dowdle *et al.*, 2014; Goodwin *et al.*, 2017; Kuno *et al.*, 2022; Mancias *et al.*, 2014; Ohshima *et al.*, 2022).

Proteasomal degradation of ferritin•NCOA4 fragments.

Whereas ferritinophagy proceeds through the lysosome by definition, previous studies have also observed proteasomal ferritin degradation (De Domenico *et al.*, 2009; Kwok & Richardson, 2004), and inhibition of autophagy has been shown to result in compensatory degradation of ferritin via the proteasome (De Domenico *et al.*, 2009). Furthermore, export of iron from the cell via ferroportin overexpression has been demonstrated to cause ferritin ubiquitination and subsequent degradation via the proteasome in the cytosol (De Domenico *et al.*, 2006). Despite these observations, the

exact mechanism by which proteasomal ferritin degradation occurs is unclear. The model of ferritin cage dismantling we present here may help elucidate this mechanism. In our model, the ferritin•NCOA4 fragments that result from NCOA4-dependent cage dismantling could be degraded via the proteasome following iron release. NCOA4 is known to be ubiquitinated by the E3 ligase HERC2, and if HERC2 more promiscuously targeted an NCOA4•ferritin complex, this observation could provide a plausible mechanism for the previously observed ferritin ubiquitination (Mancias *et al.*, 2015). Following this model, we propose that once released from ferritin, the oxidized iron (Fe^{3+}) would be reduced to usable iron (Fe^{2+}) by reductants present in the cytosol such as glutathione (Hamed *et al.*, 1983; Hider *et al.*, 2021). Notably, direct release of iron into the cytosol would seemingly allow for a less energy intensive cellular response to changing iron levels. Taken together, this proposed direct dismantling of ferritin cages by NCOA4 in the cytosol and subsequent degradation of ferritin•NCOA4 by the proteasome presents an attractive model for ferritin proteasomal degradation and warrants further study.

Role of cage dismantling in NCOA4³⁸³⁻⁵²²•ferritin condensate formation.

Recent work has proposed that full length NCOA4 drives the phase separation of NCOA4•ferritin condensates to facilitate lysosomal ferritinophagy (Kuno *et al.*, 2022; Ohshima *et al.*, 2022). Indeed, Ohshima and colleagues showed that in cells NCOA4 caused the formation of ferritin phase separated condensates, dependent on both the NCOA4•hfH interaction and the NCOA4 N-terminal self-oligomerization domains. They further demonstrated that this condensate formation was required for ferritin degradation in some conditions (Ohshima *et al.*, 2022). Similarly, it was observed that under prolonged

exposure to high levels of iron, NCOA4 formed condensates via multivalent self-interactions both *in vivo* and *in vitro* (Kuno *et al.*, 2022). However, the detailed mechanism by which these NCOA4•ferritin condensates form is unknown.

The model of ferritin cage dismantling we have proposed here could provide additional context in assessing likely mechanisms of NCOA4-dependent ferritin phase separation. Specifically, it is possible that ferritin•NCOA4 fragments, when present in high concentrations cannot be efficiently cleared by the proteasome, and instead may oligomerize using the well characterized NCOA4 coiled-coil dimerization domain to form a condensate, or through alternative interfaces as it been previously reported that the NCOA4³⁸³⁻⁵²² fragment can oligomerize, despite lacking the N-terminal self-oligomerization domains of the full-length protein (Gryzik *et al.*, 2017). We note that if such phase separated condensates do form in a concentration-dependent manner, their presence may also explain why we failed to observe dismantling products in our SEC or cryo-EM studies, and only observed such products in our mass photometry assays, which were performed in much lower concentration regimes that typically disfavor condensate stabilization (Alberti *et al.*, 2019; Wang *et al.*, 2023). A final prediction of our model is that phase separated condensates could be removed from the cell via an alternative autophagy pathway, including those reliant on TAX1BP1 or SQSTM1, which have each been associated with autophagy-dependent degradation of condensates (Bauer *et al.*, 2024; Ohshima *et al.*, 2022).

3.5 MATERIALS AND METHODS

Protein expression and purification.

Human ferritin heavy chain (hfH) was expressed in *E. coli* strain BL21 (DE3) (st_JD494) transformed with plasmid (pl_JD160), which was obtained from Addgene (122652, Trevor Douglas, unpublished). Human ferritin light chain (hfL) was also expressed in *E. coli* strain BL21 (DE3) (st_JD494) transformed with plasmid (pl_JD159), which was obtained from Addgene (122653, Trevor Douglas, unpublished). For both hfH and hfL, expression cultures (2L) were grown in 2xYT media at 37°C with aeration, and induced with 1mM isopropyl β -D-1-thiogalactopyranoside at an optical density of ~0.6. Expression proceeded for four hours at 37°C before cells were harvested via centrifugation. Cell pellets were resuspended in 50mL buffer P (20mM Tris, 150mM NaCl pH 7.5), dounced until homogenous and sonicated on ice using a Qsonica Sonicator (5sec on, 10sec off for 5min, amplitude 35%). Sample was then centrifuged at 14,460g for 20min in a Ti60 rotor. The soluble supernatant was incubated with 1 μ L benzonase (Thomas Scientific 9025-65-4) and 2mM MgCl₂ for 10 min at room temperature. Ammonium sulfate precipitation was performed by adding 26.15g NH₄SO₄ per 50mL sample and the solution incubated at 4°C for 2 hrs before centrifugation at 14,460g for 30min. The resulting pellet was resuspended in 20mM Tris 150mM NaCl pH 7.5 (buffer P) and dialyzed overnight at 4°C. The sample was centrifuged again at 14,460g for 20min and the soluble material loaded onto a Superose6 10/300 size exclusion column, equilibrated buffer P. Fractions bearing ferritin cages (~0.6CVs) were identified by SDS-PAGE, pooled, and concentrated via centrifugation in a 3kDa concentrator (Millipore Sigma UFC900324).

To generate iron-loaded hfH₂₄ cages (Fe-hfH₂₄), hfH was incubated with ferrous ammonium sulfate (Fe(NH₄)₂(SO₄)₂·6H₂O) at a 1:1,000 molar ratio and stirred for 30min at room temperature. Absorbance at 310nm was monitored in a UV/Vis spectrophotometer to monitor iron uptake, as described in (Santambrogio *et al*, 1993). Sample was then dialyzed overnight at 4°C in buffer P.

To generate cages with a mixture of light and heavy ferritin chains (hfHL), isolated hfH and hfL samples were denatured with 6M guanidine hydrochloride (10mL volume each, 10µg/mL) overnight at 4°C before being mixed together in a 1:1 molar ratio. The solution was buffer exchanged into buffer P by via serial spin-concentration to approximately 100µL (1mg/mL) in a 3kDa centricon filter (Millipore Sigma UFC900324).

For NCOA4 constructs, a g-block gene fragment (IDT) containing the sequence for NCOA4³⁸³⁻⁵²² was cloned into plasmids bearing the appropriate N- and C-terminal fusions (see plasmids pl_JD141, pl_JD132 and pl_JD123) via HiFi assembly (New England Biolabs) to generate MBP-TEV-NCOA4³⁸³⁻⁵²²-TEV-mNeon-His₁₀ (MBP-NCOA4³⁸³⁻⁵²²-mNeon) and His₆-3C-NCOA4³⁸³⁻⁵²²-TEV-sfGFP-3C-FLAG₃ (NCOA4³⁸³⁻⁵²²-GFP). Resulting plasmids were transformed into E. coli strain BL21 (DE3) st_JD494 for protein expression.

MBP-NCOA4³⁸³⁻⁵²²-mNeon expression cultures (2L) were grown in 2xYT media at 37°C with aeration, and induced with 100µM isopropyl β-d-1-thiogalactopyranoside at an optical density of ~0.6. Expression proceeded overnight at 25°C before cells were harvested via centrifugation. Cell pellets were resuspended in 50mL buffer NLB (10mM K₂HPO₄, 300mM NaCl, 20mM KCl, 10mM imidazole, 5mM 2-mercaptoethanol, pH 8.0), dounced until homogenous and sonicated on ice using a Qsonica Sonicator (5sec on,

10sec off for 5min, amplitude 35%). Sample was then centrifuged at 251,000g for one hour in a Ti60 rotor. Supernatant was loaded onto a 5mL Ni-NTA column (Bio-Rad), washed with two column volumes of buffer NLB, and eluted over 20 column volumes in a linear gradient of buffer NLB with imidazole increasing from 10mM to 1M. Pooled fractions were then concentrated to 2mL using 3kDa centricon spin concentrator (Millipore Sigma UFC900324) and purified over an S75 16/600 size exclusion column in buffer P. To generate tagless cNCOA4³⁸³⁻⁵²², and MBP-NCOA4³⁸³⁻⁵²²-mNeon proteins were cleaved by incubation with TEV protease (prepped in house, st_JD638) in a 1:100 molar ratio for 2 hrs at 30°C before purification of the cleaved product on an S75 16/600 SEC in buffer P. The resulting protein eluted at ~0.7 CVs.

NCOA4³⁸³⁻⁵²²-sfGFP expression cultures (2L) were grown in 2xYT media at 37°C with aeration, and induced with 100µM isopropyl β-d-1-thiogalactopyranoside at an optical density of ~0.6. Expression proceeded for six hours at 30°C before cells were harvested via centrifugation. Cell pellets were lysed, clarified and purified as described above for MBP-NCOA4³⁸³⁻⁵²²-mNeon. Purified NCOA4³⁸³⁻⁵²²-sfGFP was cleaved with TEV as above to generate His₆-NCOA4³⁸³⁻⁵²². Cleaved material was run over a 5mL Nuvia Q column with Q wash buffer (20mM Tris, 100mM NaCl, 5mM BME, pH 7.4) and Q elution buffer (20mM Tris, 750mM NaCl, 5mM BME, pH 7.4). Relevant fractions were identified, pooled, concentrated and further purified on an S75 16/600 SEC in buffer P to isolate His₆-NCOA4³⁸³⁻⁵²², which eluted at ~0.7 CVs.

Far-Western blots.

hfH or hfL at the noted concentrations was spotted (2 μ L) on a nitrocellulose membrane (Amersham Protran) and allowed to dry at room temperature for 12 minutes. The membrane was then blocked in buffer TBST (20mM Tris, 150mM NaCl, 0.1% Tween-20, pH 7.5) supplemented with 3% bovine serum albumin for 15 minutes at room temperature before being incubated with a 0.5 μ M solution of MBP-NCOA4³⁸³⁻⁵²²-mNeon. After washing three times for three minutes with TBST, the membrane was imaged for mNeon fluorescence signal using an Azure Biosystems imager with excitation and emission filters at 472nm and 513nm. All membranes being compared were imaged concurrently to ensure that they were comparable in signal intensity.

Analytical size exclusion chromatography (SEC).

The relevant ferritin construct was diluted to 2 μ M in buffer P and incubated with 24-fold molar excess of noted NCOA4 construct or equivalent volume of buffer P for 1.5hrs at 4°C. 100 μ L of the solution was injected onto a Superose6 10/300 SEC, run for 1.5CV in buffer P and the resulting trace plotted and analyzed in Python.

Mass photometry.

The relevant ferritin construct was diluted to 75nM in buffer P and incubated with a 24-fold molar excess of His₆-NCOA4³⁸³⁻⁵²² for 5min at room temperature. The mixture was then diluted to a final concentration of 5nM ferritin in 20 μ L buffer P for loading onto the mass photometry gasket. All data was collected on a One^{MP} mass photometer (Refeyn Ltd, Oxford, UK) using the Acquire^{MP} software. The resulting data was fit using a Gaussian Mixture Model in Python to obtain masses for each peak. Note the mass photometer was recalibrated prior to each data collection session.

Cryo-EM grid preparation and imaging.

Purified hfH₂₄ or Fe-hfH₂₄ (~1mg/mL, ~0.25mg/mL) was incubated with His₆-NCOA4³⁸³⁻⁵²² at a 24-fold molar excess or buffer P overnight at 4°C. Samples were diluted to a final concentration of 250ng/μL or 70ng/μL ferritin for hfH₂₄ and Fe-hfH₂₄ respectively in buffer P. 3μL of each sample was blotted and plunged using a Vitrobot onto a C-flat 1.2/1.3 Au grid that was glow discharged using a PELCO easiGlow™ set to “Auto” (60s, -15 mA). Blotting parameters were as follows: 5s wait, Δ(+10) force, 3s blot, 10°C, 95% relative humidity. Grids were clipped and then screened on a Talos Arctica G2 microscope with Falcon 3EC detector at the following settings: 200kV, 190,000X magnification, 0.7656Å pixel size, 75 e/Å² total electron dose and -1.8 to -4.8 in 0.3μm steps defocus.

ACKNOWLEDGMENTS

We thank Andrew Grasseti for helpful discussion, Barrett Powell for help blotting, plunging and collecting cryo-EM images and the MIT Biophysical Instrumentation Facility for supporting access to key instrumentation. This work was supported by NIH grants 5T32-GM007287, R01-GM, NSF-CAREER grant 2046778, and the Whitehead Family.

AUTHOR CONTRIBUTIONS

AL and JHD conceived the work, designed and interpreted the experiments and wrote the manuscript. AL performed all experiments. The authors declare that they have no conflict of interest.

3.6 FIGURES

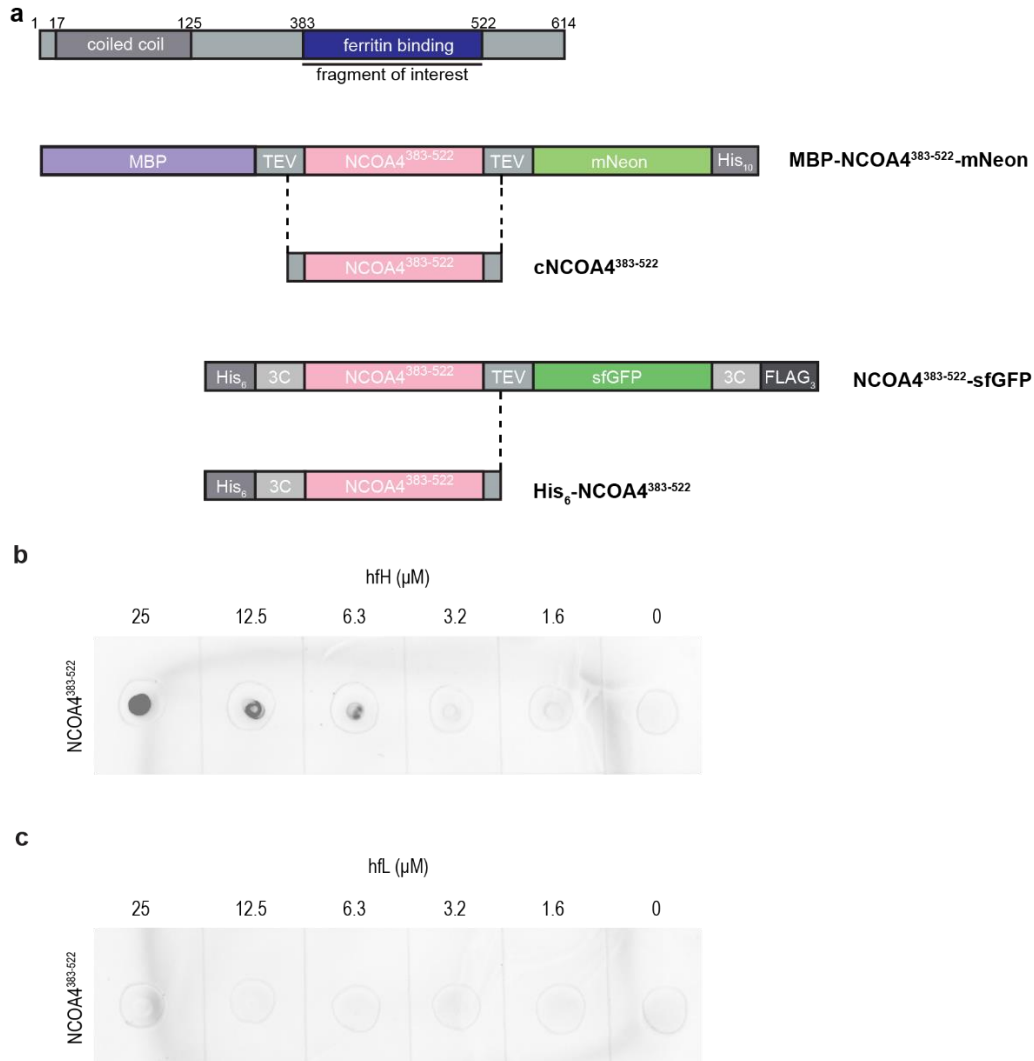


Figure 3.1: MBP-NCOA4³⁸³⁻⁵²²-mNeon binds specifically to hfH.

(a) Schematics of NCOA4 domain architecture and NCOA4³⁸³⁻⁵²² constructs used in assays for this chapter. The fragment of interest (NCOA4³⁸³⁻⁵²²) used here is noted (pink). MBP-TEV-NCOA4³⁸³⁻⁵²²-TEV-mNeon-His₁₀ (MBP-NCOA4³⁸³⁻⁵²²-mNeon) can be cleaved with TEV protease, as indicated by dashed lines, to generate cNCOA4³⁸³⁻⁵²². His₆-3C-NCOA4³⁸³⁻⁵²²-TEV-sfGFP-3C-FLAG₃ (NCOA4³⁸³⁻⁵²²-sfGFP) cleaved with the TEV protease, as indicated by dashed lines, results in His₆-NCOA4³⁸³⁻⁵²².

(b) Far-western of MBP-NCOA4³⁸³⁻⁵²²-mNeon binding to hfH, which was spotted on membrane at indicated concentrations. Binding was detected using fluorescent signal from mNeon (excitation: 472nm; emission: 513nm), which was incubated on membrane at a concentration of 0.5μM.

(c) Far-western of MBP-NCOA4³⁸³⁻⁵²²-mNeon binding to hfL, with assay performed as described in (a).

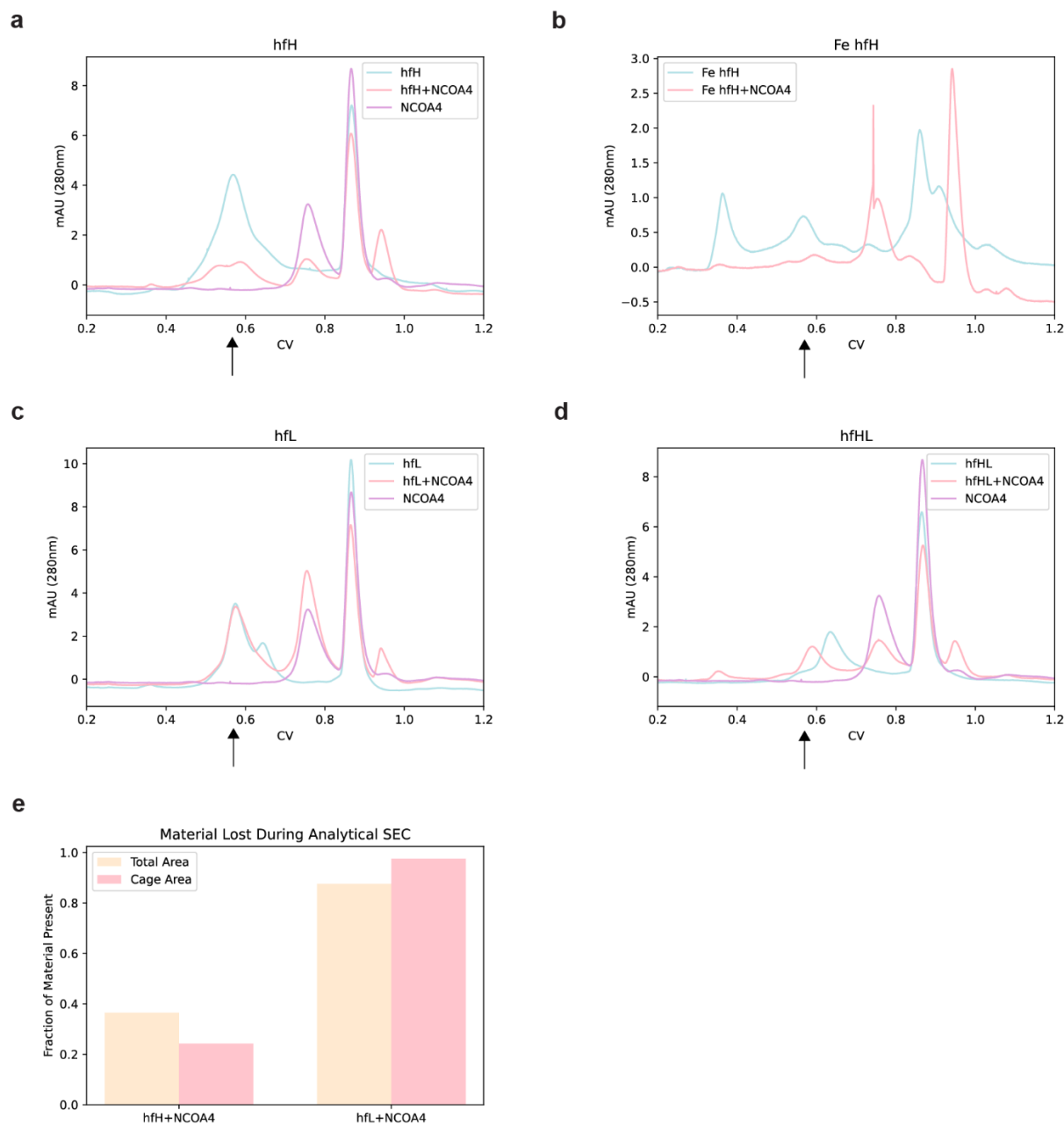


Figure 3.2: NCOA4³⁸³⁻⁵²² dependent loss of heavy ferritin cages in analytical SEC.

(a) Analytical SEC traces on Superose6 10/300 of hfH₂₄ alone (blue), hfH₂₄ with His₆-NCOA4³⁸³⁻⁵²² (pink) and His₆-NCOA4³⁸³⁻⁵²² alone (purple). Note full 24-mer cage is expected to elute at 0.56 CV, denoted by arrow. Samples incubated with 24-fold molar excess of His₆-NCOA4³⁸³⁻⁵²² (see Methods). SEC traces are as described in (a) for Fe-hfH₂₄ **(b)**, hfL₂₄ **(c)** and hfHL **(d)**.

(e) Quantification of material lost for hfH₂₄ and hfL₂₄ with His₆-NCOA4³⁸³⁻⁵²² added from traces shown in (a) and (c). Total area (orange) and area specific to cage peak (pink) shown.

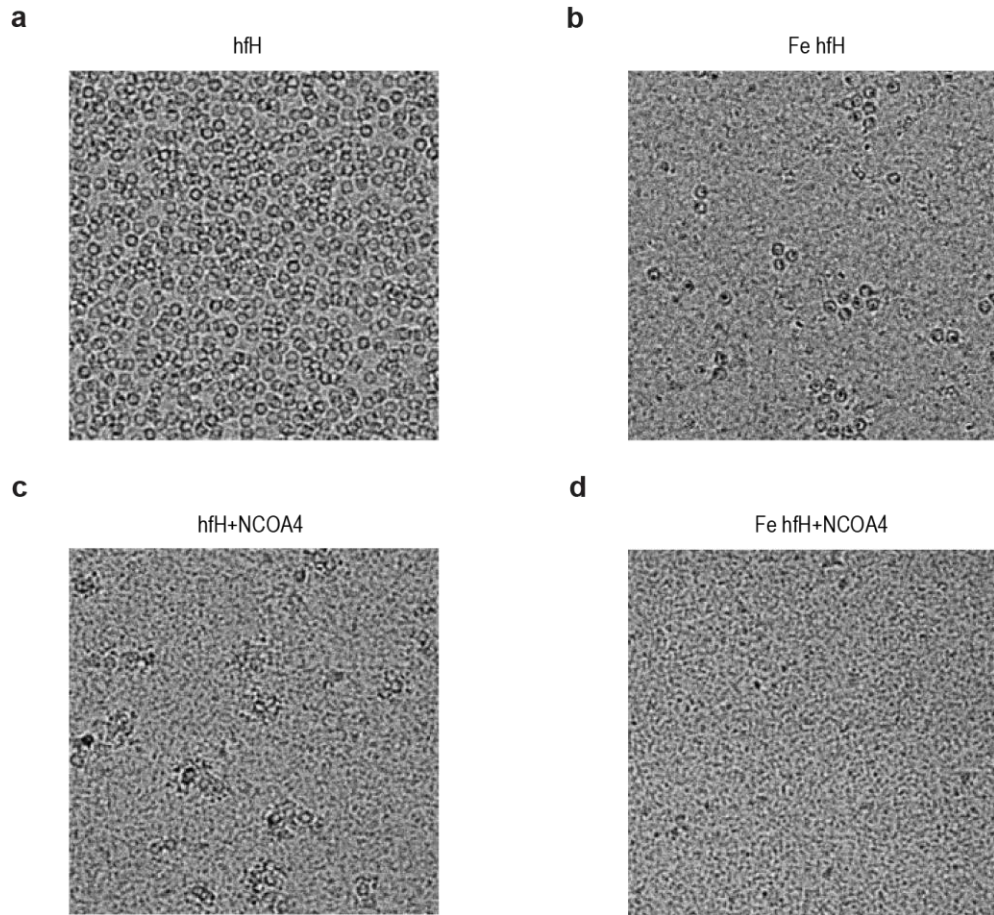


Figure 3.3: NCOA4³⁸³⁻⁵²² dependent loss of heavy ferritin cages in cryo-EM.

Representative cryo-EM micrographs of hfH₂₄ alone **(a)**, Fe-hfH₂₄ alone **(b)**, hfH₂₄ with His₆-NCOA4³⁸³⁻⁵²² **(c)** and Fe-hfH₂₄ with His₆-NCOA4³⁸³⁻⁵²² **(d)**. Samples incubated with 24-fold molar excess of His₆-NCOA4³⁸³⁻⁵²² (see Methods).

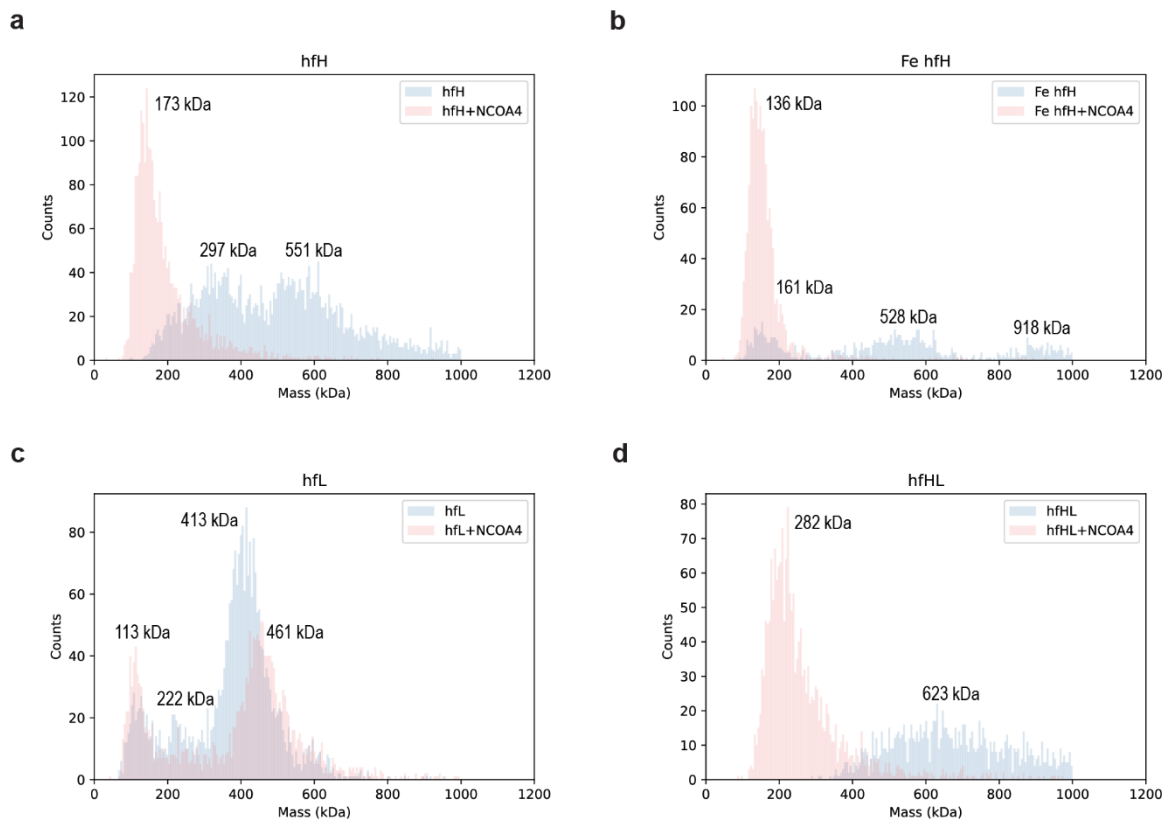


Figure 3.4: NCOA4³⁸³⁻⁵²² dependent loss of heavy ferritin cages in mass photometry.

(a) Mass photometry traces of hfH₂₄ alone (blue) and hfH₂₄ with His₆-NCOA4³⁸³⁻⁵²² (pink). Masses of each peak denoted on graph. His₆-NCOA4³⁸³⁻⁵²² added at a 24-fold molar excess of ferritin.

Mass photometry traces as described in (a) for Fe-hfH₂₄ **(b)**, hfL₂₄ **(c)** and hfHL **(d)**.

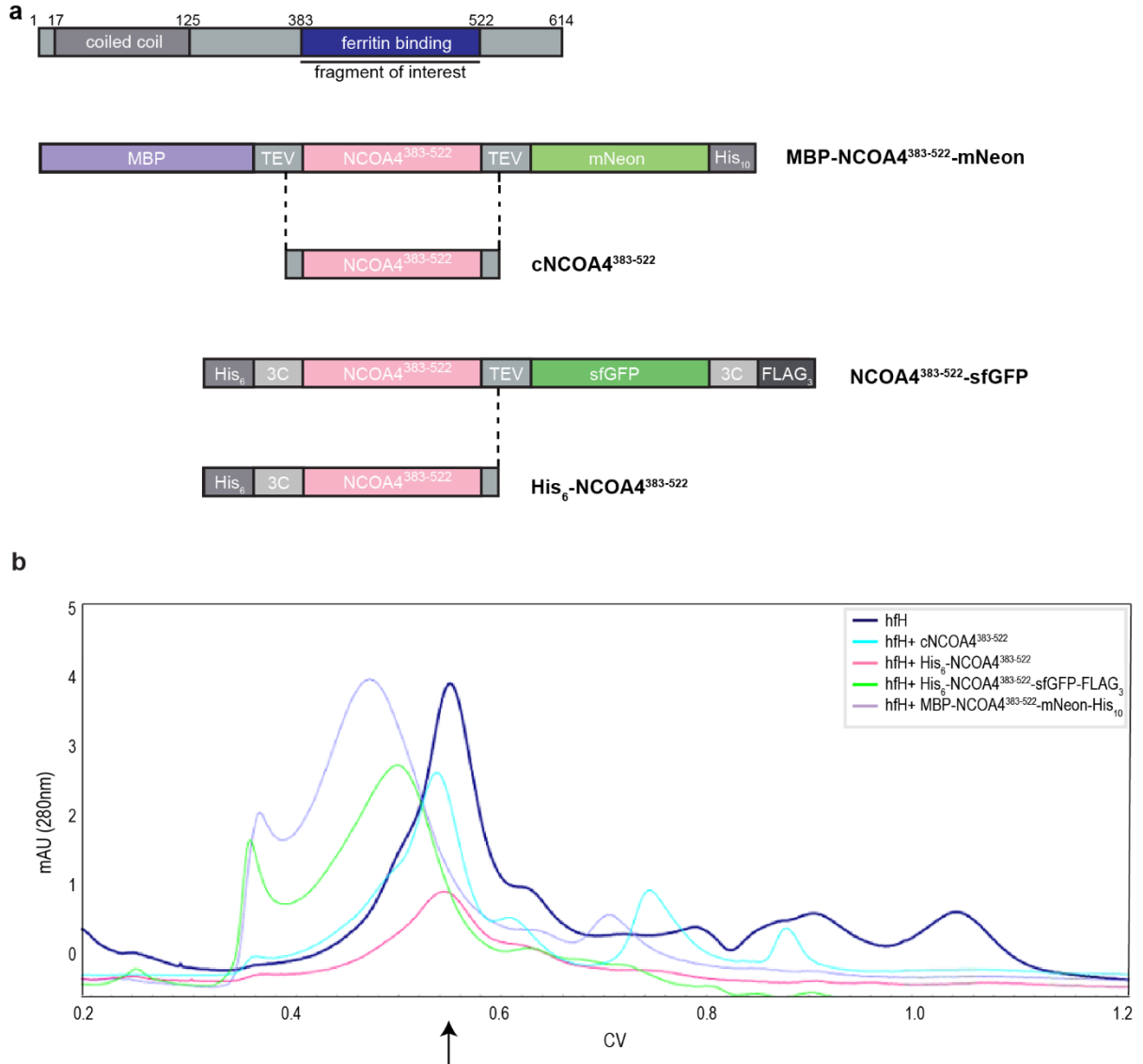


Figure 3.5: Cage dismantling activity of NCOA4³⁸³⁻⁵²² requires free C-terminus.

(a) Schematics of NCOA4 domain architecture and NCOA4³⁸³⁻⁵²² constructs used in **(b)**.
(b) Analytical SEC traces on Superose6 10/300 of noted NCOA4³⁸³⁻⁵²² constructs incubated in 24-fold molar excess with hfH₂₄. Note full cage expected to elute at 0.56 CV, denoted by arrow.

3.7 REFERENCES

- Alberti S, Gladfelter A, Mittag T (2019) Considerations and Challenges in Studying Liquid-Liquid Phase Separation and Biomolecular Condensates. *Cell* 176: 419-434
- Arosio P, Elia L, Poli M (2017) Ferritin, cellular iron storage and regulation. *IUBMB Life* 69: 414-422
- Bauer B, Idinger J, Schuschnig M, Ferrari L, Martens S (2024) Recruitment of autophagy initiator TAX1BP1 advances aggrephagy from cargo collection to sequestration. *Embo j* 43: 5910-5940
- De Domenico I, Vaughn MB, Li L, Bagley D, Musci G, Ward DM, Kaplan J (2006) Ferroportin-mediated mobilization of ferritin iron precedes ferritin degradation by the proteasome. *Embo j* 25: 5396-5404
- De Domenico I, Ward DM, Kaplan J (2009) Specific iron chelators determine the route of ferritin degradation. *Blood* 114: 4546-4551
- Dikic I (2017) Proteasomal and Autophagic Degradation Systems. *Annu Rev Biochem* 86: 193-224
- Dowdle WE, Nyfeler B, Nagel J, Elling RA, Liu S, Triantafellow E, Menon S, Wang Z, Honda A, Pardee G *et al* (2014) Selective VPS34 inhibitor blocks autophagy and uncovers a role for NCOA4 in ferritin degradation and iron homeostasis in vivo. *Nat Cell Biol* 16: 1069-1079
- Goodwin JM, Dowdle WE, DeJesus R, Wang Z, Bergman P, Kobylarz M, Lindeman A, Xavier RJ, McAllister G, Nyfeler B *et al* (2017) Autophagy-Independent Lysosomal Targeting Regulated by ULK1/2-FIP200 and ATG9. *Cell Rep* 20: 2341-2356
- Gryzik M, Srivastava A, Longhi G, Bertuzzi M, Gianoncelli A, Carmona F, Poli M, Arosio P (2017) Expression and characterization of the ferritin binding domain of Nuclear Receptor Coactivator-4 (NCOA4). *Biochim Biophys Acta Gen Subj* 1861: 2710-2716
- Hamed MY, Silver J, Wilsonx MT (1983) Studies of the reactions of ferric iron with glutathione and some related thiols. *Inorganica Chimica Acta* 78: 1-11
- Hider R, Aviles MV, Chen YL, Latunde-Dada GO (2021) The Role of GSH in Intracellular Iron Trafficking. *Int J Mol Sci* 22
- Hoelzgen F, Nguyen TTP, Klukin E, Boumaiza M, Srivastava AK, Kim EY, Zalk R, Shahar A, Cohen-Schwartz S, Meyron-Holtz EG *et al* (2024) Structural basis for the intracellular regulation of ferritin degradation. *Nat Commun* 15: 3802

Kuno S, Fujita H, Tanaka YK, Ogra Y, Iwai K (2022) Iron-induced NCOA4 condensation regulates ferritin fate and iron homeostasis. *EMBO Rep* 23: e54278

Kwok JC, Richardson DR (2004) Examination of the mechanism(s) involved in doxorubicin-mediated iron accumulation in ferritin: studies using metabolic inhibitors, protein synthesis inhibitors, and lysosomotropic agents. *Mol Pharmacol* 65: 181-195

Lane DJ, Merlot AM, Huang ML, Bae DH, Jansson PJ, Sahni S, Kalinowski DS, Richardson DR (2015) Cellular iron uptake, trafficking and metabolism: Key molecules and mechanisms and their roles in disease. *Biochim Biophys Acta* 1853: 1130-1144

Lee A, Davis JH (2024) NCOA4 initiates ferritinophagy by binding GATE16 using two highly avid short linear interaction motifs. *bioRxiv*

Mancias JD, Pontano Vaites L, Nissim S, Biancur DE, Kim AJ, Wang X, Liu Y, Goessling W, Kimmelman AC, Harper JW (2015) Ferritinophagy via NCOA4 is required for erythropoiesis and is regulated by iron dependent HERC2-mediated proteolysis. *Elife* 4

Mancias JD, Wang X, Gygi SP, Harper JW, Kimmelman AC (2014) Quantitative proteomics identifies NCOA4 as the cargo receptor mediating ferritinophagy. *Nature* 509: 105-109

Ohshima T, Yamamoto H, Sakamaki Y, Saito C, Mizushima N (2022) NCOA4 drives ferritin phase separation to facilitate macroferritinophagy and microferritinophagy. *J Cell Biol* 221

Santambrogio P, Levi S, Cozzi A, Rovida E, Albertini A, Arosio P (1993) Production and characterization of recombinant heteropolymers of human ferritin H and L chains. *Journal of Biological Chemistry* 268: 12744-12748

Srivastava AK, Flint N, Kreckel H, Gryzik M, Poli M, Arosio P, Bou-Abdallah F (2020) Thermodynamic and Kinetic Studies of the Interaction of Nuclear Receptor Coactivator-4 (NCOA4) with Human Ferritin. *Biochemistry* 59: 2707-2717

Wang J, Pantopoulos K (2011) Regulation of cellular iron metabolism. *Biochem J* 434: 365-381

Wang Y-L, Zhao W-W, Shi J, Wan X-B, Zheng J, Fan X-J (2023) Liquid-liquid phase separation in DNA double-strand breaks repair. *Cell Death & Disease* 14: 746

Wang Z, Gao H, Zhang Y, Liu G, Niu G, Chen X (2017) Functional ferritin nanoparticles for biomedical applications. *Front Chem Sci Eng* 11: 633-646

Zhang N, Yu X, Xie J, Xu H (2021) New Insights into the Role of Ferritin in Iron Homeostasis and Neurodegenerative Diseases. *Molecular Neurobiology* 58: 2812-2823

Zhang Y, Mikhael M, Xu D, Li Y, Soe-Lin S, Ning B, Li W, Nie G, Zhao Y, Ponka P (2010) Lysosomal proteolysis is the primary degradation pathway for cytosolic ferritin and cytosolic ferritin degradation is necessary for iron exit. *Antioxid Redox Signal* 13: 999-1009

Zhao H, Lu Y, Zhang J, Sun Z, Cheng C, Liu Y, Wu L, Zhang M, He W, Hao S, Li K (2024) NCOA4 requires a [3Fe-4S] to sense and maintain the iron homeostasis. *J Biol Chem* 300: 105612

Chapter 4

Conclusions and future directions

AUTHOR CONTRIBUTIONS

AL wrote following text with editorial support from JHD.

4.1 NCOA4 initiates ferritinophagy by binding GATE16 using two highly avid short linear interaction motifs.

Ferritinophagy was previously identified as an integral part of iron regulation, facilitating the degradation of ferritin cages via the lysosome, and thereby releasing iron into the cell under iron-limiting conditions (Mancias *et al.*, 2014). This process is thought to require the protein Nuclear Receptor Coactivator 4 (NCOA4), which acts as a selective receptor for ferritin. NCOA4 was first identified in an LC-MS/MS based proteomics approach that targeted proteins that co-purified with autophagosomes. It was subsequently shown to interact with LC3s via co-immunoprecipitations from cell lysates and in cell colocalization (Mancias *et al.*, 2014). Additionally, the biochemically amenable fragment of NCOA4, consisting of residues 383-522 (NCOA4³⁸³⁻⁵²²), was demonstrated to bind directly to ferritin (Mancias *et al.*, 2015). Selective autophagy receptors typically bind to LC3s via short linear motifs termed LC3 interacting regions (LIRs), although no LIRs had been previously identified within NCOA4. Despite these observations, whether NCOA4³⁸³⁻⁵²² interacted directly with GATE16, one of the strongest interactors of the LC3 family based on prior experiments (Mancias *et al.*, 2014), and if it did so, through which motifs, was unknown. Thus, we sought to biochemically define the interaction and binding mode of NCOA4³⁸³⁻⁵²² and GATE16 and to ascertain the cellular relevance of this interaction interface.

In chapter 2, I determined the molecular contacts and modes of interaction that support NCOA4 binding to GATE16 and, presumably by extension, to other LC3 family members. Specifically, I found that the minimal fragment, NCOA4³⁸³⁻⁵²², binds directly to GATE16 through two short LIR-like motifs. These two motifs each bind with weak affinity

but are highly avid and work in concert to support high affinity association of the overall complex. In assessing complex stoichiometry, I found that one NCOA4³⁸³⁻⁵²² binds for each GST-dimerized pair of GATE16 molecules, and thus infer that each motif on NCOA4³⁸³⁻⁵²² interacts with a separate unit of GATE16. Furthermore, I found that NCOA4³⁸³⁻⁵²² is sufficient to direct the lysosomal degradation of ferritin and that this process requires both NCOA4³⁸³⁻⁵²² motifs. Thus, I have concluded that this avidity model is important *in vivo* as well as *in vitro* and that GATE16 must be oligomerized or in a high local concentration to facilitate ferritinophagy. As previous studies have indicated that ferritinophagy can proceed without lipidation of LC3s by ATG7, I also tested the ability of LC3 to form puncta in ATG7 Δ cells. Under ferritinophagy inducing conditions, I found that LC3 puncta form in ATG7 Δ cells, indicating that oligomerization of GATE16 can still occur and may play a key role in these conditions. Importantly, this avidity model provides a mechanism by which selective autophagy receptors could discriminate between inactive, monomeric LC3s and their active, oligomeric forms. Finally, I have shown that iron binding to NCOA4³⁸³⁻⁵²² decreases its affinity for GATE16, and I propose that this iron-dependent binding may act as an extra layer of iron regulation in the pathway.

4.2 Future directions in interrogating NCOA4•GATE16 interactions.

Following the experiments described in this thesis, there are some open areas of research surrounding the NCOA4•GATE16 interaction that would be interesting to pursue. First, the formation of iron deposits is linked to a variety of neurodegenerative diseases including Alzheimer's (Ward *et al*, 2014) and Parkinson's (Sofic *et al*, 1988), suggesting that disruptions to iron homeostasis may affect the progression of these

diseases. Since accumulation of free, reactive iron, is common in these diseases (Zeng *et al*, 2024), some have hypothesized that dysregulation of ferritinophagy contributes to these pathologies (Quiles Del Rey & Mancias, 2019; Tran *et al*, 2022). Furthermore, it was been found that some cells associated with Parkinson's disease have an increased ratio of heavy to light chain ferritin compared to control cells (Friedman & Galazka-Friedman, 2012). Of note, NCOA4 specifically binds heavy ferritin, so this compositional change may elevate ferritinophagy activity in this context. It would be interesting to test whether blocking ferritinophagy could alleviate some of the Parkinson's disease phenotypes, as such inhibition is predicted to prevent the release of reactive iron. Using the studies from this thesis, one could develop inhibitors specific to the NCOA4³⁸³⁻⁵²² motifs identified here, such as therapeutic antibodies raised against these motifs, and test whether blocking NCOA4-dependent ferritin degradation reduces the presence of iron deposits in cell models of neurodegenerative diseases. In support of this notion, some early studies suggest that blocking the NCOA4•ferritin interaction, which also decreases ferritinophagy, mitigates degeneration in Parkinson's cells by decreasing ROS-mediated cell death (Zhao *et al*, 2024). Further studies into modulating ferritinophagy via the NCOA4•GATE16 axis could contribute both to understanding the role of iron regulation in this class of neurodegenerative disorders, and could serve as a new target for work towards the development of therapeutics.

Focusing on the molecular contacts supporting NCOA4³⁸³⁻⁵²²•GATE16 binding, it would be intriguing to obtain an NCOA4³⁸³⁻⁵²²•GATE16 structure. This structure would be informative as it could show the full extent of the interaction of NCOA4³⁸³⁻⁵²² and GATE16 and visually demonstrate how the non-canonical cysteine residue of the FAECV motif

docks into the LIR-docking site on GATE16, with clear implications in the potential binding modes of other cysteine-containing LIR motifs. In data not presented in this thesis, I obtained a 1.6-Å resolution crystal structure of GATE16 alone but was unable to identify reproducible conditions supporting formation of a co-crystal with either motif bound to GATE16, potentially due to the low affinity of each isolated motif. I also attempted to obtain a cryo-EM structure of NCOA4³⁸³⁻⁵²² in complex with GATE16, but was unable to resolve these structures at an informative resolution, likely due to the small overall size of the co-complex. Based on these observations, I believe the most promising method to obtain a co-structure would be to perform cryo-EM on the higher order ferritin•NCOA4³⁸³⁻⁵²²•GATE16 complex, which would allow us to use the mass and contrast inherent to ferritin to aid in particle picking. My initial attempts to resolve such a structure were also unsuccessful as the extent of complex formation was minimal in my conditions. However, the observations I presented in Chapters 2 and 3 that NCOA4³⁸³⁻⁵²² binds GATE16 and ferritin more tightly when lacking iron provides key insight to direct a new set of conditions expected to increase the likelihood of obtaining the desired structure. Note that because NCOA4³⁸³⁻⁵²² is predicted to be largely unstructured outside of the GATE16 and ferritin binding interfaces, we would focus our analyses on the interface surfaces while recognizing the possibility of resolving the low-resolution topology of the superstructure through the use of heterogeneous analysis tools, such as cryoDRGN (Zhong *et al*, 2021).

4.3 Putative role of NCOA4 in dismantling ferritin cages.

In chapter 3, I uncovered a potentially novel function for NCOA4³⁸³⁻⁵²² as it relates to its role in ferritin degradation. I demonstrated that the soluble, C-terminally tagged

construct I generated of NCOA4³⁸³⁻⁵²² bound specifically to the heavy chain of ferritin. Surprisingly, using analytical SEC and cryo-EM, I found that addition of NCOA4³⁸³⁻⁵²² lacking this C-terminal tag to ferritin caused a loss of heavy ferritin cages and that this behavior was specific to the NCOA4³⁸³⁻⁵²²•ferritin heavy chain interaction. Of note, this loss of material could be explained by either the phase separation (i.e. formation of higher order NCOA4³⁸³⁻⁵²²•ferritin complexes) or dismantling of ferritin cages. Either of these outcomes are not predicted by existent models of NCOA4³⁸³⁻⁵²² activity and would indicate that NCOA4³⁸³⁻⁵²² has an additional function beyond ferritin and GATE16 binding. To differentiate between these two models, I probed the NCOA4³⁸³⁻⁵²²•ferritin interaction with mass photometry. Our assays with mass photometry recapitulated the loss of heavy ferritin cages but also showed an appearance of a new species with an apparent molecular weight consistent with a partially formed cage, most consistent with the NCOA4³⁸³⁻⁵²² cage dismantling model. Furthermore, I found that this apparent cage dismantling activity requires a free C-terminus of NCOA4³⁸³⁻⁵²². This work, although highly preliminary, suggests a novel model in which NCOA4³⁸³⁻⁵²² dismantles ferritin cages, potentially providing a mechanism for cells to directly release iron into the cytosol.

4.4 Future directions for NCOA4³⁸³⁻⁵²² dependent cage dismantling.

The main set of data that discriminates between ferritin cages being disassembled versus phase separating as whole cages is the appearance of the partial cage peak in the described mass photometry assay. Given that my hypothesis is that I was only able to visualize these partial cages due to the dilute nature of the assay, these mass photometry experiments should be repeated at a range of concentrations. Doing so would

enable us to determine if there is a concentration-dependent determinant as to whether cages are degraded or potentially begin to aggregate, either as full or partial cages. Additionally, one could more directly test the condensate formation model using a dye-labeled ferritin and probing for condensate formation via confocal microscopy. This could be conducted with addition of either NCOA4³⁸³⁻⁵²² or MBP-NCOA4³⁸³⁻⁵²²-mNeon, which lacks the free C-terminus putatively required for its cage dismantling or phase separation promoting activity.

Additionally, complementary functional assays probing the outcomes of NCOA4³⁸³⁻⁵²²•ferritin binding should be conducted. My proposed model of cage dismantling predicts that NCOA4³⁸³⁻⁵²² interacting with iron loaded heavy ferritin should liberate iron in the absence of proteases, whereas the solely phase-separation promoting model predicts no liberation of iron from the cages. Given this, in work not shown, I have begun optimizing a colorimetric dye-based iron release assay, which could be performed using the various NCOA4³⁸³⁻⁵²² and ferritin reagents I've described in this thesis. As designed, this assay (AbCam Iron Assay Kit ab83366) should only detect free iron in the solution, implying that changes in measured iron upon addition of iron-free NCOA4³⁸³⁻⁵²² would have to originate from inside ferritin after cage dismantling.

4.5 Contribution to the role of NCOA4 in ferritinophagy regulation.

In both Chapters 2 and 3 of this thesis, I have biochemically interrogated the role of NCOA4³⁸³⁻⁵²² in regulating ferritinophagy, both in its interaction with GATE16 (Chapter 2) and with ferritin (Chapter 3). I have uncovered that NCOA4³⁸³⁻⁵²² uses two highly avid motifs to efficiently bind GATE16 and in doing so elucidated a model by which selective

autophagy receptors can specifically recognize active (*i.e.* oligomerized) LC3s to drive autophagy (**Figure 4.1a**). Additionally, I have found that binding of iron to NCOA4³⁸³⁻⁵²² decreases its affinity for GATE16, thus revealing a new layer of iron regulation for ferritinophagy (**Figure 4.1b**). Furthermore, I have observed a potentially novel role for NCOA4³⁸³⁻⁵²² wherein it either directly disassembles heavy ferritin cages, or supports the formation of higher-order condensates of these cages. These proposed models of NCOA4-dependent changes in cage topology present alternate pathways for ferritin regulation and, in the case of the cage dismantling model, would allow for direct release of iron into the cytosol (**Figure 4.2**). Excitingly, I believe the further exploration of the models emerging from my thesis could profoundly impact our overall understanding of cellular iron homeostasis mechanisms aimed at regulating levels of this vital yet often toxic metal.

4.6 FIGURES

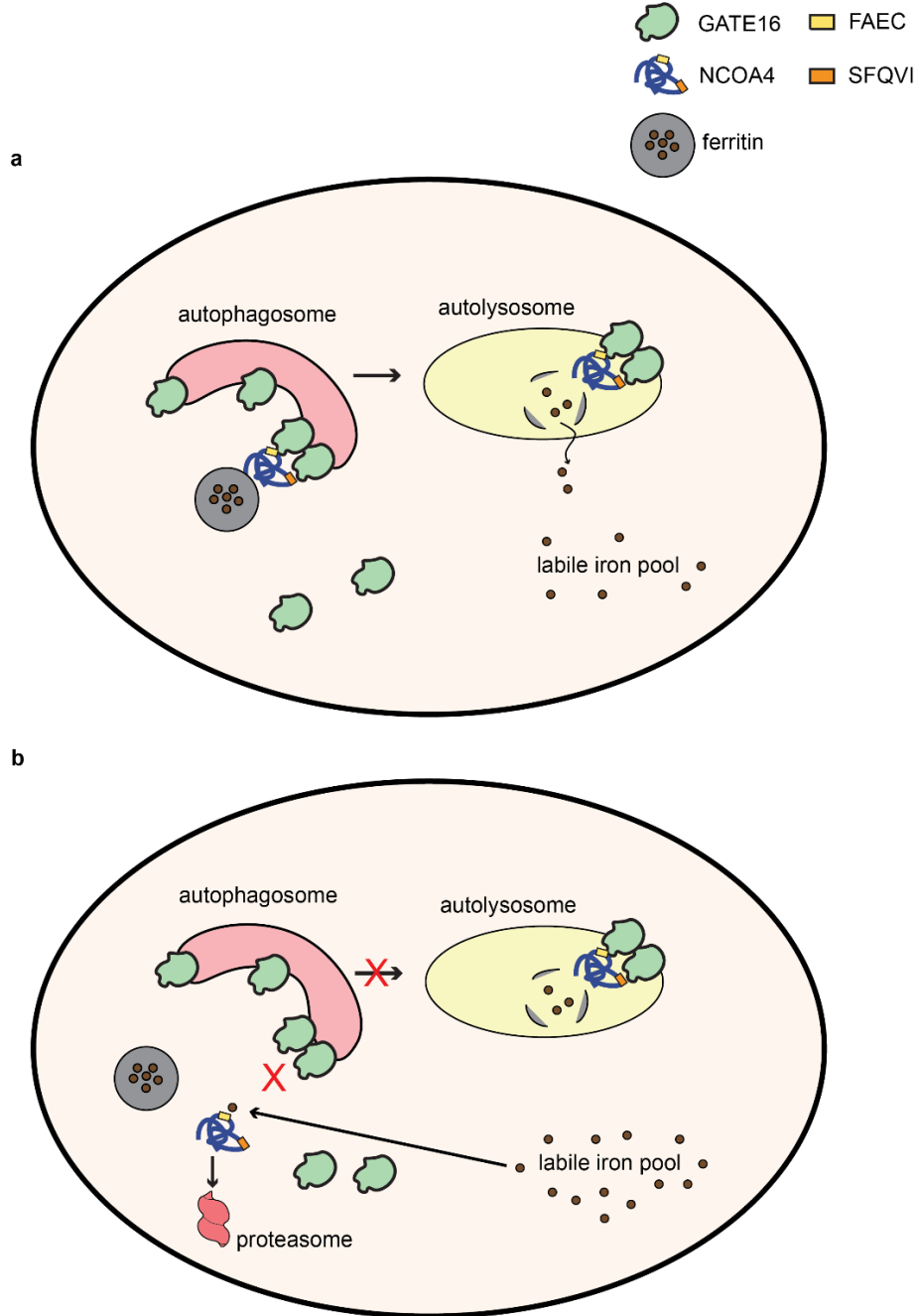


Figure 4.1: Iron regulation of NCOA4•GATE16 dependent ferritinophagy.

(a) In iron limiting conditions, NCOA4 binds to an GATE16 oligomer via its two LIR-like motifs, facilitating ferritin degradation via the lysosome.

(b) In iron replete conditions, the FAECV motif of NCOA4 is occupied by iron, preventing binding to GATE16 and the progression of ferritinophagy. NCOA4 is instead degraded by the proteasome.

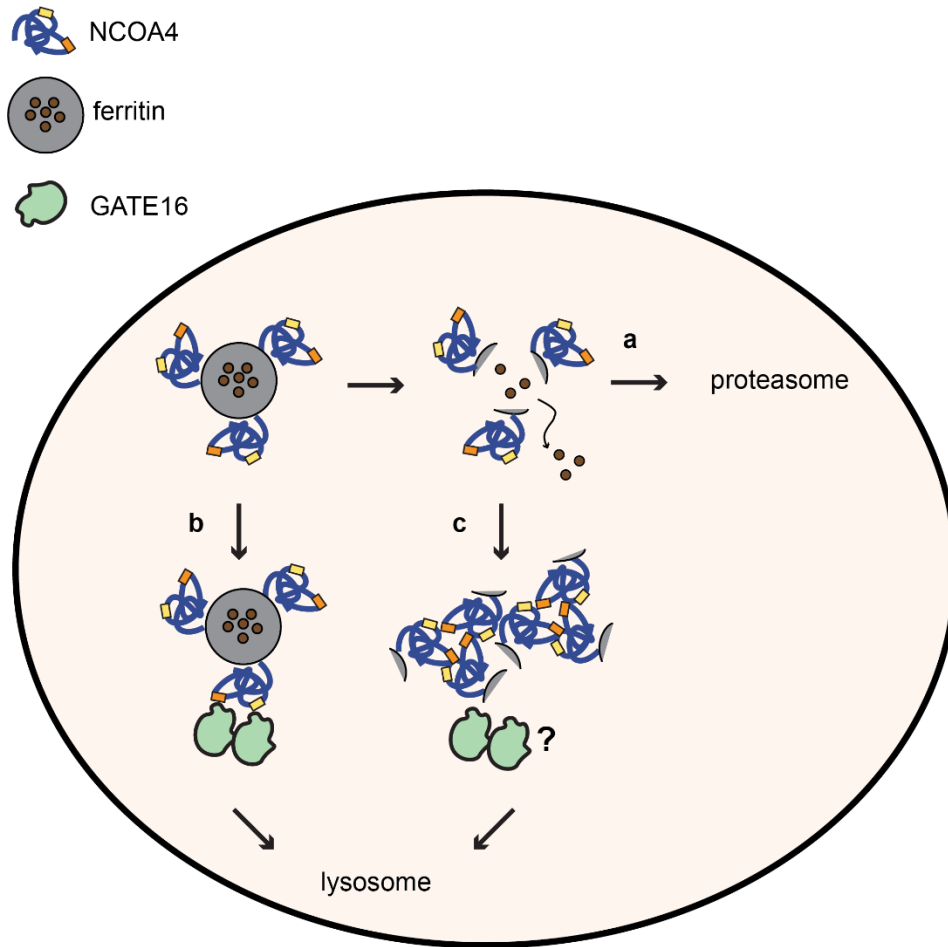


Figure 4.2: Hypothesized NCOA4 dependent degradation of ferritin via the proteasome and lysosome.

(a) NCOA4 disassembles ferritin cages, releasing iron into the cytosol. The resulting ferritin•NCOA4 fragments are degraded by the proteasome.

(b) Binding of GATE16 to NCOA4 occludes the cage dismantling activity site of NCOA4, instead promoting canonical ferritinophagy via the lysosome.

(c) When ferritin•NCOA4 fragments are present in high concentrations, NCOA4 oligomers drive the formation of ferritin•NCOA4 phase condensates, which are cleared by the lysosome, potentially by a GATE16 dependent mechanism.

4.7 REFERENCES

Friedman A, Galazka-Friedman J (2012) The history of the research of iron in parkinsonian substantia nigra. *Journal of Neural Transmission* 119: 1507-1510

Mancias JD, Pontano Vaites L, Nissim S, Biancur DE, Kim AJ, Wang X, Liu Y, Goessling W, Kimmelman AC, Harper JW (2015) Ferritinophagy via NCOA4 is required for erythropoiesis and is regulated by iron dependent HERC2-mediated proteolysis. *Elife* 4

Mancias JD, Wang X, Gygi SP, Harper JW, Kimmelman AC (2014) Quantitative proteomics identifies NCOA4 as the cargo receptor mediating ferritinophagy. *Nature* 509: 105-109

Quiles Del Rey M, Mancias JD (2019) NCOA4-Mediated Ferritinophagy: A Potential Link to Neurodegeneration. *Front Neurosci* 13: 238

Sofic E, Riederer P, Heinsen H, Beckmann H, Reynolds GP, Hebenstreit G, Youdim MB (1988) Increased iron (III) and total iron content in post mortem substantia nigra of parkinsonian brain. *J Neural Transm* 74: 199-205

Tran D, DiGiacomo P, Born DE, Georgiadis M, Zeineh M (2022) Iron and Alzheimer's Disease: From Pathology to Imaging. *Front Hum Neurosci* 16: 838692

Ward RJ, Zucca FA, Duyn JH, Crichton RR, Zecca L (2014) The role of iron in brain ageing and neurodegenerative disorders. *Lancet Neurol* 13: 1045-1060

Zeng W, Cai J, Zhang L, Peng Q (2024) Iron Deposition in Parkinson's Disease: A Mini-Review. *Cellular and Molecular Neurobiology* 44: 26

Zhao X, Kang Z, Han R, Wang M, Wang Y, Sun X, Wang C, Zhou J, Cao L, Lu M (2024) JWA binding to NCOA4 alleviates degeneration in dopaminergic neurons through suppression of ferritinophagy in Parkinson's disease. *Redox Biology* 73: 103190

Zhong ED, Bepler T, Berger B, Davis JH (2021) CryoDRGN: reconstruction of heterogeneous cryo-EM structures using neural networks. *Nat Methods* 18: 176-185